

Received 2 September 2025, accepted 18 September 2025, date of publication 24 September 2025, date of current version 30 September 2025.

Digital Object Identifier 10.1109/ACCESS.2025.3614064



# **Applications of Robust Statistics in Autonomous Driving**

# TINO WERNER

German Aerospace Center (DLR), Institute of Systems Engineering for Future Mobility, 26121 Oldenburg, Germany e-mail: tino.werner@dlr.de

This work was supported in part by German Federal Ministry for Economic Affairs and Climate Action within the Project "KI Wissen—Entwicklung von Methoden für die Einbindung von Wissen in maschinelles Lernen," and in part by the V&V4NGC Project of German Aerospace Center.

**ABSTRACT** Autonomous vehicles have to interact with their environment with the goal to fulfill their tasks while respecting all desired constraints such as not causing dangerous situations, driving comfortable maneuvers, enabling a smooth traffic flow, or avoiding overly polluting driving behavior. All steps require a suitable perception of the environment conditions, such as the estimation of the own position, a prediction of the trajectories of other traffic participants, or the assessment of parameters corresponding to vehicle dynamics. However, classical estimation algorithms are known to be easily distorted by outliers in the data. In addition, apart from rule-based systems, it becomes more convenient to train autonomous agents by machine learning algorithms. Again, such algorithms need to be robust in order to cope with model misspecification or outliers in the data. Robust Statistics is a discipline of statistics which exactly addresses these challenges. This paper provides an extensive and systematic overview of current applications of Robust Statistics in autonomous driving in a unified notation, discusses different notions of the term "robustness" and identifies directions for future work.

**INDEX TERMS** Autonomous driving, contaminated data, outliers, robust statistics.

## I. INTRODUCTION

17

18

23

Autonomous vehicles in operation have to interact with their environment by repeatedly successfully performing three tasks: Perceiving the current environment state, predicting the future states of all relevant traffic participants up to some prediction horizon, and planning their own maneuvers and therefore necessary control actions. Apart from rule-based systems, which operate according to a deterministic plan, works such as [19] have demonstrated that an autonomous agent can also be trained via machine learning (ML), here Imitation Learning (IL).

A major drawback of IL is the necessity to provide expert trajectories according to which the agent is trained. An alternative class of algorithms is given by Reinforcement Learning (RL), where no training data are required but where the agent learns by trial-and-error. However, while

The associate editor coordinating the review of this manuscript and approving it for publication was Zhiguang Feng .

knowledge about correct maneuvers is implicitly encoded in the expert trajectories in IL training, and while traffic rules can be implemented in rule-based systems, RL agents learn according to a reward function which assigns a real value to a state-action pair, so that the agent learns by experience which actions were useful (i.e., resulted in higher rewards) for which states. Projects such as KI Wissen<sup>1</sup> consider the formalization of prior knowledge and their integration into Artificial Intelligence (AI) training for autonomous driving, see [331] for an extensive overview of knowledge integration into AI.

The perception, the prediction and, for an agent trained by machine learning, even the training is based on statistical estimation, which is well-known to be vulnerable to contamination of the data in the sense that the true model differs from the assumed model, the "ideal model", so that observations from the real distribution may appear as outliers

1https://www.kiwissen.de/

31

39

41

45



(w.r.t. the "ideal model"), with the potential to severely distort a statistical estimator (see, e.g., [121], [153], [213]). Robust Statistics has provided numerous techniques in order to safeguard against such perturbations in the sense that the estimator still works reasonably well, even in the presence of a certain fraction of contaminated data.

Due to the rising interest in autonomous systems and the constant progress made in robustifying estimation and machine learning algorithms, this paper aims at systematically collecting concrete applications of Robust Statistics in autonomous driving, to formalize these approaches in a consistent mathematical notation, and to identify possible extensions and directions for further research. Although this paper is not accompanied with own experiments, it also makes suggestions for future experimental studies.

This paper is organized as follows. Sec. II provides a description of each tasks considered in this paper, a placement into the "sense, plan, act" workflow, and a roadmap across the different application areas considered in this paper. Moreover, potential sources of contamination are identified and how such contamination appears in the data. Sec. III collects the necessary concepts from Robust Statistics and relates them to other notions of robustness that one encounters in the autonomous driving literature. Sec. IV is devoted to approaches from Robust Statistics in perception tasks such as tracking, point cloud detection, or state estimation. Sec. V reviews robustifications for planning/prediction tasks, in particular for RL, IL, and model-predictive control (MPC) algorithms. In Sec. VI, potential topics for future work are discussed.

### II. OVERVIEW

### A. GENERAL TASKS

An autonomous vehicle has to continuously observe its surroundings (perception, "sense"). This is realized in practice by potentially multiple types of sensors such as cameras, LiDAR or radar sensors. The collected information is used in order to predict the movements of the surrounding traffic participants, such as other vehicles or pedestrians, which is necessary in order to plan its own maneuvers ("plan"/"think"). The planning outcomes are finally used in order to perform the correct actions so that the planned next state is reached ("act"). A graphical illustration, including selected tasks corresponding to each of these phases, is provided in Fig. 1.

In the following subsections, we briefly describe each task which has already been addressed by techniques from Robust Statistics that we review in greater detail later. They should provide a quick overview for the reader and already collect the main challenges corresponding to the respective task concerning sources of contamination and the impact of contamination on inference and optimization. Mathematical formulations of the respective optimization problems and the methodology are postponed to the main sections Sec. IV and Sec. V.

### **B. SIMULTANEOUS LOCATION AND MAPPING**

Simultaneous location and mapping (SLAM) consists of two main tasks: Tracking the position of the robot (strictly speaking, the sensor) and estimating its ego-motion; and computing the map of the unknown surrounding environment (e.g., [168]). The robot may use different types of sensors such as camera, LiDAR, sonar or infrared. Camera-based SLAM is referred to as visual SLAM (e.g., [353]).

In odometry, the goal is to estimate the ego-motion of the robot. In contrast to SLAM, which requires global consistency of the estimated trajectory in regard of a localization of the agent within its environment, odometry considers local consistency and incrementally estimates the robot's trajectory. Odometry can be considered as part of SLAM, e.g., [128].

In particular, one has to distinguish between different types of sensors that are used for odometry, e.g., wheel odometry, GNSS/INS (global navigation satellite system/ intertial navigation system), GPS, sonar, LiDAR or camera (e.g., [13]). Using camera data corresponds to visual odometry (VO), using LiDAR data to LiDAR odometry (e.g., [177]).

Depending on the used sensor type and the actual task, one may find different types of contamination in the collected data, which we specify in the following subsections.

### 1) VISUAL ODOMETRY

As for camera models in VO, the most common is the perspective camera model (e.g., [353]). All camera models map the 3D world into an 2D image plane. In the perspective model, more distant objects appear smaller. For 2D image coordinates (u, v) and 3D coordinates (x, y, z), the perspective model is given by

$$\lambda \begin{pmatrix} u \\ v \\ 1 \end{pmatrix} = \begin{pmatrix} f_x & 0 & c_x \\ 0 & f_y & c_y \\ 0 & 0 & 1 \end{pmatrix} \begin{pmatrix} x \\ y \\ z \end{pmatrix},$$

where  $\lambda$  is a depth factor and where the matrix is referred to as the intrinsic calibration matrix, with the focal lengths  $f_x$  and  $f_y$  and the projection center  $(c_x, c_y)$ .

In general, cameras are vulnerable to illumination changes (e.g., [63]). Other sources of contamination can be self-shadowing, camera saturation, camera shaking or rotation, motion blur or defocus [219].

In direct odometry, the image data are used as they are and a projection of the images on reference images is computed. The quality is then quantified via the photometric errors [125]. Alternatively, [62] use brightness intensities at the positions instead of the position coordinates themselves. In the sample consisting of the collected 2D points, contamination manifests itself in points that are not in accordance with the rest of the sample, resulting in high photometric and/or geometric errors when comparing the source and the reference image. A robust approach allows to cover situations (regardless whether photometric or geometric errors are quantified) where the image taken by the camera is contaminated, but in principle, it would also allow for



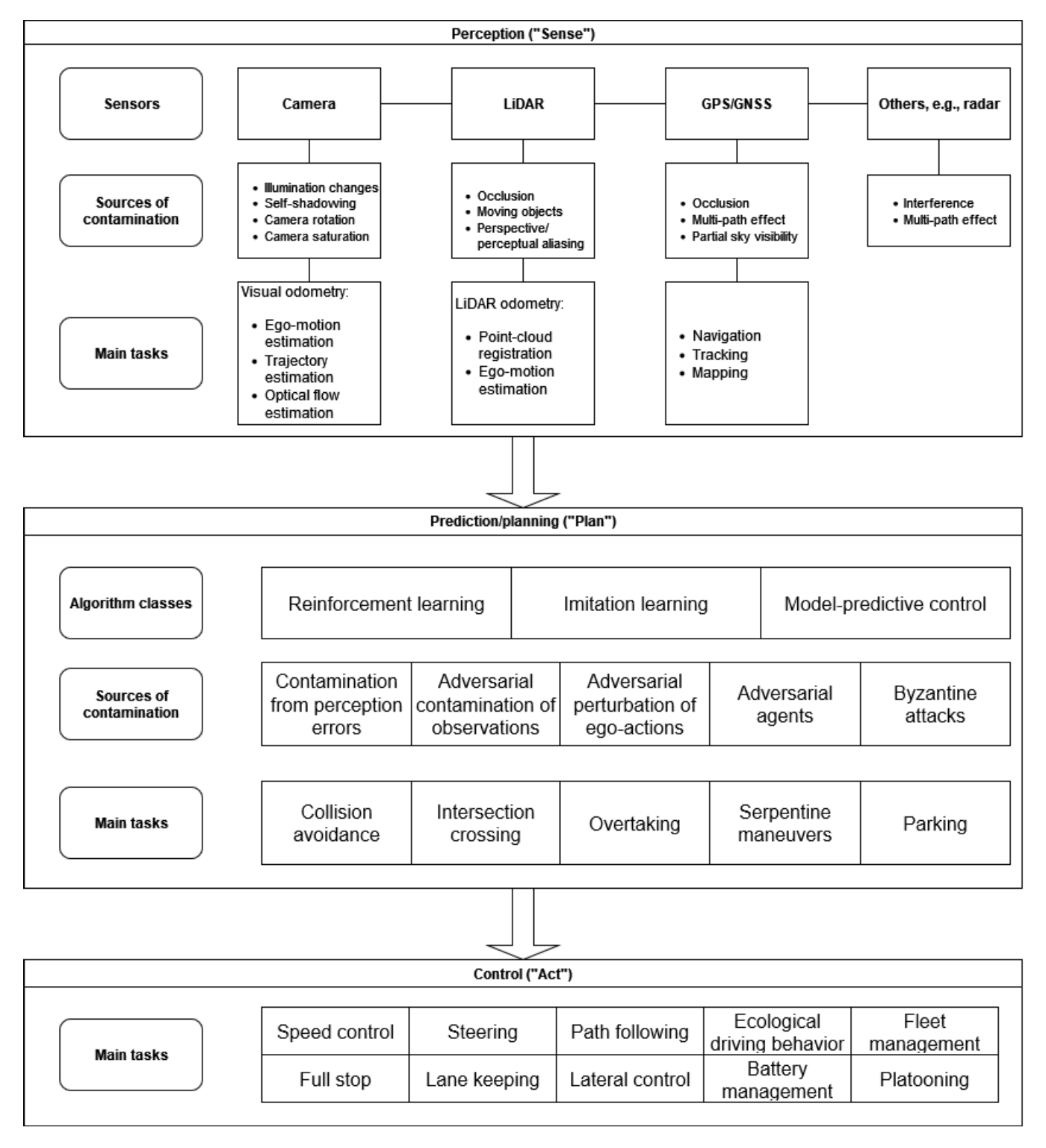


FIGURE 1. Overview of perception, planning, and control tasks as well as corresponding sources of contamination.

the usage of contaminated reference images or reference intensities.

154

155

156

158

Reference [219] mention that a stereo camera pair increases the robustness for the cost of slightly increased computational complexity.

Optical flow estimation slightly differs from VO since the only goal is to estimate the optical flow, i.e., the velocity between subsequent images, but not necessarily the camera position itself. According to [155], the optical flow can be related to the position, translational and rotational velocity

166

168

169

170

171

172

173

174

175

176

177

178

180

181

182

184

185

187

189

190

192

193

194

195

197

199

200

202

204

206

207

209

210

211

212

214

216



220

222

224

225

228

230

231

232

233

235

236

238

243

245

248

250

251

252

253

257

259

260

262

264

267

269

271

of the camera. Therefore, one can extract the positions and velocities by regression from the sample. Contamination in the sample is induced by measurement errors of the optical flow, maybe due to the lack of a visible ground surface. References [33] and [34] elucidate that optical flow estimation is usually accompanied by assumptions such as the brightness constancy assumption which indicates that the brightness only varies smoothly (w.r.t. to both position and time), or a spatial coherence assumption that indicates that neighboring pixels are likely to be part of the same object, and hence change similarly. Note that drifts of the sensors usually do not violate these assumptions as they do not affect the relative correspondences between the pixels. Those assumptions however are violated in the presence of reflections, shadows, or motion boundaries, which imply outliers in the data in the sense that they violate these assumptions. In other words, outliers are likely to produce large loss values and therefore capable to let the estimation break down. Therefore, robust approaches are required.

# 2) LIDAR ODOMETRY/POINT CLOUD REGISTRATION

LiDAR data are usually point clouds. In contrast to cameras, LiDAR has the advantage to be immune to light variations [177], but the analysis of 3D data may cause high computational costs [13]. When using LiDAR data, contamination may result from occlusions [381], moving objects [62], [63], perspective and perceptual aliasing, i.e., different but similar places cannot be distinguished [210], or from environments with self-similar structures where false associations are generated that appear as outliers [4]. [245] argue that outliers not only occur due to measurement errors but also due to changes in the object itself or overlapping point clouds in the sense that they represent overlapping but not the same details of an object. Reference [330] point out that moving objects appear as dynamic obstacles and hence occlude the static environment from the sensors of an autonomous vehicle, inducing outliers. See [187] for an overview of potential sources of contamination in point cloud data.

Point cloud registration addresses the registration of sets of 2D or 3D points in computer vision. One of the best known algorithms for this problem is the iterative closest point algorithm (ICP). Here, one has some reference surface (a "model" point cloud), with which the observed point cloud, the "data" point cloud, has to be aligned. To this end, the goal is to find a parametric transformation between the points of both point clouds. In the simplest form, this is done iteratively by finding the closest model point for each data point, respectively, for the current parameter, and to update the transformation parameter by minimizing the sum of squared distances over all data points (e.g., [93]). Note the similarity of this approach to transform data points in order to match model points and the transformation of 2D positions or brightness values in order to match their reference counterparts in VO.

Such outliers potentially induce large values of the loss function that is to be minimized, in particular, when using the squared loss as in the standard ICP algorithm. A typical robustification is to use a robust loss function that allows for a certain fraction of such erroneous points without significant distortion of the matching procedure.

### 3) NAVIGATION

For satellite data, contamination may occur due to occlusion, i.e., where the line-of-sight between emitter and receiver is blocked [231], [237], [269]. Reference [9] argue that a common source of contamination in GNSS data is the multi-path effect, i.e., the signals from satellites in a low orbit can reach the receiving antenna by multiple paths due to reflection on the ground or on surrounding objects. Reference [65] additionally mention partial sky visibility and non-line-sight as sources of contamination. Another source of contamination can be electromagnetic propagation in the sensors [334]. Radar data may be contaminated due to the multi-path effect and interference [192].

In odometry, although the models may receive sequential data, they usually do not include a time component in the form of a time series or state space model. All navigation or tracking approaches where time series data are used are discussed separately and are therefore contained in the individual section Sec. IV-A3. The often used filtering approaches assume a state space model where the observations at time t depend on the current system state, and the current system state depends recursively on the system state at time (t – 1). In contrast to localization problems that are solved via regression or image translation where contamination appears statically in the responses, regressor matrices, or point clouds/images, contamination can propagate through the recursive state space model, and the error distribution may be non-stationary.

Usually, one assumes outliers that only affect the observations, indicating that the observations can be drawn from a different than the assumed ideal distribution with a certain probability (cf. [269]). However, contamination may also appear in the state equation, indicating that the state at time (t+1) is drawn from a different than the assumed conditional distribution w.r.t. the current state at time t. This phenomenon is referred to as innovation outliers (cf. [269]), and results, due to the recursivity of the state equation, also in contamination in the subsequent states.

Filtering approaches mostly amount to the application of the standard or an extended Kalman filter (which covers non-linear state and observation equations), or by noise modeling, usually by variational inference. Inference in Kalman filtering can be identified with least squares regression, opening the path for robust approaches by performing robust regression instead. In variational inference, assumptions on the measurement and process noise distributions are required. By using a heavy-tailed distribution for each type of noise, both additive and innovation outliers can be adequately captured when computing the posterior state distributions.

333

336

338

339

341

343

344

346

348

350

351

353

355

356

357

358

359

360

361

362

363

365

366

367

370

371

372

373

375

377

273

275

277

278

280

282

283

284

285

287

289

290

292

294

295

296

301

303

304

305

306

308

309

311

313

314

316

318

319

320

321

322

323

325

Reference [343] point out that many approaches try to achieve robustness by focusing on high-level features such as lines and edges, however, the computational burden can hinder real-time performance. Reference [211] point out that robust features (e.g., [27], [203]) that are constructed in order to be less invariant towards illumination changes are not suitable for realistic situations where the spectrum and the direction of the light can change.

In SLAM, the data may consist of relative information such as (pseudo)range measurements, i.e., distances between the receiver and the emitter, collected from GPS or radar. By a regression model, one can infer the vehicle (i.e., receiver) location from the range data. Since the measurement function that quantifies the relative information is usually non-linear, a good initial guess for the true positions is required in order to find the global optimum (cf. [141]). Contamination appears not only from measurement errors but is also implied by bad initial guesses, and their location may be random or grouped (e.g., [4]). Contamination in the sense of measurement errors of the ranges appear as outliers in the responses. A robust (regression) approach therefore not only safeguards against measurement errors but also against bad initializations (maybe resulting from measurement errors in the data) and allows for contamination in the regressor matrix, maybe due to erroneous receiver coordinates or clock offsets.

# C. BOUNDING BOX ESTIMATION

Bounding box estimation is crucial in object detection and tracking. The goal is to find a box which completely surrounds the desired object and which is as tightly as possible. Typical approaches for bounding box detection invoke both a classification loss, because the object corresponding to the box needs to be identified, as well as a regression loss that quantifies the quality of the bounding box coordinates (e.g., [108]).

A source of contamination could be errors made by the annotators, which is a known problem and has been studied for example in [224] and [306]. Suppose that an annotator provided a bounding box that is much wider or narrower than it should be. This could induce wrong patterns during training, maybe when there are many similar objects in the data, so that the neural network learns to fit reliable bounding boxes for the similar objects and, therefore, also for the object with the wrong bounding box, which implies a large regression loss for this particular bounding box. However, if for some reason a reference bounding box immensely differs from the optimal one, it could have a leverage effect, similarly as one large outlier in least-squares regression, and distort the whole model. Having already annotated data, is seems implausible that they would be checked again by the data scientist, so in this case, one could find contamination by inspecting the losses during neural network training or during testing, and may identify such "outliers". By a robust approach, even large outliers may not result in a distorted model. Reference [154] provided another argumentation why

contamination may appear, namely that object detection is accompanied with an uncertainty that grows as a function of time, i.e., when performing tracking and iteratively predicting a bounding box for a future time step. In this sense, the true bounding box coordinates could appear as outliers under the assumption of the current predictive model for the coordinates.

### D. ESTIMATION OF VEHICLE PARAMETERS

Vehicle parameters need to be inferred in order to operate a vehicle safely. Such parameters can correspond to vehicle dynamics like longitudinal and lateral velocities, moments of inertia, or tractive forces, or be related to electric vehicles only, which are voltages or the state of charge of batteries.

Contamination appears once measurement errors occur, either in the training data for the parameters of interest, resulting in errors in the response variables, or for the regressor variables, which leads to contamination in the features. Outliers in the responses or regressors can be identified individually by outlier detection procedures, applied onto the response column or the regressor matrix, however, in a regression setting, both procedures alone would not find outliers that are inconsistent with the regression model. In other words, if for example a response variable has been measured wrongly but still lies within the range of the majority of response values, it would not appear as outlier when considering the response column alone. However, if the contamination is inconsistent with an assumed underlying regression model, it is detected when computing the residuals. Robust procedures hence allow to deal with even large measurement errors, which may never be completely avoidable, and can provide models that only marginally suffer from contamination.

# E. DETECTION OF ROAD FEATURES

Road feature detection includes to find the position of road features such as road markings or to even extract road surfaces from measured 3D point clouds. This is achieved by a regression approach.

A typical source of contamination are measurement errors and false positives of the tracker (e.g., [302]). In road surface detection, contamination may arise from non-surface points in the point cloud [234], which would imply large residuals.

# F. PREDICTION AND PLANNING

Apart from the applications of Robust Statistics in perception tasks as illustrated in the previous subsections, robust procedures also entered approaches for prediction and planning, i.e., RL, IL, and MPC.

In most of these approaches, one either considers adversarial robustness or robustness against noise induced by measurement errors, where either the observed state is perturbed (e.g., [282]) or even the true state [316]. Robust approaches usually amount to a minimax game, where one does not optimize the expected future reward, but a

381

382

384

386

388

389

390

391

393

395

396

398

401

402

405

406

407

408

410

411

417



419

424

425

427

429

430

431

432

434

435

436

437

439

442

443

444

446

451

452

453

456

458

459

460

461

463

464

465

worst-case future reward under unfavorable transitions [131], maybe induced by adversarial agents that are trained in order to hinder the ego-agent to reach its goal (e.g., [256]). Even perturbations of the ego-actions have been considered [298].

However, as RL does not need data but uses the data generated during training, finding a reasonable amount of contamination is more difficult than in settings where one can just use contaminated real-world data. One challenge, when training adversarial agents, is to ensure that these agents at least behave plausibly, i.e., that the ego-agent is not trained solely on extreme edge cases that are very unlikely to be encountered in the real world.

In IL, reference trajectories are given, where contamination can appear by random perturbations [19]. With annotation errors from bounding box estimation in mind, one can interpret such perturbations as a manifestation of a non-perfect human driver, similarly to annotation errors due to non-perfect human annotators. Alternatively, single state-action pairs may be contaminated [198], a fraction of transitions [366] or even a fraction of transitions and rewards [365].

### III. KEY CONCEPTS OF ROBUST STATISTICS

This section provides the necessary notions and concepts of Robust Statistics.

### A. CONTAMINATION MODELS

Contamination models formalize mismatches of the assumed ("ideal") and the real distribution. They are given by sets of probability distributions whose distance, quantified in some metric, to the ideal distribution is bounded by some constant.

Before we start with formal definitions, we provide small examples in order to illustrate how the contamination models have to be understood and how they deviate from adversarial attacks.

Example 1: Consider the regressor matrix  $X = \begin{pmatrix} 2 & 0 & 3 \\ -1 & 1 & 2 \\ -2 & 1 & 0 \\ 4 & -1 & 3 \end{pmatrix}$  and the following perturbed versions:

$$X^{(1)} = \begin{pmatrix} 1 & -1 & 2 \\ -2 & 0 & 1 \\ -3 & 0 & -1 \\ 3 & -2 & 2 \end{pmatrix}, \quad X^{(2)} = \begin{pmatrix} 8 & -4 & 6 \\ -1 & 1 & 2 \\ -2 & 1 & 0 \\ 4 & -1 & 3 \end{pmatrix},$$

$$X^{(3)} = \begin{pmatrix} 2 & 0 & 3 \\ 8 & 9 & 8 \\ -2 & 1 & 0 \\ 9 & 8 & 11 \end{pmatrix}.$$

Let us start with adversarial attacks. Here, we interpret the perturbed matrices as sums of the form  $X^{(k)} = X + V^{(k)}$ , k = 1, 2, 3, for perturbation matrices  $V^{(k)}$ . These matrices

are therefore given by

$$V^{(3)} = \begin{pmatrix} 0 & 0 & 0 \\ 9 & 8 & 6 \\ 0 & 0 & 0 \\ 5 & 9 & 8 \end{pmatrix}.$$

Can these perturbation matrices stem from an adversarial attack scheme? It depends on the budget, usually quantified in the Frobenius norm. The Frobenius norm of a matrix  $M \in \mathbb{R}^{m \times n}$  is defined as  $||M||_F = \left(\sum_{i=1}^m \sum_{j=1}^n |m_{ij}|^2\right)^{1/2}$ . Therefore, we have  $||V^{(1)}||_F = \sqrt{12}$ ,  $||V^{(2)}||_F = \sqrt{61}$ ,  $||V^{(3)}||_F = \sqrt{351}$ . In other words, with a perturbation budget of 7 for an adversarial attack scheme on X, it is possible to generate  $X^{(1)}$ , but it is impossible to generate  $X^{(2)}$  or  $X^{(3)}$ . With a budget of 20, it is possible to generate each of the perturbed matrices.

Now, consider a probabilistic contamination model in the sense that with a certain probability, 1 - r, a row of X stems from its original distribution, and with probability r, from some other distribution G. The first consequence is that the  $V^{(k)}$  are no longer needed here, as there is no additive perturbation matrix. We assume for simplicity in this example that when a row of  $X^{(k)}$  equals the respective row of X, it stems from the original distribution. We start with  $X^{(2)}$ . Only the first row differs from X. In this simplified example, it follows that for r = 0.1, the probability that only one row stems from another than the original distribution is  $4 \cdot 0.1 \cdot 0.9^3$ . However, whether realizing  $X^{(2)}$ is possible and its likelihood also depends on the distribution G. If G is a  $\mathcal{N}_3((6, -4, 3), \Sigma)$ -distribution for some positive semi-definite matrix  $\Sigma$ , the realization of  $X^{(2)}$  is certainly possible and its likelihood is given by the density of G at (6, -4, 3). However, if G has zero density at (6, -4, 3), realizing  $X^{(2)}$  under this contamination scheme is impossible. A similar argumentation can be done for  $X^{(3)}$ . As for  $X^{(1)}$ , under our simplifying assumptions, having four rows realized from G is very improbable for a low r, but not impossible.

This example should emphasize that the main difference in the geometric distances used in adversarial attacks and the probabilistic distances that are encountered in contamination settings from Robust Statistics is that the former are deterministic in the sense that a certain adversarial contamination is either possible or impossible, while distributional contamination is more subtle and allows for a large variety of possible realized perturbations.

For the following definition, see [259, Sec. 4.2].

Definition 1: Let  $(\Omega, \mathcal{A})$  be a measurable space. Let  $\mathcal{P} := \{P_{\theta} \mid \theta \in \Theta\}$  be a family of parametric distributions  $P_{\theta} \in \mathcal{P}_{\theta}$  on  $(\Omega, \mathcal{A})$ , where  $P_{\theta_0}$  denotes the "ideal distribution". Let  $\Theta \subset \mathbb{R}^p$  be a parameter space. A **contamination model** is given by the set  $\mathcal{U}_*(\theta_0) := \{U_*(\theta_0, r) \mid r \in \mathcal{U}_*(\theta_0, r) \in \mathcal{U}_*(\theta_0, r)$ 

522

523

524

525

526

527

528

529

530

532

535

537

539

542

545

546

551

552

553

554

556

559

561

562

565



469

472

473

474

476

478

480

481

483

485

486

488

491

492

493

495

498

502

503

505

507

509

510

512

514

515

516

 $[0,\infty]$ } of **contamination balls**  $U_*(\theta_0,r)=\{Q\in\mathcal{M}_1(\mathcal{A})\mid d_*(P_{\theta_0},Q)\leq r\}$ , where  $\mathcal{M}_1(\mathcal{A})$  denotes the set of probability distributions on  $\mathcal{A}$ . One refers to r also as the "contamination radius".

One can consider the "ideal distribution" to be the distribution that one assumes for the underlying data, often idealized, e.g., Gaussian.

Example 2: The convex contamination model  $U_c(\theta_0)$  considers a convex combination of distributions, leading to convex contamination balls of the form

$$U_c(\theta_0, r) = \{(1 - r) + P_{\theta_0} + \min(1, r)Q \mid Q \in \mathcal{M}_1(A)\}.$$

The convex contamination model is intuitive in the sense that with a probability of  $\min(1, r)$ , an instance in a dataset, a gradient in neural network training, an action of an agent, or whatever the data consist of, is contaminated, i.e., in expectation, a  $\min(1, r)$ -fraction of the considered objects is not generated from the ideal distribution. In Ex. 1, convex contamination has been considered.

### B. BREAKDOWN POINT

The breakdown point (BDP), roughly speaking, quantifies the amount of contamination that is necessary in order to achieve a breakdown of the estimator in the sense that the estimator may output unreasonable values. For a given dataset, the so-called finite-sample BDP [78] is the relative fraction of instances that have to be contaminated in order to achieve such a breakdown. For regression, let the dataset consist of instances  $(X_i, Y_i) \in \mathbb{R}^{p+1}$  and assume the model  $\mathbb{E}[Y_i] = h(X_i)\boldsymbol{\beta}$  for some unknown coefficient vector  $\boldsymbol{\beta} \in \mathbb{R}^p$ . The BDP is then defined as follows.

Definition 2: Let  $Z_n := \{(X_1, Y_1), \dots, (X_n, Y_n)\}$  for instances  $(X_i, Y_i)$ . The **case-wise finite-sample breakdown point** of an estimator  $\hat{\beta}$  for the regression parameter  $\beta$  is defined by

$$\varepsilon^*(\hat{\boldsymbol{\beta}}, Z_n) = \min \left\{ \frac{m}{n} \mid \sup_{Z_n^m} (||\hat{\boldsymbol{\beta}}(Z_n^m)||) = \infty \right\}. \tag{1}$$

Here, the set  $Z_n^m$  denotes any sample that has exactly (n-m) instances in common with  $Z_n$ . The coefficient  $\hat{\beta}(Z_n)$  denotes the estimated parameter on  $Z_n^m$ .

Note that the fraction given by the BDP is deterministic in the sense that, for example, in federated learning, one assumes that exactly m out of n gradients can be intercepted and manipulated by an attacker. In contrast, the convex contamination balls are stochastic in the sense that even if the contamination radius r is fixed, the number of contaminated objects follows an  $B(n, \min(1, r))$ -distribution. The BDP of many estimators has already been computed in the literature on Robust Statistics.

We continue the Ex. 1 in order to illustrate the contaminations that are covered in BDP examinations.

Example 3: Consider the matrices X,  $X^{(1)}$ ,  $X^{(2)}$ , and  $X^{(3)}$  from Ex. 1. In contrast to the modeling approach with ideal and contaminating distributions as in Ex. 1, we inspect

the situation where a breakdown point of some algorithm operating on X should be discussed. For comparison, we first consider adversarial attacks. Here, the question is whether some adversarial attack that can be crafted using the allowed budget can lead to a large deviation in the output of a trained model. Usually, one has a classification model and tries to find adversarial perturbations that cause the model to predict a different label for the perturbed input than for X (e.g., [42], [111]).

When dealing with poisoning attacks, one does not assume an already trained model as when considering adversarial attacks, but examines the impact of an adversarial perturbation w.r.t. some budget on the trained model itself, i.e., whether adversarial perturbations can distort the model during training.

For BDP inspections, the goal is similar as when considering poisoning attacks. Here, one is also interested in the impact of perturbations on the training process, but the contamination is injected differently. While poisoning attacks consider perturbations that are bounded by a geometric argument, e.g., the Frobenius norm, BDP discussions consider the fraction of perturbed observations only. In this sense, the perturbed matrices  $X^{(k)}$  can appear in poisoning attack settings provided that the budget is sufficiently high. For BDP discussions however, the set  $Z_n^m$  is considered. In this example, the set  $Z_n^m$  consists of all  $4 \times 3$ —matrices for which exactly (n - m) rows are identical with the respective rows of X. In this sense, the matrix  $X^{(2)}$  lies in the set  $Z_n^m$  for all m = 1, ..., 4, while the matrix  $X^{(3)}$  can only be considered for m > 1. The matrix  $X^{(1)}$  would correspond only to m = 4, however, in nearly all settings, one would not allow for m > n/2 = 2, so one can assume that  $X^{(1)}$  would not appear in BDP discussions.

The BDP concept has also been formulated, e.g., for classification (rotation of decision boundaries; [370]), ranking (order inversion; [325]), and clustering (dissolution of clusters; [136]).

In particular, in the context of high-dimensional data, [10] propose to consider the contamination of single cells. As one contaminated cell already contaminates the corresponding instance, in high-dimensional settings, one can easily contaminate each instance with a few outlying cells. One can nevertheless consider the relative fraction of contaminated cells as (cell-wise) BDP concept, see, e.g., [310], when analyzing cell-wise robust algorithms that are tailored to this setting.

# C. INFLUENCE CURVE

Robust Statistics interprets estimators as statistical functionals, i.e., functionals which take a distribution as input. For example, the expected value of some distribution P can be denoted by the mean functional  $T^{\text{mean}}(P) = \int xP(dx)$ . The influence curve goes back to [123]. The goal is to determine the local behavior of an estimator in a neighborhood around the ideal distribution by a suitable linearization of the

**IEEE** Access

underlying functional. Given such a linearization, i.e., a van-Mises expansion [311] of the statistical functional in the sense

$$T(Q) - T(P) = \int T'(P)d(Q - P)(x) + \text{rem}$$

for some stochastic remainder term rem, the (Gâteaux-) deritative can be identified with the influence curve, i.e., T'(P) = IC(x, T, P).

Formally, the influence function is defined as follows (e.g., [259]).

*Definition 3:* Let  $\mathcal{Z}$  be a normed function space. Let further the parameter space  $\Theta$  be a normed real vector space and let  $T: \mathcal{Z} \to \Theta$  be a statistical functional. The **influence curve** of T at  $\mathbf{x}$  for a distribution P on  $\mathcal{Z}$  is given by

$$IC(\mathbf{x}, T, P) := \lim_{r \to 0} \left( \frac{T((1-r)P + r\delta_{\mathbf{x}}) - T(P)}{r} \right)$$
$$= \partial_r \left[ T((1-r)P + r\delta_{\mathbf{x}}) \right] \Big|_{r=0}$$

for the Dirac measure  $\delta_x$  at x.

The influence curve determines the infinitesimal impact of a single observation on the estimator. Robustness of the estimator in the sense of the influence curve requires that  $|IC(x, T, P)| < \infty$  for all x. This property is called B-robustness.

# D. ROBUST LOSSES AND AGGREGATION METHODS

Let a general M-estimator be given by

$$\hat{\boldsymbol{\theta}}^{M} = \operatorname{argmin}_{\boldsymbol{\theta}} \left( \frac{1}{n} \sum_{i=1}^{n} \rho(r_i(\boldsymbol{\theta})) \right)$$

for a loss function  $\rho : \mathbb{R} \to \mathbb{R}$  and residuals  $r_i(\theta)$ . If  $\rho$  is differentiable, one can equivalently consider the corresponding Z-estimator

$$\operatorname{zero}_{\boldsymbol{\theta}} \left( \frac{1}{n} \sum_{i=1}^{n} \psi(r_i(\boldsymbol{\theta})) \right)$$

for  $\psi = \rho'$ . The influence function of an M-estimator is (e.g., [121])

$$IC(\mathbf{x}, \hat{\boldsymbol{\theta}}^{M}, P_{\boldsymbol{\theta}_0}) = -\frac{\psi(\mathbf{x})}{\mathbb{E}_{P_{\boldsymbol{\theta}_0}}[\psi'(\mathbf{X})]}.$$
 (2)

Therefore, a robustification of an M-estimator can be done by bounding the derivative  $\psi$  of the loss function, which leads to "robust loss functions". A popular example is the Huber loss

$$\rho_H(r) = \begin{cases} r^2, & |r| \le k \\ 2k|r| - k^2, & |r| \ge k \end{cases}$$

for a hyperparameter k. One can interpret location M-estimators as weighted means of the form (e.g., [213])

$$\sum_{i=1}^{n} w(X_i - \hat{\boldsymbol{\theta}})(X_i - \hat{\boldsymbol{\theta}}) = 0, \quad \hat{\boldsymbol{\theta}} = \frac{\sum_{i} w_i X_i}{\sum_{i} w_i},$$
$$w_i = w(X_i - \hat{\boldsymbol{\theta}}).$$

In the case of the Huber loss, the weight function is given by

$$w_H(r) = \min\left(1, \frac{k}{|r|}\right).$$

A disadvantage of the Huber loss is that the loss function is still unbounded, which makes Huberized M-estimators vulnerable against large outliers or heavy-tailed distributions. In order to cope with such situations, one uses loss functions which are bounded, implying that their derivatives  $\psi$  tend to zero again in the sense  $\lim_{|r|\to\infty} (\psi(r)) = 0$ . Therefore, such derivatives are sometimes called "redescenders". A popular loss function of this type is the Tukey-biweight loss, given by

$$\rho_T(r) = \begin{cases} 1 - \left(1 - \left(\frac{r}{k}\right)^2\right)^3, & |r| \le k \\ 1, & |r| \ge k \end{cases}$$

Further losses with redescending derivative are the Welsch loss

$$\rho_W(r) = 1 - \exp\left(-\frac{1}{2}\left(\frac{r}{k}\right)^2\right),\tag{623}$$

the Geman-McClure loss

$$\rho_{GM}(r) = \frac{r^2}{r^2 + k^2},$$

and the Cauchy loss

$$\rho_C(r) = \frac{k^2}{2} \ln \left( 1 + \left( \frac{r}{k} \right)^2 \right).$$

Another technique, which still allows for using standard loss functions such as the squared loss, is to robustify the aggregation of the losses corresponding to the individual instances. This is done by trimming, leading to approaches such as the least median of squares [262]

$$\operatorname{argmin}_{\boldsymbol{\theta}}(\operatorname{med}(r_i(\boldsymbol{\theta}))).$$

Due to a slow convergence rate, [262] proposed the least trimmed squares (LTS) estimator

$$\operatorname{argmin}_{\boldsymbol{\theta}} \left( \sum_{i=1}^{h} (r^2(\boldsymbol{\theta}))_{i:n} \right),$$
 63

where  $z_{1:n}$  denotes the smallest element of a vector  $z \in \mathbb{R}^n$ ,  $z_{2:n}$  the second smallest element and so forth. In other words, the LTS estimator intends to minimize the sum of squares for the  $h \leq n$  observations with the smallest squared residuals (the set of these instances is sometimes called "clean subset"). Due to the computational complexity of LTS, [264], [265] proposed an iterative algorithm that starts with an initial subset  $I_h^{(0)}$  of size h so that the parameters of the model are computed solely using the instances  $I_h^{(0)}$ . Then, the residuals for all instances are computed, leading to the next iterate  $I_h^{(1)}$  that consists of the h instances with the smallest residuals. Due to only attaining a local minimum, this algorithm is repeated for several initial sets, so that the final h-set with the smallest sum of residuals (over this h-set) is taken. This technique has been extended to high-dimensional models by



654

656

658

659

660

662

666

670

672

673

675

680

681

683

686

688

693

695

700

the Sparse LTS (SLTS) method [7] where Lasso models are computed in each iteration.

In regression, one may have to estimate both the regression parameter  $\hat{\beta}$  and a scale  $\hat{\sigma}$ . This can be done by first estimating  $\hat{\sigma}$  and by solving

$$\operatorname{argmin}_{\beta} \left( \frac{1}{n} \sum_{i} \rho \left( \frac{r_{i}(\beta)}{\hat{\sigma}} \right) \right),$$

for a bounded loss function  $\rho$ . The idea of MM-estimators is to first compute a consistent and highly robust estimator  $\hat{\boldsymbol{\beta}}^{(0)}$ , to compute a robust scale estimator  $\hat{\boldsymbol{\sigma}}$  and to find a solution of the problem above, allowing for both robustness and high efficiency.

# E. OTHER NOTIONS OF ROBUSTNESS IN AUTONOMOUS

The term "robustness" is often used in the AI literature, including that on autonomous driving, in a dictionary-sense such as robustness against error propagation by the simplification of computation steps or against hyperparameter settings of a certain algorithm. Robustness can also be understood as a better accessibility of model parameters (e.g., [81]).

The closest understanding of robustness to that from Robust Statistics is the consideration of challenging environment conditions such as GPS in the presence of tunnels and canyons [219], sensor fusion in "hostile environments" [339] or rain [360], or in general the gap between a simulation and the real world, e.g., [8], [11]. Sensors such as LiDAR or Radar that can cope with varying lightning or weather conditions are also called "robust" [89].

In deep learning in general, the term "robustness" is often understood as **adversarial robustness** (e.g., [156]; see, e.g., [24], [266] for details on adversarial robustness), which is not the core understanding of robustness in the sense of Robust Statistics, because the perturbation occurs after model training, while Robust Statistics considers the effect of contamination onto the estimator, i.e., the contamination appears before training and therefore potentially affects the trained model. Reference [104] point out that there are different understandings of the term "robustness" and focus themselves on the classical robustness in terms of the breakdown point. Moreover, they correctly emphasize that robustness in the sense of the BDP does not guarantee adversarial robustness.

At least two measures for adversarial robustness have been proposed in the literature, the error-rate-based measure [212] where adversarial samples are generated given a certain perturbation radius and the relative number of errors is investigated, or the radius-based measure [296] where one searches for the minimum perturbation radius in order to generate a misclassification. In the adversarial setting, one uses the term "certified robustness" which indicates some guarantee that an adversary does not have success provided that the perturbation norm is smaller than some threshold.

The counterpart from Robust Statistics is the property of a non-zero BDP in order to guarantee global robustness here.

Sometimes even the convex contamination setting is interpreted as adversarial setting [371]. Reference [382] use the terminology "robust loss" for a worst-case loss in adversarial training. Reference [338] call the property that machine learning models perform well even in the presence of adversarial attacks as "robust accuracy" or "robust generalization". Reference [112] define "over-robustness" (for Graphical Neural Networks (GNNs)) as unwanted robustness in the sense that even the semantic context has changed due to the perturbations, the robust classifier does not react, which they call "robust beyond the point of semantic change". The term "trigger/backdoor robustness" has been coined in [118] who consider backdoor and poisoning attacks.

711

714

716

719

721

724

731

732

733

734

735

737

742

744

749

751

752

753

754

Reference [135] speak of "common corruptions" of images such as blur, Gaussian noise or due to certain weather conditions such as fog. They propose not to only consider the worst-case situation when assessing robustness as in adversarial attacks (and, notably, also in BDP computations) but to also take these common corruptions into account. They introduce the term "corruption robustness" which does not refer to the minimum probability that the classifier predicts the correct class over a perturbation ball as in adversarial robustness but which refers to the expectation over a set of corruptions. Note that this idea is similar to the expected finite-sample BDP from [268] where one abstains from considering the worst-case contamination in the context of heavy-tailed distributions.

### F. RANSAC

A popular algorithm that entered autonomous driving application is RANSAC (random sample consensus), going back to [92]. The idea of RANSAC is to iteratively identify the worst points (usually time points) and to remove them from the data. More precisely, RANSAC samples m < n instances, computes a model  $f_{\hat{a}}$  and determines the consensus set, which is given by the instances for which the loss is smaller than some threshold. If the size of this set is larger than h for some h, one uses this set to re-compute the model, otherwise, one samples another random subset of size m and repeats the procedure. At the end, the largest consensus set (which one may again interpret as "clean" subset) observed is reported. The elements of this consensus set are interpreted as inliers here. This procedure can be interpreted as a brute-force counterpart of the iterative algorithm for the computation of the LTS.

For example, [349] use the RANSAC algorithm in order to address ego-motion estimation, segmentation, and moving object detection. They point out that RANSAC is tailored to environments with rapid changes. Reference [178] apply RANSAC for robust pose estimation of vehicles.

Reference [291] point out that on data corresponding to rotation search or point cloud registration, one can even have more than 95% outliers, see also [239], and work with up

762

765

767

768

770

772

774

775

777

781

782

786

788

789

791

792

794

798

801

804

806

808

809

811



820

822

825

827

829

835

837

841

842

844

846

847

850

851

852

854

857

to 99% outliers in their experiments. The reason is that for two point clouds  $\mathcal{P} = (\mathbf{P}_i)_{i=1}^n$ ,  $\mathcal{P}^* = (\mathbf{P}_i^*)_{i=1}^n$ ,  $\mathbf{P}_i$ ,  $\mathbf{P}_i^* \in \mathbb{R}^3$ , mismatched keypoints or localization errors can result in a lot of false correspondences  $(P_i, P_i^*)$  [178], [291]. From the perspective of Robust Statistics, such a high contamination radius is uncommon, and most concepts can at most deal with contamination radii of 0.5 because the BDP of an equivariant estimator cannot exceed 0.5 asymptotically [71]. There are however at least two cases where the number of outlying instances is allowed to be higher. First, when aggregating models, e.g., [326] proposed a trimmed Stability Selection where only the models corresponding to the smallest out-of-sample losses are considered for aggregation, theoretically allowing for a higher rate of outliers in the data set than 0.5 because resampling can result in sufficiently clean training batches (where the outlier ratio is at most 0.5). On the other hand, an instance is considered to be outlying if at least one cell is contaminated [10]. In such situations, cell-wise robust algorithms provide an alternative to classical robust algorithms as they can deal with the situation that each instance is contaminated, provided that the cell-wise contamination rate is lower than their cellwise BDP. However, this requires sufficiently many predictor variables, e.g., in the setting of point cloud registration, the data set only consists of the pairwise point correspondences, making the notion of cell-wise robustness obsolete.

RANSAC has disadvantages, such as the long computation time, the dependence on the minimum number of instances that is required for defining a model [254], the problem to apply it to data with only a few samples due to sparse measurements or many dropouts [210], the increased complexity for large outlier fractions [283], the sensitivity to the outlier threshold [210], its non-deterministic nature (e.g., [239], [280]), and the difficulty to apply it to highdimensional problems [280]. RANSAC clearly depends on the error threshold, which leads to the problem that, in contrast to trimming approaches such as LTS where the trimming rate (i.e.,  $\alpha$  such that  $h = \lceil (1 - \alpha)n \rceil$ ) is fixed, defining a threshold does not provide ex ante information to how many non-trimmed instances it corresponds. According to [341], RANSAC can deal with 80% outliers but becomes very expensive due to re-adaptations when the outlier rate is higher than 90%.

Reference [210] experimentally compare different Mestimators with the squared, absolute, Huber, Cauchy, Geman-McClure, the dynamically scaled covariance loss [4] and a clipped squared loss on a dataset for visual localization, with the result that the Geman-McClure loss, optionally combined with clipping in the sense that the last iterations are done w.r.t. the clipped squared loss as loss function instead of the Geman-McClure loss, lead to the best results in the presence of large contamination radii. RANSAC cannot be applied due to the large contamination radius, resulting in too few correct correspondences in each images. Reference [225] showed that RANSAC in combination with

robust base estimators such as LTS or LMS performs better in the presence of contamination than RANSAC with standard least squares. The methods were evaluated by the number of inliers they identified on simulated data where this number is known. Reference [182] point out that the iterative closest point algorithm (ICP), which is the standard tool for point cloud registration, heavily depends on the initializations of the transformations and that it cannot deal with cross-source point clouds, for example, from multiview stereo. They combine RANSAC with the Tukey biweight in order to overcome the problem of a very high required number of trials of RANSAC.

Reference [140] propose VODRAC (voting-based double-point random sampling with compatibility weighting). The idea is to overcome to computational complexity of RANSAC by using the pairwise compatibility constraint. That is, for the model  $\tilde{p}_i^* = R\tilde{p}_i + \tilde{t} + \epsilon_i$  for  $\tilde{p}_i$  and  $\tilde{p}_i^*$  from point clouds  $\mathcal{P}, \mathcal{P}^*$ , respectively, a rotation operator  $R \in SO(3)$  and a translation  $\tilde{t} \in \mathbb{R}^3$ , the constraint is

$$r_{ij} := ||\tilde{\boldsymbol{p}}_i^* - \tilde{\boldsymbol{p}}_i^*|| - ||\tilde{\boldsymbol{p}}_i - \tilde{\boldsymbol{p}}_i|| \le 2\eta$$

for the inlier threshold  $\eta$ . This norm difference equals  $2||\epsilon_i - \epsilon_j||$  under the model above. This allows for checking whether two correspondences are compatible, then, one can check whether a third correspondence is compatible with each of these two correspondences and so forth, facilitating the search for the inlier set. This technique is referred to a double-point random sampling. In addition, they aim at putting more weight onto clear inliers, i.e., for which  $r_{ij}$  is small, by invoking Tukey's biweight loss function, leading to the weights

$$w_{ij} = \begin{cases} \left(1 - \frac{r_{ij}^2}{(2\eta)^2}\right)^2, & r_{ij}^2 \le (2\eta)^2\\ 0, & r_{ij}^2 > (2\eta)^2, \end{cases}$$

which allows a sorting of the correspondence set in the sense that the minimal subset is formed by the correspondences with the highest weights.

# IV. APPLICATIONS IN AUTONOMOUS DRIVING: PERCEPTION

This section collects approaches based on Robust Statistics in perception tasks for autonomous driving. In each subsection, we address one of the sub-tasks that we already listed in Fig. 1. Robust perception refers to strategies that allow for corrupted data, such as outliers in camera or LiDAR data, that may result from challenging weather conditions, light reflections, occlusions, or just measurement errors. The extraction of realiable state information from those data is vital in order to suitably predict the maneuvers of other traffic participants and to plan own maneuvers.



A. SLAM

Reference [141] propose to use the Cauchy loss for a robust graph-based SLAM for the model

$$z_{ij} = h_{ij}(\boldsymbol{p}_i, \boldsymbol{p}_j) + \boldsymbol{\epsilon}_{ij}$$

for a non-linear measurement function  $h_{ij}$ , positions  $p_i$ , errors  $\epsilon_{ij}$  and measurements  $z_{ij}$  from  $p_i$  to  $p_j$ . The goal is to estimate the true locations  $p_i$ , so the residuals that enter the Cauchy loss function are

$$r_{ij} = ||\Sigma_{ij}^{1/2}(\boldsymbol{z}_{ij} - h_{ij}(\boldsymbol{p}_i, \boldsymbol{p}_j))||_2$$

for the covariance matrix  $\Sigma_{ij}^{-1}$  of the ideal model  $\epsilon_{ij} \sim \mathcal{N}(\mathbf{0}, \Sigma_{ii}^{-1})$ . The objective is then

$$\operatorname{argmin}_{(\boldsymbol{p}_1,\dots,\boldsymbol{p}_n)} \left( \sum\nolimits_{(i,j)\in E} \rho_C(r_{ij}) \right)$$

for the edge set *E* of the corresponding SLAM graph.

Reference [4] also consider a graph-based approach of the SLAM model which aims to minimize

$$\sum_{t} ||h_{t,t+1}(\boldsymbol{p}_{t}, \boldsymbol{p}_{t+1}) - z_{t,t+1}||_{\Sigma_{t}}^{2} + \sum_{t} \sum_{t'} ||f(\boldsymbol{p}_{t}, \boldsymbol{p}_{t'}) - z_{t,t'}||_{\Lambda_{t,t'}}^{2}$$

where the indices t and t' correspond to time steps. The covariance matrices of the odometry and sensor measurements are given by  $\Sigma_t$  and  $\Lambda_{t,t'}$ , respectively. The goal is to find the positions  $p_t$  that minimize the loss. They propose the dynamically scaled covariance loss,

$$\begin{split} \sum_{t} ||h_{t,t+1}(\pmb{p}_{t}, \pmb{p}_{t+1}) - z_{t,t+1}||_{\Sigma_{t}}^{2} \\ + \sum_{t} \sum_{t'} ||\Psi(\zeta_{t,t'})h_{t,t'}(\pmb{p}_{t}, \pmb{p}_{t'}) - z_{t,t'}||_{\Lambda_{t,t'}}^{2} \\ + \sum_{t} \sum_{t'} ||1 - \zeta_{t,t'}||_{\Xi_{t,t'}}^{2}, \end{split}$$

where the  $\zeta_{t,t'} \in [0, 1]$  are switching variables,  $\Psi : [0, 1] \rightarrow [0, 1]$  is a scaling function and where  $\Xi_{t,t'}$  is a switching prior. This loss is minimized w.r.t. both the  $p_t$  and the  $\zeta_{t,t'}$ . They show that the solution is given by

$$\zeta_{t,t'} = \min \left( 1, \frac{2\Xi_{t,t'}^{-1}}{\Xi_{t,t'}^{-1}} + ||h_{t,t'}(\pmb{p}_t, \pmb{p}_{t'}) - \pmb{z}_{t,t'}||_{\Lambda_{t,t'}}^2 \right).$$

References [3] and [210] show that, inserting the unconstrained solution for the  $\zeta_{t,t+1}$  (so that they are not upper bounded by 1) for dynamically scaled covariance into the loss function, one replicates the Geman-McClure loss function, up to a constant factor. Reference [210] identify the dynamically scaled covariance loss therefore with a variant of the Huber loss where the squared loss is used for small residuals, and the Geman-McClure loss for large residuals.

Reference [3] propose a Bayesian approach for estimating the posterior of the state (position) variables, so that robust loss functions can be implicitly encoded via corresponding distributions such as corrupted Gaussian in a mixture approach. They test their procedure using real data from Google StreetView maps from which the necessary poses and 3D points are extracted.

Reference [303] use the truncated least squares loss for location estimation, i.e.,

$$\sum_{i} \sum_{j} \rho(r_{ij}^{2}), \quad \rho(r) = \begin{cases} r^{2}, & |r| \leq k \\ k^{2}, & |r| \geq k \end{cases},$$

for the geodesic distances  $r_{ij}^2$  between the average poses and the measured poses.

Reference [202] consider multimodal motion prediction and propose a loss function composed by several losses, one is a regression loss w.r.t. the coordinate offsets for which they use the Huber loss. The goal is to predict trajectories until a given horizon.

Many SLAM approaches consider GPS or GNSS data, where one usually has the (pseudo)range as response variable.

Reference [96] compare several robust regression methods for positioning estimation in challenging areas such as urban canyons or city centers. Their model is given by

$$Y_i = X_i \boldsymbol{\beta} + \epsilon_i \tag{3}$$

where the  $Y_i$  are the differences between measured and predicted pseudoranges, the  $X_i$  are the geometry matrices and  $\beta$  is a vector consisting of the receiver coordinates and the clock offset of the receiver and the satellite, scaled with the speed of light. As for the robust methods, LTS and M-estimation with the Huber loss and the IGGIII weight function

$$w_{\text{IGGIII}}(r) = \begin{cases} 1, & |r| \le k_1 \\ \frac{k_1}{|r|} \left( \frac{k_2 - |r|}{k_2 - k_1} \right)^2, & k_1 \le |r| \le k_2 \\ 0, & |r| \ge k_2 \end{cases},$$

respectively, are applied.

Another comparison has been made in [173] who compare several robust regression and outlier detection methods, including LTS, LMS, robust M-estimators, S-estimators, and MM-estimators, on simulated GPS data where the response variable is the pseudorange. The goal of [173] was to study how many outliers were correctly detected by the individual methods. They point out that the robust methods are time-consuming and may hinder real-time performance.

Reference [9] apply robust regression methods on GNSS data, where they consider the linear model Eq. 3 where  $X_i$  at least contains information about the satellite ID, the epoch and the elevation and where  $Y_i$  are the pre-fit pseudoranges. They apply LTS, LMS and a forward search, where one starts searching for a clean subset of size h and increases this number iteratively. They achieve real-time capability on a real-world dataset and propose to not analyze large chunks of data at once but to use a sliding-window approach. Reference [6] consider MM-regression.

Reference [12] propose to apply the Huber M-estimator for GPS position estimation. The underlying model is given by

$$Y_i = X_i^{(d)} + X_i^{(b)} + \epsilon_i,$$

955

957

958

960

961

963

965

967

968

970

972

973

974

975

977

980

982

983

984

985

989

991

993

998

1000

1001



1002

1006

1008

1012

1013

1015

1017

1018

1020

1024

1025

1027

1028

1029

1030

1032

1033

1034

1035

1036

1037

1039

1040

1044

where Y is a pseudorange measurement,  $X^{(d)}$  is the geometric distance from satellite to receiver and  $X^{(b)}$  is a receiver clock offset. In the linear model Eq. 3, the parameter vector  $\beta$  contains the incremental corrections to the unknown variables (receiver coordinates and clock offsets). Due to linear relationships of the residuals and measurement errors, they compute the redundancy matrix which is used to modify the residuals. See also [64] for an application of robust M-estimators for GNSS in urban scenarios, where a three-satellite constellation is considered, which is reflected by three clock offsets in the features. References [216], [217], and [218] consider the regression problem from [12] with the tropospheric and ionospheric corrections as additional features in the model above and also use S- and MMestimators. Reference [40] also integrate ionospheric and tropospheric corrections and replace the WLS estimation by an estimation based on the Huber loss. Reference [361] additionally include multi-path delays and ionospheric and tropospheric corrections in the pseudorange model. Using real-world data from open-sky, semi-urban and dense-urban environments, they apply different robust loss functions, including the Huber, Tukey, Cauchy, Geman-McClure and Welsch loss.

Reference [114] propose to adapt the threshold of Tukey's biweight loss for GNSS position estimation. This is done in dependence of the detected fraction of multi-paths in the data when applying a CNN. The higher this fraction, the lower the threshold, which is chosen in order to maintain a given efficiency or BDP. Alternatively, they propose a robust Mestimator, which is computed via IRWLS.

Reference [358] aim at discarding pseudorange and Doppler measurements in GNSS. They point out that Doppler measurements are also affected by reflections from buildings or trees, although to a smaller extent than pseudorange measurements. Based on the NFA (number of false alarms) criterion, i.e.,

$$NFA(D) = \eta \frac{1}{\Gamma(|D|/2)} \int_0^{\delta_D^2/(2\sigma^2)} e^{-t} t^{|D|/2-1} dt,$$

for the set D of observations, a normalization constant  $\eta$ , the variance  $\sigma^2$  of the underlying assumed normal distribution of the measurement noise, and the sum of squares  $\delta_D^2$  of the standardized residuals, they propose an iterative algorithm in order to find a "clean subset" of the data that minimizes this criterion.

Reference [320] propose a cross-view localization based on both satellite and ground views. Given feature maps extracted by a CNN from the satellite and ground-view images, the residuals  $r_i$  between the components of these feature maps are computed. Then, the individual points are weighted according to weights that are proportional to the derivative of some robust loss function so that points with large residuals are downweighted.

Reference [237] consider robust range estimation and propose to use a tanh-type robust loss function of the form

$$\rho(Y_i, \hat{Y}_i) = \frac{1}{c} \tanh\left(\frac{c}{2} \frac{(Y_i - \hat{Y}_i)^2}{\sigma^2}\right),$$

where the  $Y_i$  are the measured ranges,  $\hat{Y}_i$  their predicted counterparts, and where  $\sigma > 0$  is a scale parameter. The parameter c is estimated by LMS,  $\sigma$  by the MAD. They also propose a robust Bayesian algorithm, which is initiated by the weights

$$w(Y_i, \hat{Y}_i) = \frac{1}{\sigma^2} \operatorname{sech}^2 \left( \frac{c(Y_i - \hat{Y}_i)^2}{2\sigma^2} \right),$$

computed from the M-estimation.

Reference [323] propose the GNSS measurement model

$$Y_{ij} = ||X_i - a_j|| + c(\delta_i^s - \delta_j) + I_{i,j} + T_{i,j} + b_{i,j} + \epsilon_{i,j}$$

for the pseudorange between vehicle i and satellite j, where  $a_j$  is the position of satellite j, where  $\delta_i^s$  and  $\delta_j$  are the clock offset of vehicle i and satellite j to the satellite system s, respectively, and where  $\epsilon_{i,j}$  is the measurement noise, which appears as a stochastic noise term for which some distribution needs to be assumed. Furthermore, c denotes the speed of light and  $I_{i,j}$  and  $T_{i,j}$  denote measurement errors that are induced by the ionosphere and the troposphere, respectively. Lastly,  $b_{i,j}$  are latent variables for modeling unknown measurement biases. As for vehicle to vehicle measurements, they use the model

$$Y_{ij} = h(X_i, X_j) + b_{ij} + \epsilon_{ij},$$

for latent variables  $b_{ij}$ , measurement noise  $\epsilon_{ij}$  and the states  $X_i$  and  $X_j$  of vehicle i and vehicle j, respectively. Assuming that the measurement noise is Gaussian, any contamination is modelled by the latent variables. To this end, Gaussian-Gamma prior distributions are assumed, and the joint distribution of the states and latent variables are approximated via variational inference. They apply their method on a real-world data set with three vehicles. Reference [40] consider the same GNSS model, but without latent variables. In a differential GNSS approach, the differences

$$\boldsymbol{\rho}^b = h(\boldsymbol{X}) - h(\boldsymbol{X}^b) + \boldsymbol{\epsilon}^b$$

are modelled, where  $X^b$  denotes the position of the base station. First-order linearization leads to

$$\boldsymbol{\rho}^b \approx h(\boldsymbol{X}_0) + H_r \boldsymbol{\delta} - h(\boldsymbol{X}^b) + \boldsymbol{\epsilon}^b,$$

for  $\delta = X_0 - X$  and geometry matrix  $H_r$ . The residuals are given by  $\mathbf{r}^b \approx H_r \delta + \epsilon^b$  and modelled by a Gaussian distribution. In the collaborative localization setting, the measurements of all individual vehicles are concatenated. Denoting the concatenated counterparts of the quantities



above by  $\tilde{r}$ ,  $\tilde{H}_r$  and  $\tilde{\delta}$ , the Gaussian assumption allows for a WLS formulation of the form

$$\hat{\tilde{\delta}} = \operatorname{argmin}_{\tilde{\boldsymbol{\delta}}} \left( (\tilde{r} - \tilde{H}_r \tilde{\boldsymbol{\delta}})^T \tilde{W} (\tilde{r} - \tilde{H}_r \tilde{\boldsymbol{\delta}}) \right),$$

where the weight matrix is the inverse joint covariance matrix.

Reference [107] propose a baro-radar odometry approach based on barometry and radar and use robust loss functions for the barometry and Doppler residuals. Radar data are also considered in [192] who propose to use a truncated least squares loss function.

# 1) VISUAL ODOMETRY/EGO-MOTION ESTIMATION

Many approaches intend to find a linear transformation that relates the 2D images collected from the camera and 2D reference images.

References [62] and [63] consider dense visual tracking under large illumination changes. Given a stereo camera pair, making n intensity measurements each, these observations are stored into two sets I and I'. Let  $\mathcal{I} = (I, I')^T$  be the current view pair, let  $\mathcal{I}^*$  be the reference view pair, and let  $\mathcal{P}^* = \{p, p'\}$  be a set of stereo image correspondences (the pixel locations) from a pair of reference templates from the set  $\mathcal{P}_n^* = \{\{p^*, (p')^*\}_1, \dots, \{p^*, (p')^*\}_n\}$ . Let f be the motion model, which is quadrifocal warping in [62], represented by a transformation  $T \in SE(3)$ . If  $\bar{T}$  is the true transformation, and if  $\hat{T}$  is the estimated transformation until time step (t-1), the tracking problem then amounts to estimating the incremental transformation  $T(\xi)$  at the current time step t, under the assumption that there exists  $\xi_0$  such that  $T(\xi_0)\hat{T} = \bar{T}$ . Then, the standard criterion based on the least-squares cost is

$$\sum_{\mathcal{P}^* \in \mathcal{P}_n^*} (I(f(\mathcal{P}^*, T(\boldsymbol{\xi})\hat{T}) - \mathcal{I}^*(\mathcal{P}^*)))^2,$$

where the quadratic loss is replaced by the Huber loss in [62] and [63]. Experiments on real-world data show that their approach allows for real-time performance. They also make suggestions for further computational improvement.

Reference [219] propose a hybrid approach between model-based optimization, where the error between the current model and the transformed current image is minimized, and VO, which minimizes the distance between the previous and current transformed image. More precisely, for model-based tracking, they assume the relation

$$i^*(\mathcal{P}^*) = \alpha i_t(f(\mathcal{P}^*, \bar{T}) - \gamma$$

between the reference image intensities,  $i^*$ , and the current image intensities  $i_t$  at time t, leading to the Huberized objective

$$\sum\nolimits_{\mathcal{P}^* \in \mathcal{P}^*_n} \rho_H(\alpha i_t(f(\mathcal{P}^*, T(\boldsymbol{\xi})\hat{T}) - \gamma - i^*(\mathcal{P}^*))).$$

In the VO approach, they consider augmented reference images that include the warped image  $i_{t-1}^f$  from the previous time step, where

$$i_{t-1}^f(\mathcal{P}^*) = i_{t-1}(f(\mathcal{P}^*, T_{t-1})),$$

leading to a similar objective as above but where  $i^*(\mathcal{P}^*)$  is replaced by  $i_{t-1}^f(\mathcal{P}^*)$ . As the model-based approach suffers from illumination changes (apart from the fact that it requires an à priori model, which may be very difficult to obtain, as pointed out in [63]), and the VO approach is prone to drift due to the accumulation of errors during feature extraction and matching [63], [219] combine both approaches, the robust loss functions corresponding to both approaches are stacked so that a joint optimization is performed. Reference [219] achieve near real-time performance on real-world data with a stereo camera pair.

Reference [229] propose a Huberized approach in model-based visual tracking by downweighting the contribution of all pixels whose photometric error is higher than some iteratively decreasing threshold. The standard average photometric error is given by

$$C_r(\boldsymbol{p}, \boldsymbol{d}) = \frac{1}{|\mathcal{J}^*|} \sum_{I \in \mathcal{J}^*} ||\boldsymbol{r}_{\mathrm{ph}}(I, \boldsymbol{p}, \boldsymbol{d})||_1,$$
 1110
$$\boldsymbol{r}_{\mathrm{ph}}(I, \boldsymbol{p}, \boldsymbol{d}) = \boldsymbol{I}^*(\boldsymbol{p}) - \boldsymbol{I}(\pi(KT\pi^{-1}(\boldsymbol{p}, \boldsymbol{d})))$$
 1111

for inverse depth d, a set  $\mathcal{J}^*$  of indices of reference images from the set  $\mathcal{I}^*$ ,  $I^* \in \mathcal{I}^*$ , pixel  $p = (x, y)^T$ ,  $T \in SE(3)$ , a camera-intrinsic transformation matrix K, and backprojection  $\pi^{-1}(p, d)$  of the inverse depth value to a 3D point. The robustification now invokes the Huber norm

$$||\mathbf{r}||_{\epsilon} = \begin{cases} \frac{||\mathbf{r}||_{2}^{2}}{2\epsilon}, & ||\mathbf{r}||_{2} \le \epsilon \\ ||\mathbf{r}||_{1} - \frac{\epsilon}{2}, & ||\mathbf{r}||_{2} \ge \epsilon \end{cases},$$

which enters the energy functional

$$E_{\aleph} = \int w(\boldsymbol{u})||\boldsymbol{\nabla}\aleph(\boldsymbol{u})||_{\epsilon} + \lambda C(\boldsymbol{u}, \aleph(\boldsymbol{u}))d\boldsymbol{u}$$

for the map  $\aleph$  that assigns a depth value to a pixel, and a pixel weight function w. Similar approaches based on robust loss functions can be found in [238], where the Huber function is directly applied to the  $r_{\rm ph}$ , and [110], [172], who consider the IRWLS formulation of the minimization problem w.r.t. the photometric error, where they use robust weight functions such as the Huber of Tukey weight function. Experiments on real-world datasets confirm real-time capability. References [169] and [171] consider the photometric residuals  $r_{\rm ph}$  and formulate the MAP estimation problem

$$\operatorname{argmax}_{\xi}(P(T(\xi)|(r_{\operatorname{ph}}(I,u,d))_{I\in\mathcal{J}^*})),$$

searching for the transformation  $T(\xi)$  that maximizes the posterior probability of the residuals. Here, they allow for heavy-tailed distributions such a t-distribution. Reference [171] apply their approach on data from an autonomous flight experiment and achieve real-time performance.

Reference [343] propose to minimize the geometric projection error instead of the photometric error due to a higher resistance against illumination changes. The idea is to find a distance transform map  $D_c$  that computes the Euclidean



distance to the closest edge for each pixel. For an edge pixel  $e_i$  from the current frame  $I_t$ , it should therefore hold that  $D_c(e_i) = 0$ . Let the reprojection residual for an edge pixel  $e_i^*$  from a reference image  $I^*$  be

$$r(\boldsymbol{e}_i^*) = D_c(\hat{\boldsymbol{e}}_i)$$

for the reprojection position  $\hat{e}_i$  computed by the underlying rotation and translation model. The objective is

$$\sum\nolimits_{\boldsymbol{e}_{i}^{*} \in \mathcal{E}^{*}} ||\boldsymbol{r}(\boldsymbol{e}_{i}^{*})||_{\epsilon}$$

for the Huber norm  $||\cdot||_{\epsilon}$  and the set  $\mathcal{E}^*$  of all edges in  $I^*$ . Real-time performance has been shown on real-world datasets.

Reference [17] consider dense VO [169], which does not only use matched features as sparse VO does, i.e., dense VO uses all pixels, resulting usually in a higher precision but at higher computational costs. They point out that using a *t*-distribution for both geometric and photometric errors ignores the physical process, resulting in photometric errors not being well-represented by such a noise model. Therefore, they propose to use a *t*-distribution for photometric errors but a probabilistic sensor noise model for geometric errors (which in turn is not suitable for photometric errors), and estimate the transformation between the 3D camera coordinates and 2D image points.

Reference [381] argue that photo bundle adjustment (PBA), which estimates scene geometry and camera motion in VO, is usually done by minimizing the photometric error. Motivated by works such as [169], they point out that PBA must be robustified against outliers that may arise due to widely separated active key frames so that the photo-consistency assumption may be violated by occlusions and reflections. In [381], their PBA error function for the total photometric error has the form

$$\sum \sum \sum w(r_i)r_i^2(\xi)$$

for the parameters  $\xi$ , the squared residuals  $r_i^2$  and weights  $w(r_i)$ , where the quadruple sum goes over all pixels in all points corresponding to the active keyframes. The problem is that the usually used Levenberg-Marquardt algorithm in order to optimize this objective picks keyframes according to photometric consistency, so that frames with occlusions or reflections are prone to be ignored here. Although [381] consider sparse VO, they conclude that a t-distribution is also suitable for the photometric errors as in dense VO considered in [17]. They first derive that the approach based on the t-distribution is also suitable here, and also make experiments with the Huber weights

$$w(r_i) = \begin{cases} \sigma^{-2}, & |r_i| < k \\ k\sigma^{-2}|r_i|^{-1}, & |r_i| \ge k \end{cases},$$

where  $\sigma^2$  is the variance of the ideal Gaussian distribution of the photometric errors. Experiments reveal that the *t*-distribution leads to even better performance because the

weights drop even faster at the tails. In their experiments, they also flag points as outliers if the number of outlying pixels (flagged as such if the photometric error exceeds the 95%—quantile of the error in the respective keyframe) exceeds some threshold and delete them from the set of observations. The Huber loss is also used in [94] and [221]. Experiments on KITTI and other datasets confirm real-time performance.

Reference [155] consider the problem of camera ego-motion estimation and propose a robust ego-motion estimation procedure. They argue that the noise in real-time flow data is often non-Gaussian and that violations of the scene-rigidity assumption due to objects moving independently result in outliers. The underlying model is

$$u(\mathbf{p}_i) = \delta(\mathbf{p}_i)A(\mathbf{p}_i)v_t + B(\mathbf{p}_i)v_r$$

for the optical flow  $u(p_i)$  at image position  $p_i \in \mathbb{R}^2$ , the translational velocity  $v_t \in \mathbb{R}^3$ , the rotational velocity  $v_r \in \mathbb{R}^3$ , the inverse  $\delta$  of the scene depth and linear transformations A and B. Motivated by [363], who already proposed a robust ego-motion estimation procedure based on IRWLS, they write the problem as a regression problem as [363], i.e.,

$$\min_{\boldsymbol{\nu}_r,\boldsymbol{\nu}_t,\boldsymbol{\delta}}(||A\boldsymbol{\nu}_t\boldsymbol{\delta}+B\boldsymbol{\nu}_r-\boldsymbol{u}||^2),$$

with the linear transformations  $Av_t$  and B in matrix notation, but they allow for confidence weights for each individual flow vector. For a least-squares estimate  $\hat{v}_r$  of  $v_r$  and a re-formulation that allows to drop  $\delta$ , this leads to

$$\min_{\mathbf{v}_r}(||\mathbf{v}_r \circ A^{\perp}(t)^T (B\hat{\mathbf{v}}_r(\mathbf{v}_t) - \mathbf{u})||_2^2).$$

In an expected residual likelihood approach, they directly estimate these confidence weights, based on an assumed Laplacian distribution of the residuals.

Reference [251] first derive a model for a monocular visual-inertial system and aim at making robust state estimations, where the states consist of positions and depths. To this end, the residuals for the visual measurement are minimized, but they are robustified in advance by the function  $\rho(r) = I(r \ge 1) + (2\sqrt{r} - 1)I(r < 1)$ . On a real-world dataset, they achieve real-time performance. See [272] for a similar robustness approach. Reference [372] include 3D to 2D reprojection errors, which enter via the Huber norm.

The Huber loss is also used in [51] where the reprojection error of the estimated trajectory from a linear projection of feature points w.r.t. the estimated trajectory from tracking key points.

References [33] and [34] use robust loss functions for optical flow estimation. Let  $(X_t, y_t)$  be an image point at time t and let  $v_t \in \mathbb{R}^2$  be the vector containing the horizontal and vertical image velocity. For the image intensity I = I(x, y, t) of pixel (x, y) at time t, the objective suggested by [33] is

$$\sum_{s=(x,y)} \sum_{\mathcal{R}_s} \rho_1(\partial_x I v_1 + \partial_y I v_2 + \partial_t I, \sigma_1)$$

$$+ \lambda \sum_{i \in \mathcal{N}_s} [\rho_2(v^{(s)}_1 - v^{(i)}_2, \sigma_2) + \rho_2(v^{(s)}_2 - v^{(i)}_2, \sigma_2)],$$
<sub>1239</sub>



1242

1244

1245

1246

1247

1249

1251

1252

1253

1254

1255

1256

1257

1259

1261

1262

1263

1264

1265

1266

1268

1269

1270

1271

1273

1276

1278

1280

1281

1282

1283

1285

1287

where  $\mathcal{N}_s$  containts all neighboring pixels of pixel s, where  $\mathcal{R}_s$  is some local neighborhood of s, for  $\sigma_1, \sigma_2, \lambda > 0$ , and where  $\rho_1, \rho_2$  are loss functions. The objective has to be optimized w.r.t.  $v_1, v^{(s)}_1$  and  $v^{(s)}_2$ . The first summand encourages the data conservation constraint that the intensity structure of small regions should persist over time, while the second summand encourages the local optical flow of a pixel to be close to that of neighboring pixels. Alternatively, they consider a line-process approach where discontinuities between pixels are modelled separately by binary variables, which leads to a similar objective, and also consider a robust alternative where the truncated squared loss is taken as loss function.

### 2) LIDAR ODOMETRY/POINT CLOUD REGISTRATION

Reference [93] robustify ICP by using the Huber loss function, aiming to minimize the distance

$$\sum_{i} w_{i} \min_{j} (\rho_{H}(||\tilde{\boldsymbol{p}}_{j}^{*} - T(\boldsymbol{\xi})(\tilde{\boldsymbol{p}}_{i})||),$$

where the  $w_i$  are just indicator variables that take the value one if and only if there is a match between reference and data points.

Welsch's loss function has been applied as a robust error metric for ICP in point cloud registration in [73] in order to quantify the distance between a set of intersection points on the source surface and the target surface, respectively, i.e.,

$$D(x, y) = \rho_W(||x - y||_2^2).$$

Reference [31] consider the objective

$$\min_{\boldsymbol{R}, \boldsymbol{\vec{t}}} \left( \sum\nolimits_{i} \rho(||\boldsymbol{R} \tilde{\boldsymbol{p}}_{i} + \boldsymbol{\vec{t}} - \tilde{\boldsymbol{P}}^{*}||) \right)$$

for a rotation matrix  $R \in \mathbb{R}^{3\times 3}$  and a translation vector  $\vec{t} \in \mathbb{R}^3$  for point cloud registration and use IRWLS with the Huber, the Tukey or the Cauchy loss function as robust loss functions  $\rho$ .

The Huber loss is applied in [333] for motion-prediction from point clouds, where it is used as motion-prediction loss, spatial and temporal consistency loss.

Reference [125] propose a LiDAR-based direct odometry method with the goal to efficiently find the matching points for the point clouds extracted from the LiDAR data. Direct odometry methods usually compare 2D images, therefore, they first project the 3D LiDAR point to a 2D sphere. As a re-projection of the entire projected 2D image would be time-consuming, this re-projection is only done on selected key points. Let  $p^* \in \mathbb{R}^2$  be the 2D image coordinates of the reference data and let f be a parametric conversion function between sensor and reference data so that  $f = f(T(\xi), F)$  for a parameter  $\xi$  that encodes rotation and translation, a frame F, and a translation  $T(\xi)$  from the Lie group SE(3). Let the residuals from the 2D image coordinate map be  $r(F_s, F^*, T(\xi))$  for a sensor frame  $F_s$  and a reference frame  $F^*$ . Then, let a new frame  $F_0$  be given with the goal to adjust

the corresponding  $T_0(\xi_0)$ , which is done by minimizing

$$\sum_{j} \sum_{F} \rho_{H}(r(F_{s}, F^{*}, T_{0}(\xi_{0})T_{j}^{-1}))$$
1290

1289

1291

1292

1294

1296

1297

1299

1302

1303

1304

1305

1307

1309

1310

1311

1312

1313

1315

1317

1318

1320

1322

1323

1324

1326

1328

1329

1330

1331

1332

1333

1334

1336

at the key points, where the  $T_j$ ,  $j=1,\ldots,n$ , are frame-specific transformations. Afterwards, the  $T_j$  are updated similarly, but where Tukey's biweight loss is used. Experiments on KITTI data and real-world data with an autonomous vehicle confirm real-time performance.

Reference [144] use the Huber loss function when computing functional map matrices that parameterize pairwise correspondences of point clouds in order to better deal with occlusions or deformations. The objectives

$$\sum_{i=1}^{I_{kl}} \rho_H(||\Phi_{l,i}^{(kl)} - \Phi_{k,i}^{(kl)}C||)$$
1300

have to be minimized w.r.t. the map C for all (k, l), which represent the edges in the point cloud graph, and where  $\Phi_k^{(kl)}$  are the matrices that represent the matched points from point cloud  $\mathcal{P}_k$  to point cloud  $\mathcal{P}_l$ , for the number  $I_{kl}$  of matches.

The squared loss in the ICP algorithm has been replaced with the LMS criterion in [214] and [375], and with the LTS criterion for example in [59] and [243]. Reference [245] proposed the so-called fractional root mean squared distance as distance measure for ICP, which is essentially an LTS criterion, up to taking the square root. Reference [145] consider a truncated absolute loss. Reference [115] propose a differentiable variant of the Huber loss. Reference [68] use the family of parametrized robust loss functions from [23] and propose an algorithm where one alternatingly optimizes for the parameters of this loss function and the actual regression parameter. Reference [346] propose a graduated non-convexity approach where a non-convex robust loss is optimized by iteratively optimizing a sequence of surrogates, which are initially convex but gradually become non-convex. This method is applied to point cloud registration with the Geman-McClure and the truncated least squares criterion.

Reference [193] consider matching a data and a reference point cloud, resulting in the objective

$$\mathrm{argmin}_{R \in \mathrm{SE}(3), \vec{\boldsymbol{t}} \in \mathbb{R}^3} \left( \sum\nolimits_i \sum\nolimits_j \rho(r(\tilde{\boldsymbol{p}}_j^* - R\tilde{\boldsymbol{p}}_i - \vec{\boldsymbol{t}})) \right)$$

for a robust loss function  $\rho$ . Experiments on different data sets confirm a total computational time of less than one second, confirming real-time performance.

A similar approach has been used in [335] for point-toplane matching, where the distance between a point from the point cloud and the nearest point from a local plane on the map is considered. They use the Huber loss function. In [376], the truncated least squares loss is used in order to find a transformation that aligns points from a LiDAR frame with points from a local map for ego-motion estimation. Experiments on KITTI data and real-world data collected from a robot confirm real-time performance of their overall LiDAR-only odometry and mapping pipeline.

Reference [143] propose a loss function that can be interpreted as a soft counterpart of a truncated least squares



loss, namely  $\rho(\mathbf{r}, k, w) = w^2 ||\mathbf{r}||^2 + (1 - w)^2 k^2$ . In other words, each residual is accompanied with a weight which decides the trade-off between the squared loss and a constant loss. This loss function is not used directly as objective for the estimation of the optimal transformation  $T \in SE(3)$  but as a penalty term, i.e., the objective is

$$\sum_{i} ||(\mathbf{r})^{(i)})^*||^2 + \sum_{i} \rho(w_i, ||\mathbf{r}^{(i)}||^2),$$

where  $(\mathbf{r}^{(i)})^*$  denotes the residuals w.r.t. a reference point cloud and where  $\mathbf{r}^{(j)}$  denotes residuals from the LiDAR point cloud. The objective is optimized w.r.t. the weights and the transformation alternatingly. The optimization w.r.t. the weights leads to the closed-form solution  $w_j^* = k^2(||\mathbf{r}^{(j)}||^2 + k^2)^{-1}$ , implying the loss  $\rho(||\mathbf{r}^{(j)}||^2, k, w_j) = k^2||\mathbf{r}^{(j)}||^2(k^2 + ||\mathbf{r}^{(j)}||^2)$ . This is just a scaled Geman-McClure loss. They achieve real-time performance on different real datasets. A similar objective function has been proposed in [373]. On real-world data from urban areas in Hong Kong, they achieve real-time performance.

Reference [330] use the Huber kernel loss as loss function in laser localization. The objective is then

$$\sum_{i} w_{i} \rho_{H}(r(T(\boldsymbol{\xi})(\tilde{\boldsymbol{p}}_{i}), \tilde{\boldsymbol{P}}^{*})),$$

where  $w_i$  an indicator which is zero if  $\tilde{p}_i$  is considered to be an outlier, which is done by comparing the median of the error of the posterior predictive corresponding to this point with the population median of the error.

### 3) NAVIGATION/TRACKING VIA FILTERING

An important class of state estimation techniques are **Kalman filters** (KF). The linear KF assumes a state space model of the form (e.g., [269])

$$X_t = F_t X_{t-1} + v_t, \quad Y_t = Z_t X_t + \epsilon_t,$$

with transition matrices  $F_t \in \mathbb{R}^{p \times p}$ ,  $Z_t \in \mathbb{R}^{q \times p}$ , and noise variables  $\epsilon_t \sim \mathcal{N}_q(\mathbf{0}_q, V_t)$ ,  $\mathbf{v}_t \sim \mathcal{N}_p(\mathbf{0}_p, Q_t)$ . The first equation is the state equation, describing the evolution of the states of the system, while the second equation is the measurement equation that describes the generation of noisy measurement outputs from the underlying true states. In control theory, one would also include a controller input in the state equation (see Sec. V-C). The state space model described here is time-discrete and time-variant. In the less general time-invariant settings, one has static transition matrices F and Z. The goal in Kalman filtering is to estimate the true states  $X_t$  when measuring the  $Y_t$ . There are several ways how to robustify the KF, for example, by robustifying the loss function is the least-squares interpretation of the KF, by assuming a different noise distribution that is capable to model large errors which would appear as outliers under the Gaussian assumption, or outlier detection. In this paper, since we are not aware of any robust approach for autonomous driving in a continuous-time setting, we always have a discrete-time setting.

Reference [269] distinguish between **additive outliers** (**AOs**), which affect the observations, i.e.,

$$\boldsymbol{\epsilon}_t^{\text{re}} \sim (1 - r_{AO}) \mathcal{L}(\boldsymbol{\epsilon}_t^{\text{id}}) + r_{AO} \mathcal{L}(\boldsymbol{\epsilon}_t^{ru}),$$

and **innovation outliers (IO)**, which affect the innovations, i.e.,

$$\mathbf{v}_t^{\text{re}} \sim (1 - r_{IO})\mathcal{L}(\mathbf{v}_t^{\text{id}}) + r_{IO}\mathcal{L}(\mathbf{v}_t^{ru}),$$

where  $\mathcal{L}(\boldsymbol{\epsilon}_t^{\mathrm{id}})$ ,  $\mathcal{L}(\boldsymbol{\epsilon}_t^{ru})$ ,  $\mathcal{L}(\boldsymbol{\nu}_t^{\mathrm{id}})$ ,  $\mathcal{L}(\boldsymbol{\nu}_t^{ru})$  denote the distributions of the ideal and contaminated noise terms, respectively, and where  $r_{AO}$ ,  $r_{IO} \in [0,1]$  are the respective contamination radii. The main difference is that IOs affect subsequent states, covering level shifts or linear trends, so that not only the current observation is affected. One can also define **substitutive outliers (SO)**, which directly manipulate the observation distribution and not the noise distribution, i.e.,

$$Y_t^{\text{re}} \sim (1 - r_{SO})\mathcal{L}(Y_t^{\text{id}}) + r_{SO}\mathcal{L}(Y_t^{ru}).$$

The Kalman filtering algorithm, going back to [164], is given by the following recursive scheme (here, in the notation of [269]): Initialization

$$X_{0|0} = a_0, \quad \Sigma_{0|0} = Q_0, \tag{4}$$

prediction

$$X_{t|t-1} = F_t X_{t-1|t-1}, \quad \Sigma_{t|t-1} = F_t \Sigma_{t-1|t-1} F_t^T + Q_t,$$
 (5)

and correction

$$X_{t|t} = X_{t|t-1} + K_t \Delta Y_t, \quad \Sigma_{t|t} = (I_p - K_t Z_t) \Sigma_{t|t-1}, \quad (6)$$

for

$$\Delta X_t = X_t - X_{t|t-1}, \quad \Delta Y_t = Y_t - Z_t X_{t|t-1} = Z_t \Delta X_t + \epsilon_t,$$
(7)

and

$$\Delta_t = Z_t \Sigma_{t|t-1} Z_t^T + V_t, \quad K_t = \Sigma_{t|t-1} Z_t^T \Delta_t^-.$$
 (8)

Here, the quantity  $K_t$  is referred to as the Kalman gain.

This recursive scheme can also be interpreted as a least-squares approach (e.g., [288]). In the notation of [65], denoting

$$\begin{pmatrix} Y_t \\ X_{t|t-1} \end{pmatrix} = \begin{pmatrix} Z_t \\ I \end{pmatrix} X_t + \begin{pmatrix} \epsilon_t \\ r_t \end{pmatrix}$$

for

$$\mathbf{r}_t = X_{t|t-1} - X_t,$$
 1425

one can compactly write

$$\tilde{Y}_t = \tilde{Z}_t X_t + \tilde{r}_t,$$

where  $\tilde{r}_t$  has a block diagonal covariance matrix  $\tilde{R}_t$ . The estimation of the states via a squared loss leads to a least-squares solution with prediction

$$\hat{X}_{t|t} = (\tilde{Z}_t^T \tilde{R}_t^{-1} \tilde{Z}_t)^{-1} \tilde{Z}_t^T \tilde{R}_t^{-1} \tilde{Y}_t.$$
 (9)



In non-linear dynamics, suitable versions of the linear KF have been proposed in the literature, where the state-space model is given by

$$X_t = f(X_{t-1}) + \mathbf{v}_t, \quad Y_t = h(X_t) + \epsilon_t,$$

for differentiable functions f and h. In the recursive KF scheme however, the linear maps  $F_t$  and  $Z_t$  are required. For the EKF, a first-order linearization of f is done at  $X_{t-1|t-1}$ , while a linearization of h is done at  $X_{t|t-1}$ .

The **unscented Kalman filter** (UKF) also allows for non-linear transformations but does not perform a linear approximation as the EKF. Instead, a so-called unscented transformation [162], [312] in order to approximate the posterior mean and variance of the underlying function is computed.

The **cubature Kalman filter** (CKF) uses the radial-spherical cubature rule [14] instead of the unscented transformation as in the UKF in order to estimate the posterior mean and variance.

The following approaches consider robust loss functions.

Reference [49] propose to replace the squared loss of the linear KF by the maximum correntropy (MMC) criterion, which is a local similarity measure and therefore insensitive to large outliers. The MMC criterion is given by

$$\int \kappa(x,y)dF(x,y)$$

for a shift-invariant Mercer kernel  $\kappa$ , e.g., the Gaussian kernel  $\kappa(x,y)=G_{\sigma}(r)=\exp(-r^2/(2\sigma^2))$ . Given residuals  $r_t$ , one can therefore estimate the correntropy by the arithmetic mean of the  $G_{\sigma}(r_t)$ . In the KF context, they define the errors

$$\tilde{\epsilon}_t = \begin{pmatrix} -(X_t - \hat{X}_{t|t-1}) \\ \epsilon_t \end{pmatrix}$$

and denote  $\mathbb{E}[\tilde{\epsilon}_t \tilde{\epsilon}_t^T] = B_t B_t^T$  with a matrix  $B_t$  that can be computed by a Cholesky decomposition of  $\mathbb{E}[\tilde{\epsilon}_t \tilde{\epsilon}_t^T]$ . It follows that  $D_t = W_t X_t + r_t$  for

$$\boldsymbol{D}_{t} = B_{t}^{-1} \left( \hat{\boldsymbol{X}}_{t|t-1} \, \boldsymbol{Y}_{t} \right), \quad W_{t} = B_{t}^{-1} \begin{pmatrix} I \\ H_{t} \end{pmatrix}, \quad \boldsymbol{r}_{t} = B_{t}^{-1} \tilde{\boldsymbol{\epsilon}}_{t},$$

$$\tag{10}$$

where  $\mathbf{r}_t$  is white noise. Now, the correntropy objective leads to

$$\hat{X}_{t|t-1} = \operatorname{argmax}_{\boldsymbol{x}} \left( \frac{1}{p+q} \sum_{i=1}^{p+q} G_{\sigma}((\boldsymbol{D}_t)_i - (W_t)_i \boldsymbol{x}) \right).$$

They derive an iterative fixed-point algorithm in order to find the optimal solution and prove a sufficient condition for convergence.

A CKF based on the MMC criterion has been applied for cooperative localization of underwater vehicles. Reference [378] apply an MCC-based cubature information filter for tracking aerial autonomous vehicles. In their numerical simulations with a step size of 1 s, their filter requires a computation time of around 0.2 s. Reference [293] propose to combine a UKF with the MCC criterion based

on the *t*-kernel with an additional weighting scheme in order to safeguard the estimation against extreme outliers. As weight function, applied to the individual components of the states, they consider the biweight, Huber, Hampel and Andrews function. On real-world data collected from an autonomous underwater vehicle, their algorithm achieves real-time performance. Reference [195] use a KF with the MCC criterion for pseudorange estimation. They consider localizing and tracking in real-world experiments and achieve similar computational efficiency than the standard KF.

Reference [185] consider collaborative localization and propose an EKF updating scheme with the MCC. Here, as for the required Mercer kernel, they consider a Cauchy kernel. Reference [88] consider a Laplacian kernel and apply the resulting MCC-based EKF for cooperative localization of autonomous underwater vehicles. In their simulations, the computation time was around twice as much as for the standard EKF.

An alternative loss function for robust state estimation with the KF has been proposed by [72] who consider the residual least entropy-like loss function

$$H_{k}(D_{k}, q_{1}, ..., q_{k})$$

$$= I(D_{k} \neq 0) \cdot \frac{-1}{\ln(k)} \sum_{i=1}^{k} q_{i} \ln(q_{i}),$$

$$D_{k} = \sum_{i=1}^{k} ||\mathbf{r}_{i}||^{2},$$

$$q_{i} = \frac{||\mathbf{r}_{i}||^{2}}{\sum_{i=1}^{k} ||\mathbf{r}_{j}||^{2}},$$
1502

for the residuals  $r_i$ . This loss function is used as a penalty term for the weighted least-squares objective which encourages a large entropy of the residuals and hence many small and few large residuals.

Reference [65] consider GNSS/INS integration and propose a robust KF by robustifying the update step with an M-estimator. They point out that robust methods require a larger number of measurements than classical ones (which is a consequence of the efficiency loss, since the least-squares estimator is the maximum likelihood estimator under Gaussian noise and hence achieves maximum efficiency) but that GNSS applications usually do not have many satellites in view. They consider the standardized version  $W_t$  of  $\tilde{R}_t^{-1}$  from Eq. 9 by standardizing the measurements first. Then,  $W_t$  is updated using IRWLS, which is robustified by the Huber estimation

$$(W_t)_{ii} = w_H([\bar{\boldsymbol{Y}}_t - \bar{\boldsymbol{Z}}_t \hat{\boldsymbol{X}}_{t|t}]_{ii})$$

for the respective standardized measurements  $\bar{Y}_t$  and  $\bar{Z}_t$ . In their experiments, they consider different types of contamination, which are single biases, multiple biases, and ramps.

Reference [97] consider, in addition to innovation and observation outliers, so-called **structural outliers**, i.e., where the linear mapping  $Z_t$  resp.  $F_t$  in the state space model may be misspecified. They assume that the observations



are synchronized, otherwise, delayed observations may be treated as outlying data. First, they aim at robustly estimating the covariance matrix in the least-squares interpretation of the KF. To this end, they consider the Stahel-Donoho estimator

$$\sup_{||\boldsymbol{u}||=1} \left( \frac{|\boldsymbol{h}_t^T \boldsymbol{u} - \text{med}_j(\boldsymbol{h}_j^T \boldsymbol{u})|}{\text{MAD}_j(\boldsymbol{h}_j^T \boldsymbol{u})} \right)$$

for the data points h, which are here the matrices  $(Z_t^T, I)^T$ . However, they argue that applying the estimator in each time step would detect only structural outliers and therefore propose to use the vector  $\tilde{Y}_t = (Y_t^T, \hat{X}_{t|t-1}^T)^T$  instead of the  $h_t$  as it already captures the effects of all three types of outliers. Points whose value s of the Stahel-Donoho estimator is larger than some threshold  $\tau$  are downweighted in the sense that their new weight is  $\tau^2/s^2$ , where  $\tau=1.5$  in [97]. As structural outliers appear as leverage points in the least-squares interpretation of the KF, a GM-estimator with the Huber loss function and the weights arising from the Stahel-Donoho estimator is applied, i.e., one minimizes

$$\sum_{i} w_i \rho_H(\tilde{r}_i),$$

with the residuals  $\tilde{r}_i = r_i s^{-1} w_i^{-1}$  with the MAD s of the vector of residuals  $r_i$ . Due to non-linearity, this problem is solved using IRWLS. Finally, the update filter error has to be adapted. They therefore compute the IC of the GM-estimator, given by

$$IC(x, X, P) = \frac{\psi(\tilde{x})}{\mathbb{E}_P[\psi'(x)]} (A^T A)^{-1} X w$$

for  $\tilde{x} = xs^{-1}w^{-1}$ , which enables to compute the asymptotic covariance matrix  $\Sigma_{t|t} = \mathbb{E}_P[\mathrm{IC}(x, X, P)(\mathrm{IC}(x, X, P))^T]$ .

Reference [364] propose distributionally robust filtering, where a minimax problem is solved. Let  $\mathbf{Z}_t = (X_t, Y_t)$  and let  $F_{\mathbf{Z}_t | Y_{t-1}}$  denote the conditional joint state-measurement distribution at time step t. The new state is estimated by

$$\hat{X}_{t+1} = \min_{s} (\max_{F \in \mathcal{U}(F_{Z_t|Y_{t-1}})} (\mathbb{E}[(X_t - s)(X_t - s)^T])),$$

for an uncertainty set  $\mathcal{U}(F_{\mathbf{Z}_t|Y_{t-1}})$  around  $F_{\mathbf{Z}_t|Y_{t-1}}$ . In their algorithm, they construct this set by mean and covariance constraints around a nominal distribution. The problem can be re-written as a nonlinear semi-definite program. In their experiments, they consider tracking a hypersonic vehicle.

Reference [284] replace the least-squares regression problem arising in the KF by a minimax problem. In particular, they propose to minimize the worst-case expected squared residuals over an uncertainty set. As for this uncertainty set, they either use all normal distributions with the same mean as the ideal distribution but whose covariance lies within a certain radius around the ideal covariance, or a Wasserstein-based contamination ball containing all normal distributions whose  $W_2$ -distance from the ideal distribution is bounded by the contamination radius. On real-world data, the performance of their algorithm is comparable to that of the standard EKF, thus allowing for real-time performance.

Reference [74] consider aircraft ground inspection, which is vulnerable to large GNSS positioning errors. They consider a robust EKF based on M-estimation. They essentially robustify the KF in the same manner as [49], but where the  $r_t$  from Eq. 10 do not enter the correntropy criterion but a weighted least squares objective, i.e.,

$$\min_{\mathbf{r}}(\mathbf{r}_t^T(\mathbf{x})W\mathbf{r}_t(\mathbf{x})),$$

for the weight matrix  $W = \text{diag}(w_H(\mathbf{r}_{t,i}))$  with the Huber weight function  $w_H$ . Reference [75] propose a grid search in order to select the hyperparameter K of the Huber function in a data-driven way, according to the horizontal accuracy. More precisely, the hyperparameter is chosen according to a difficulty level of the scenario, and this level is predicted using a neural network. In order to make the predictions more interpretable, [76] replace the neural network by a SVM.

Reference [28] propose a robustification of the EKF by downweighting measurement outliers. They use the formulation

$$\hat{X}_{t} = \operatorname{argmin}_{X_{t}}(||X_{t} - f(\hat{X}_{t-1})||_{\hat{V}_{t}}^{2} + ||Y_{t} - h(X_{t})||_{\tilde{O}_{t}}^{2})$$

for  $\tilde{Q}_t = \hat{Q}_t^{1/2} W^{-1} \hat{Q}_t^{T/2}$ . Here,  $Q_t^{1/2}$  is the Cholesky factorization of  $Q_t$ . The weight matrix W is given by  $W = \mathrm{diag}(w(Q_t^{1/2}(Y_t - h(X_t))))$  for a weight function w corresponding to a robust loss function. In their experiments, they use the Huber weight function. Reference [270] integrate feature maps into the EKF for GNSS positioning. Those feature maps contain information about, for example, satellite visibility or spatio-temporal features, allowing for a prior distribution of the pseudorange residuals. In the EKF, observations whose pseudorange residual deviates considerably from the expected ones are downweighted. This is done by applying the weight function corresponding to a robust loss function, for which the Huber, Tukey and Geman-McClure loss function are considered, to the predicted pseudorange residuals.

Reference [119] apply parallel robust EKFs for a Bayesian approach for robust localization from GNSS data. Instead of the Gaussian likelihood, they consider densities of the form  $p(Y_t|X_t) \propto \exp(-\rho(r_t))$  for the residual  $r_t = Y_t - h(X_t)$  and where  $\rho$  is the Huber or the Tukey loss function. The covariance matrix  $V_t$  of the measurement equation is updated via  $\tilde{R}_t = (\psi(r_t))^{-1}R_t$  for  $\psi(r_t) = \partial_r \rho(r)|_{r=r_t}$ . However, due to multi-modal uncertainties in the measurements, single Gaussian distributions are not suitable. To this end, they replace the standard posterior,

$$p(X_t|Y_{1:t}) \propto p(Y_t|X_t) \int p(X_t|X_{t-1})p(X_{t-1}|Y_{1:t-1})dX_{t-1},$$

with

$$p(X_t|X_t^l, Y_{1:t}) \propto p(Y_t|X_t^l, X_t)$$

$$\int p(X_t|X_t^l, X_{t-1})p(X_{t-1}|X_t^l, Y_{1:t-1})dX_{t-1},$$
1623



for linearization points  $X_t^l$  at which the EKF transition and the robust loss  $\rho$  are linearized. As the selection of linearization points is accompanied by uncertainties itself, [119] propose the update rule

$$p(X_t^l, Y_{1:t}) \propto p(Y_t|X_t^l) \int p(X_t^l|X_{t-1}^l) p(X_{t-1}^l|Y_{1:t-1}) dX_{t-1}^l.$$

In their algorithm, one starts with an initial set of linearization points and iteratively updates this whole set and corresponding weights that are computed via the posterior  $p(Y_t|X_t^l)$ , so that the distribution  $p(X_t|Y_{1:t})$  can finally be estimated using Rao-Blackwellization.

The UKF has been robustified by Huberization in [337]. Given the non-linear dynamics

$$X_{t+1} = f(X_t) + \mathbf{v}_t, \quad Y_t = h(X_t) + \epsilon_t,$$

one can write

$$\begin{pmatrix} Y_{t+1} \\ X_{t+1|t} \end{pmatrix} = \begin{pmatrix} h(X_{t+1}) \\ X_{t+1} \end{pmatrix} + \begin{pmatrix} \epsilon_t \\ \Delta \hat{X}_{t+1|t} \end{pmatrix}$$

for the predicted state  $\hat{X}_{t+1|t}$  at time (t+1) and its error  $\Delta \hat{X}_{t+1|t}$ . For the covariance  $V_t$  of  $\epsilon_t$  and the covariance  $\Sigma_{t+1|t}$  of  $\hat{X}_{t+1|t}$ , one computes

$$\tilde{Y}_{t+1} = S_{t+1}^{-1/2} \begin{pmatrix} Y_{t+1} \\ \hat{X}_{t+1|t} \end{pmatrix}, \quad S_{t+1} = \begin{pmatrix} V_t & 0 \\ 0 & \Sigma_{t+1|t} \end{pmatrix},$$

$$g(X_{t+1}) = S_{t+1}^{-1/2} \begin{pmatrix} h(X_{t+1}) \\ X_{t+1} \end{pmatrix}, \quad \xi_{t+1} = S_{t+1}^{-1/2} \begin{pmatrix} \epsilon_t \\ \Delta \hat{X}_{t+1|t} \end{pmatrix},$$

so that  $\tilde{Y}_{t+1} = g(X_{t+1}) + \xi_{t+1}$  holds. The objective for finding the prediction  $\hat{X}_{t+1|t}$  is then

$$\min_{\mathbf{x}} \left( \sum_{i=1}^{p+q} \rho_H(r_{t+1,i}(\mathbf{x})) \right),\,$$

where the residuals are given by  $r_{t+1}(X_{t+1}) = \tilde{Y}_{t+1} - g(X_{t+1})$ . Reference [337] use this Huberized UKF for underwater terrain matching, where  $X_t$  represents the 2D coordinates of the vehicle. Reference [46] apply it to tracking.

Reference [322] propose an adaptive variant of the robust UKF with an application in vehicle tracking. They consider the dynamics model error and the measurement model error simultaneously by treating the respective residuals separately, i.e.,

$$\min_{\mathbf{x}} (\lambda_t || \mathbf{x} - \hat{\mathbf{X}}_{t|t-1} ||_{\Sigma_{t|t-1}}^2 + || F_t \mathbf{x} - Y_t ||_{V_t^{-1}}^2)$$

with a fading factor  $\lambda_t$  which is computed by

$$\lambda_t = \begin{cases} 1, & |\Delta \tilde{X}_t| \le \tau \\ \frac{\tau}{|\Delta \tilde{X}_t|}, & |\Delta \tilde{X}_t| > \tau \end{cases},$$
$$\Delta \tilde{X}_t = \frac{||\tilde{X}_t - \hat{X}_{t|t-1}||}{\sqrt{\operatorname{tr}(\Sigma_{t|t-1}^{-1})}},$$

for some threshold  $\tau > 0$ .

Reference [21] alternatingly use the Huber and the loss corresponding to the dynamically scaled covariance approach

from [3] in the EKF and consider the navigation of autonomous underwater vehicles. On real-world data, the computation time is close to that of the standard KF, with at most around 25% overhead. Reference [22] modify the EKF by alternatingly optimizing the MSE and the Huber loss in the sense that in a first iteration,  $\hat{X}_{t|t}$  is estimated using the updating steps corresponding to the Huber loss. Then,  $\hat{X}_{t|t}$  enters as prior  $\hat{X}_{t|t-1}$  in the updating steps corresponding to the MSE. The average runtime on real-world data is around 75% higher than for the standard KF.

See further applications of Huberized Kalman Filters for spacecraft attitude estimation (linear KF; [166]), elliptical orbit rendezvous and docking (EKF; [167]), navigation (UKF; [47], [250], CKF; [307]), vehicle tracking (CKF; [124], [197]), underwater tracking (EKF; [82]), and collaborative localization (EKF; [129]).

In contrast to loss-based filters where a robustification of the loss function is done, **noise modeling and covariance scaling** approaches consider heavy-tailed distributions, assuming that the measurements can be contaminated by heavy-tailed noise, in contrast to the standard KF that assumes Gaussian noise. This idea essentially goes back to [328]. It has been shown in [267] that in the ideal, i.e., Gaussian, model, the usage of a *t*-distribution with small degrees of freedom leads to a high efficiency loss. In particular, using variational approximation allows for learning the real noise distribution in an online manner, even allowing for non-stationary (e.g., due to changing environments as argued in [152]) loss distributions.

Reference [2] propose a structured variational approach where they assume an inverse Wishart distribution of the covariance matrix  $V_t$ . As they assume that  $Y_t|X_t,R_t \sim \mathcal{N}(FX_t,R_t)$ , marginalizing out  $R_t$  leads to a t-distribution as the conditional distribution of  $Y_t|X_t$ . They derive that the marginal log-likelihood of the  $Y_t$  can be expressed as the sum of a lower bound of the marginal likelihood of the data and the KL-divergence between the true and the approximate posterior distribution of  $(X_t,R_t)$  given  $Y_t$ . For iid. noise and for a slowly-drifting noise model, where the two parameters of the inverse Wishart distribution of  $R_t$  themselves obey a first-order model, they derive an algorithm in order to compute an approximate posterior. They apply their method for GPS position estimation of a car. Reference [1] assume

$$X_t | X_{t-1} \sim \mathcal{N}(F^T X_{t-1} + \boldsymbol{b}, Q),$$
 1706  
 $Y_t | X_t, V_t \sim \mathcal{N}(Z^T X_t + \boldsymbol{d}, V_t)$  1707

where the observation noise  $V_t^{-1}$  is assumed to follow a Wishart distribution, again leading to a *t*-distribution of  $Y_t|X_t$ . The posterior  $p(X_t|Y_1,..,Y_t)$  is approximated by structured variational filtering. They apply their method for position estimation from GPS data.

The approach from [1] has been extended to the nonlinear case in [246] and [273]. Reference [150] argue that these such variational Bayes approaches as in [273] can handle slowly time-varying measurement noise covariance matrices

1718

1719

1721

1722

1723

1724

1725

1726

1727

1728

1729

1731

1733

1734

1735

1736

1738

1739

1740

1741

1743

1744

1745

1746

1748

1750

1751

1753

1754

1755

1756

1758

1760

1761

1763

1765

1767

1768

1770



1773

1774

1776

1779

1781

1783

1784

1786

1789

1791

1793

1794

1796

1798

1799

1800

1801

1803

1805

1806

1807

1808

1810

1811

1812

1813

1814

1815

1817

1818

1820

1823

1824

1825

1827

 $V_t$ , but that they assume accurate estimation of the process noise covariance matrices  $Q_t$ , otherwise, their performance decreases. Therefore, they propose to assume inverse Wishart priors for both  $V_t$  and the prediction error covariance matrix  $P_t$ , which, by the prediction step  $X_{t|t-1} = F_{t-1}X_{t-1|t-1}$ , satisfies

$$P_{t|t-1} = F_{t-1}P_{t-1|t-1}F_{t-1}^T + Q_{t-1}.$$

The new states are then inferred jointly with  $P_{t|t-1}$  and  $V_t$  via variational approximation. Their method is applied to target tracking.

Reference [233] assume that the measurement noise is skewed t-distributed and approximate the posterior observation distribution with variational inference. They apply their filter for GNNS position estimation. In their experiments, they report that the computational time of their filter exceeds that of the standard KF by a factor of around 5 to 10. Reference [374] consider GNSS positioning and assume tdistributed measurement noise. They propose to estimate the degrees of freedom outside the variational Bayes iteration via inversely scaling a baseline degree of freedom with the Mahalanobis distance of the current innovation to a Gaussian distribution with the current innovation covariance matrix. The method is applied in a field test for position estimation of a vehicle in Beijing. Reference [55] assume t-distributed process noise, while the measurement noise is assumed to be Gaussian. They consider SINS navigation in a real-world car-mounted experiment. Reference [158] model the measurement noise by a convex contamination model, where the ideal Gaussian distribution is contaminated with a Gaussian distribution with a different covariance matrix. They allow the contamination radius to vary in time. As they consider a situation where the states are observed by multiple agents, they have an observation equation for each agent j with individual transition matrices  $Z_t^j$  and noises  $\epsilon_t^j$ . In a sliding window approach, the joint posterior of the states, the process covariance matrices, the agent-specific measurement covariance matrices and contamination radii is approximated via variational inference. They apply their method in a target tracking simulation with multiple sensors. Reference [170] argue that a robust filter is less efficient than a filter with the Gaussian assumption and propose to use two models, one with Gaussian and one with t-distributed measurement noise, and to combine them using Bayesian model averaging. They use their method for target tracking. In their simulations, they observe a computational time of their filter of around twice as high as for the standard CKF, while only requiring around 40% of the time of the CKF where iterative variational Bayes approximations are used. Reference [126] propose to use  $\alpha$ -stable sub-Gaussian distributions for the measurement noise in the linear KF, and compare noise modeling with low- and heavy-tailed noise distributions, such as Gaussian mixtures or t-distributions. Reference [336] assume a mixture of a Gaussian and a Gaussian inverse-Gamma distribution for the measurement noise and apply their algorithm to the navigation of an underwater vehicle. Reference [191] invoke

a Gaussian-exponential distribution for the measurement noise.

Reference [148] propose a Gaussian-inverse-Wishart mixture distribution for the state transition. They argue that such a mixture has the advantage over a single Gaussian-inverse-Wishart distribution when only inaccurate prior information is available. As for the prior, they assume a Dirichlet distribution. For the conditional observation distribution, they assume a Gaussian-inverse-Wishart distribution and derive a variational approximation algorithm of the joint posterior of the current and previous state, the measurement and the state covariance matrices and the mixing parameters. They apply their algorithm to target tracking. Reference [86] track an autonomous surface vehicle by assuming an inverse Wishart distribution for the measurement covariance matrix and computing the posterior distribution of the states and covariances by variational inference. Reference [207] first scale the measurement covariance matrix with IGGIII weights, and propose to model the covariance matrix with variational Bayes and an inverse Wishart distribution as prior.

Reference [146] argue that the estimation accuracy of the prediction error covariance matrix,  $\Sigma_{t|t-1}$ , depends on the state noise covariance matrix,  $Q_t$ . Therefore, if only inaccurate prior information about the latter is available, they propose to not use the one-step prediction-error covariance matrix directly in their variational Bayesian adaptive KF algorithm, but estimate a prior scale matrix via the EM algorithm. They apply their strategy for collaborative localization with two surface vehicles and one autonomous underwater vehicle.

Reference [66] use the CKF with a sigma-point update rule for GNSS/INS estimation. In order to deal with measurement outliers, they propose to include switching variables which are Bernoulli-distributed, where the presence of an outlier would correspond to the value 0, with Beta prior. The measurement covariance matrix is scaled with the inverse of the expectation of the switching variable in the respective time step. The joint posterior of the states, switching variables and their priors are updated via variational inference. They apply their method in a real-world experiment with carmounted GNSS/INS.

Reference [147] assume that both the process and measurement noise are t-distributed. In a smoothing approach with nonlinear dynamics, they infer the trajectory in a fixed time window via variational inference of the joint posterior, and apply their technique to target tracking. Reference [317] consider car tracking and assume t-distributed process noise and a Gaussian-generalized hyperbolic distribution for the measurement noise in the EKF. The latter is a mixture of Gaussian distributions, where the mixture distribution is a generalized inverse Gaussian distribution, thus a joint posterior of the states, covariances, distribution and mixture parameters is computed by variational approximation. Reference [252] consider target tracking and assume a Gaussian-exponential-Gamma distribution for both the process and the measurement noise.

1883

1885

1888

1890

1892

1895

1900

1902

1905

1907

1909

1912

1915

1916

1917

1919

1921

1922

1924

1926

1928

1929

1931

1933



1828

1830

1832

1833

1834

1836

1838

1840

1841

1843

1845

1846

1847

1848

1850

1851

1852

1853

1855

1857

1858

1860

1862

1863

1865

1867

1868

1870

1871

1873

1874

1875

1876

1878

1880

Reference [152] propose a Gaussian-Student's *t* mixture distribution (GSTM) in order to address non-stationary, heavy-tailed noise distributions for both the states and the observations. The GSTM distribution is of the form

$$p(\mathbf{x}|\pi) = \pi \mathcal{N}(\mathbf{x}, \boldsymbol{\mu}, \boldsymbol{\Sigma}) + (1 - \pi)t(\mathbf{x}, \boldsymbol{\mu}, \boldsymbol{\Sigma}, \boldsymbol{\nu}),$$

where  $\pi$  is the mixing parameter, which has to be inferred and for which a Beta distribution is assumed as prior distribution. While the GSTM distribution has lighter tails than the corresponding pure t-distribution, it has heavier tails than the corresponding Gaussian distribution. Reference [152] argue, based on the influence function of the GSTM distribution, which is close to that of the Gaussian distribution in a vicinity of the mean and tends to that of the t-distribution outside, that the GSTM distribution has the same efficiency as the Gaussian distribution on clean data and the same efficiency as the t-distribution on contaminated data. The joint posterior distribution of the states, the mixing parameters and the degrees of freedom is approximated via a variational Bayes approach.

Reference [314] assume time-varying skewness in the measurement noise, which they argue to result from imperfect synchronization and a variable nonline of sight. They propose a so-called shape-parameter mixture distribution of the measurement noise, which is a mixture of Gaussian scale mixture distributions w.r.t. the shape parameters, extending the work of [149] who initially proposed the pure Gaussian scale mixture for the process and the measurement noise. As for the mixing prior, they assume a Dirichlet distribution. They apply their algorithm to robot tracking.

Reference [209] incorporate both heavy-tailed measurement noise and inequality constraints in a variational Bayes algorithm. First, they assume a skewed t-distribution for the measurement noise and an inverse Wishart distribution for the predicted error covariance matrix. As for the inequality constraints, they consider linear constraints of the form  $a_t \leq D_t X_t \leq b_t$ , for some constraint matrix  $D_t$ . These constraints are integrated into the variational approximation via truncation of one element of the predicted state, conditioning the computed distribution onto the feasible set. In their experiments, they track a mobile robot.

Reference [356] consider target tracking and extend the state-space model by multiplicative noise in the measurement equation, leading to the model

$$X_t = F_t X_{t-1} + \mathbf{v}_t, \quad Y_t = m_t Z_t X_t + \boldsymbol{\epsilon}_t.$$

They motivate the multiplicative term  $m_t$  by the multi-path effect as well as fading and scattering when considering underwater acoustics. The two additive and the multiplicative noise are modelled as generalized t-distributions, and the posteriors are approximated by variational inference.

There is further literature where variational filtering is used in situations where multiple state-space models have to be considered, for example, in sensor fusion, collaborative navigation or centralized estimation settings.

Reference [281] consider state estimation of autonomous surface vehicles and propose to perform the estimation remotely in order to save onboard computational capacities. To this end, they propose a stochastic event-triggered communication strategy. Let  $Y^{\text{old}}$  be the most recent observation that the USV transmitted to the remote station. For each following time step t, one computes  $c_t := \exp(-0.5(Y_t - Y^{\text{old}})^T A_t (Y_t - Y^{\text{old}})^T A_t (Y_t$  $Y^{\text{old}}$ ), for a symmetric positive-definite matrix  $A_t$ , and triggers a new transmission if  $U_t \sim U([0, 1])$  realizes a value larger than  $c_t$ , making a new transmission more likely if the current observation strongly deviates from the previously transmitted observation. They assume the GSTM distribution from [152] for the state distribution  $p(X_t|X_{t-1},\theta)$ , where  $\theta$ represents the USV model parameter vector. They use VB in order to compute an approximate joint posterior for  $X_t$ and  $\theta$ . They compare different adaptive and event-triggered UKF versions and the standard UKF with their method, which outperforms its competitors in terms of accuracy, both in a simulation as well as on a real-world experiment. As for an adaptive KF, the observation noise covariance parameters are stochastic, so a joint posterior for the distribution of the states and parameters must be found, which is done by an VB approximation in [274].

Reference [368] consider multi-sensor fusion and propose to robustify the single filters by assuming t-distributed noise. The posterior state distribution for each filter is approximated by variational inference. Assuming that each sensor operates independently, they derive a weighting strategy which additionally neglects any dependence between the individual state components, resulting in a diagonal weight matrix which can be easily computed, as matrix inverses are avoided, for the price of potentially reduced accuracy. They compare their algorithm with competitor robust KF and sensor fusion algorithms in a real-world experiment with an autonomous driving platform, achieving better accuracy than its competitors. As for the computational time, their algorithm requires around 4 times more time than the standard KF, but around half of the time required for the federated KF.

Reference [184] consider a leader-follower cooperative navigation setting where a fleet of follower vehicles with cheap and low-accuracy sensors is given, and one or multiple leader vehicles with high-accuracy sensors. As for the observations, they consider the range between leaders and followers. The states and measurements are the concatenated state and measurement vectors. In the resulting EKF, they model both the process noise and the measurement noises by t-distributions. The joint state and measurement posteriors are updated recursively via linearization of the state and the measurement equation. They apply their algorithm for underwater navigation in a real-world experiment with one follower and one leader vehicle. Reference [151] consider t-distributed measurement and process distributions and use variational inference for approximating the posteriors. They apply their method for collaborative localization with two



leader surface vehicles and one autonomous underwater vehicle.

Reference [297] argue that in collaborative localization with low overlap between the local maps of the individual agents, outlier data associations are likely, resulting in potentially high outlier ratios. Therefore, they compute the spatial consistency between each two matched point pairs  $\{x^{(1)}, y^{(1)}\}, \{x^{(2)}, y^{(2)}\}$ , considering them only as inliers if the difference  $|||x^{(1)} - x^{(2)}||_2 - ||y^{(1)} - y^{(2)}||_2|$  is below some threshold. Local maps with more inliers are associated with a higher overall inlier probability in an EM algorithm where the positions are updated. Their algorithm is applied to a KITTI dataset and a real-world dataset with three robots.

Reference [344] consider decentralized collaborative localization, which, in contrast to centralized collaborative localization where one central entity jointly estimates the states of all robots based on the transmitted data, allows the robots to share their own state estimates with each other. In addition to a robot-individual state equation, [344] define observation equations for the absolute range measurement  $y_{a,t}^{il}$  between robot i and landmark l at time t, given by

$$y_{a,t}^{il} = h_t^i(\boldsymbol{X}_t^i, \boldsymbol{X}_t^l) + \boldsymbol{v}_t^i,$$

and for the relative range measurements  $y_{r,t}^{ij}$  between robots i and j at time t, given by

$$y_{r,t}^{ij} = h_t^i(\boldsymbol{X}_t^i, \boldsymbol{X}_t^j) + \boldsymbol{v}_t^i.$$

While using Gaussian distributions for the state equations, [344] allow for *t*-distributed noise in the absolute and relative range measurements and propose a variational Bayes approach in order to update them for each robot. Due to shared information, interdependences between each robot pair have to be integrated into the algorithm, which themselves are updated iteratively. They apply their method for collaborative localization of 5 robots.

Reference [200] propose to robustly estimate  $V_t = \text{Cov}(\epsilon_t)$  of the KF by scaling the diagonal entries using different weight functions such as the IGGIII weight function. A similar idea has been proposed in [188] who scale the covariance matrix of the CKF using IGGIII weights. See also [294], [315], [318].

Reference [352] combine an adaptive KF and a robust KF. In the adaptive KF, the gain and covariance are scaled with Huber weights. In the robust KF, IGGIII weights are used in order to scale the measurement covariance matrix. Finally, the estimated state vector and state covariance matrix is computed as a convex combination of both predictions from the adaptive KF and from the robust KF. Here, for small residuals, the adaptive KF gets more weight, and vice versa for large residuals. They apply their algorithm for land vehicle navigation.

Reference [45] assume a linear state-space model and propose to compute the standard Mahalanobis distance of the observations and to scale the noise covariance matrix  $V_t$  in the KF with a scalar if the Mahalanobis distance exceeds some

threshold, where the scaling factor is chosen adaptively. They apply their algorithm to a kinematic positioning problem where both position and velocity have to estimated.

References [304] and [305] consider the observation equation  $Y_t = Z_t X_t + \epsilon_t + u_t$ , where  $u_t$  follows a non-ideal distribution. Note that this contamination scheme is not a convex contamination, unless one would consider the distribution of  $\epsilon_t + u_t$  as contaminating distribution and the contamination radius as 1. In particular, they follow an unknown variance prior approach where  $u_t \sim \mathcal{N}(0, \Sigma_t)$  where  $\Sigma_t$  itself follows some prior distribution. The estimation of  $\Sigma_t$  is done via the EM algorithm. They apply their approach for the localization of a marine vehicle and a quadrotor. The computation time was around 6 times higher than that for the standard KF, but lower than for the KF proposed in [2].

Reference [231] consider object tracking by sequences of images and propose to apply a Kalman smoother for each pixel in order to deal with abrupt lightning changes and occlusions. They propose to replace the square in the Gaussian distribution by the Huber function, i.e., the observation model given some template feature vector  $\boldsymbol{f}_t$  at time t is given by

$$p(Y_t|f_t) = c^{-1}|R|^{-1/2} \exp(-\rho_H(r(Y_t, f_t)))$$

for a normalizing constant c, a scale matrix R and the error

$$r(\boldsymbol{Y}_t, \boldsymbol{f}_t) = \sqrt{(\boldsymbol{Y}_t - \boldsymbol{f}_t)^T R^{-1} (\boldsymbol{Y}_t - \boldsymbol{f}_t)}.$$

They then approximate the posterior  $f_t$ , which is no longer analytically computable. In their workflow, they first match templates. Given a set of predicted feature vectors  $\hat{f}_t(x)$ , they match them to the current image in order to derive the errors for the KF at the next time step. Considering translation, rotation and scaling, they consider the transformation

$$T(\xi)(x) = (1 + \xi_4) \begin{pmatrix} \cos(\xi_3) - \sin(\xi_3) \\ \sin(\xi_3) & \cos(\xi_3) \end{pmatrix} \begin{pmatrix} x_1 \\ x_3 \end{pmatrix} + \begin{pmatrix} \xi_1 \\ \xi_2 \end{pmatrix}$$

with a parameter  $\xi \in \mathbb{R}^4$  to be estimated, which is done by robust regression w.r.t. the objective

$$\sum_{x} \rho_{H}(r(\boldsymbol{I}_{t}(\boldsymbol{p}(x,\boldsymbol{\xi})),\hat{\boldsymbol{f}}_{t}(x)))$$

for the feature vector  $I_t(p(x, \xi))$  observed at image point  $p(x, \xi)$ . The templates are updated using the robust KF and lastly, the scale matrix R is updated.

Reference [334] apply a robust particle filter on pedestrian tracking using radar. They consider a non-linear state space model and assume  $\epsilon_t \sim \mathcal{N}(\mathbf{0}, W_t^{-1}R)$  for a diagonal weight matrix  $W_t = (w_{t,m})_{m=1,\dots,d}$ , with Gamma priors

$$w_{t,m} \sim \text{Gamma}(w_{t,m}|\theta_m/2, \theta_m/2),$$

 $m=1,\ldots,q$ .

References [29] and [30] consider joint robust GNSS position and attitude estimation with the EKF. As the EKF can be interpreted as the optimization problem

$$\hat{X}_{t|t} = \operatorname{argmin}_{\mathbf{x}}(||\mathbf{x} - \hat{X}_{t|t-1}||_{\Sigma_{t|t-1}}^{2} + ||h(\mathbf{x}) - Y_{t}||_{V_{t}}^{2}),$$



they point out that generalized M-estimators such as in [97] do not allow for redescending losses, hence they use robust information filters where the optimization problem is re-formulated by replacing  $V_t$  by a weighted version  $V_t^{1/2}W^{-1}V_t^{T/2}$  for

$$W = \operatorname{diag}(w(V_t^{-1/2}(\boldsymbol{Y}_t - h(\boldsymbol{X}_t))))$$

for a weight function w, which may be the Huber loss function or the Tukey loss function. The solution to the optimization problem above can then be approximated iteratively. They further adapt this strategy to the situation where the data points belong to a manifold, as in the joint position and attitude estimation problem. Experiments are done on simulated data with an outlier rate of 20% and 25% in [29] and [30], respectively.

Apart from approaches based on a robustification of the loss function or modeling heavy-tailed noise, there are strategies that invoke other techniques for robustification, such as **outlier detection or clipping**.

If only AOs occur, [267] propose a Huberization of the Kalman gain in order to robustify the correction step, i.e., the Huberization of the Kalman gain is given by

$$H_b(K_t \Delta Y_t) := K_t \Delta Y_t \min \left(1, \frac{b}{|K_t \Delta Y_t|}\right).$$

The clipping height b may be determined so that a certain Anscombe-efficiency level is attained or by a minimax criterion w.r.t. a least favorable contamination radius. In the case of SO-outliers, they assume a convex contamination model around the true distribution  $F_{Y_t}^{\text{id}}$  of the  $Y_t$ , leading to a distribution  $F_{Y_t}^{\text{re}}$ , so that, assuming independence with the distribution  $F_{X_t}$  of the  $X_t$ , the ball

$$\mathcal{U}^{\text{SO}}(r) = \bigcup_{0 \le s \le r} \{ \mathcal{L}(\boldsymbol{X}_t, \boldsymbol{Y}_t^{\text{re}}) \mid F_{\boldsymbol{Y}_t}^{\text{re}} \in U_c(F_{\boldsymbol{Y}_t}^{\text{id}}, s) \}$$

is considered. They propose to either minimize the MSE on  $\mathcal{U}^{SO}$  or to minimize the MSE w.r.t. a bound on the bias on  $\mathcal{U}^{SO}$ . In the case of IOs, they show that the correction step can be written as

$$X_{t|t} = X_{t|t-1} + Z_t^{\Sigma} (\Delta Y_t - \mathbb{E}[\epsilon_t | \Delta Y_t]),$$
  

$$Z_t^{\Sigma} = \Sigma_{t|t-1} Z_t^T (Z_t^T \Sigma_{t|t-1} Z_t)^-,$$

so a robustification is done by Huberizing  $\mathbb{E}[\epsilon_t | \Delta Y_t]$ , which equals  $(I - Z_t K_t) \Delta Y_t$  in the ideal model, leading to the Huberized correction step

$$X_{t|t} = X_{t|t-1} + Z_t^{\Sigma} [\mathbf{\Delta} Y_t - H_b((I - Z_t K_t) \mathbf{\Delta} Y_t)].$$

In [269], the same clipping strategy is performed for the EKF. They apply their method to vehicle tracking with the goal to estimate the change of altitude. Apart from measurement errors and changes in the road surface, their data also consist of missings due to signal loss, e.g., in tunnels, leading to jumps in altitude or speed.

Reference [359] propose an iterated EKF where the linearization is considered at the updated state  $X_{t+1|t}$ . Then,

a Huberization of the Kalman gain  $K_t \Delta Y_t$ , going back to [267], is performed. They consider spacecraft navigation.

Reference [91] point out that robust KFs that allow for heavy-tailed noise distributions and that approximate the posterior by variational Bayes are only robust to additive outliers, while a Huberization of the residuals such as done in [269] also robustifies against IOs. Moreover, they point out that anomalies are often multi-modal, which cannot be represented by t-type distributions.

Reference [38] use a standard KF, but reduce the dataset to inliers using RANSAC before, for lane detection and tracking.

Reference [37] consider measurement outliers in collaborative localization and downweight them in an KF scheme where the weights are computed via the Stahel-Donoho estimator.

Reference [196] consider additive outliers and propose to identify them by computing the matrix

$$B_t = Z_t P_{t|t-1} Z_t^T + Z_t Q_t Z_t^T + V_t.$$
 2104

The *i*-th component of an observation is flagged as outlier if the *i*-th diagonal element of  $(Y_t - Z_t X_{t|t-1})(Y_t - Z_t X_{t|t-1})^T$  is larger than  $B_{ii}$ , multiplied with some weight. If an outlier is detected, the corresponding predicted state and covariance matrix are corrected via component-wise scaling. Their method is applied to aircraft tracking. They argue that their algorithm achieves real-time performance as the computation time is lower than 100 ms per frame.

Reference [380] integrate outlier detection and suppression into a variational Bayes approach by using sliding windows. First, they allow for heavy tails by using a *t*-distribution for both the measurement and process noise. In their sliding window approach, the posterior for each time step in the window are updated by using a constant measurement and state covariance matrix within each sliding window. In addition, in each window, for each covariance matrix, an auxiliary variable is considered which scales the covariance matrix, allowing for outlier suppression in the respective window. The posterior for the states, covariance matrices and auxiliary variables is approximated jointly by variational inference. They apply their method to tracking a car in a simulated and in a real-world experiment.

Reference [87] point out that the EKF performs linear approximations based on the estimations from the previous step, so that errors may even increase. They also point out that the computational complexity dramatically increases when trying to robustify the EKF. They criticize the  $\mathcal{H}_{\infty}$ -filtering approach (e.g., [285]; see Sec. V), which interprets outliers as bounded uncertainty, to be too pessimistic. The idea in [87] is to detect outliers in the innovations and to clip them, i.e.,

$$\max(-k, \min(k, Y_{i,t} - (h_i(\hat{X}_{t|t-1}))),$$

where the clipping height k is adaptively chosen.



### **B. ESTIMATION OF VEHICLE PARAMETERS**

KFs are used in order to provide an estimation of the true underlying state  $X_t$ , based on the observed noisy state  $Y_t$ . Of course, provided that an underlying state space model can be formulated, one can estimate vehicle parameters by considering them to be part of the underlying states  $X_t$ .

A Huberized linear KF has been applied in [83] for position estimation of vehicles, in [194] who estimate the position error and mounting angles and yaws as well as lever-arm residuals between data from the INS and a laser Doppler velocimeter or VO, respectively.

A Huberized EKF is applied in [332] for center of gravity estimation, which is done by using a state space model that relates the height of the center of gravity and its distance to the front axis with the velocity, [369] consider estimating the rotor angle and speed of a bus. Reference [68] apply robust KFs, including a Huberized EKF and a covariance-scaled EKF, for the estimation of attitude, position and velocity errors, and acceleration and gyro biases of a rover. Several robust KFs, including a Huberized KF, the KF from [45] and several variational filters, have been compared in [69], here with the application to improve wheel-inertial odometry for planetary rovers. The state represents the attitude, position and velocity error, and the acceleration and gyro biases.

Reference [292] use a Huberized UKF with adaptive covariance for the navigation of coupled vehicles, [313] consider vehicle state estimation, such as longitudinal and lateral velocities, yaw rate, mass, center of gravity, and moment of inertia.

Reference [190] use a Huberized CKF for rotor angle and speed estimation and confirm real-time performance as their algorithm only leads to a slight overhead in the computation time compared to the standard CKF. Reference [189] apply a Huberized CKF to an INS where the state consists of attitude, latitude, longitude, height and velocity errors, gyroscopic drifts, accelerometer biases, and a scale factor error of the Doppler velocity log. A numerically more stable version of the CKF, the square-root CKF, has been Huberized in [139], who use it for state-of-charge (SoC) estimation for lithiumion batteries. Here, the state represents the SoC and the polarization voltage.

The variational filter from [2] has been applied in [277] for the estimation of the internal resistance in the battery system of electric vehicles. Reference [357] apply an EKF with *t*-distributed observation noise for ship position estimation. Reference [127] use an adaptive KF with the MCC and allow for a time-varying noise covariance via variational Bayes in order to estimate the tire-road forces and the side slip angle of a vehicle. In numerical simulations, their algorithm only requires slightly more computation time than the standard CKF.

Reference [52] use the correntropy criterion for the linear KF for the navigation of vehicles in an urban environment. Reference [61] combine the CKF with maximum correntropy for spacecraft attitude estimation, [248] consider the

estimation of the yaw rate, the lateral and the longitudinal velocity of a vehicle, [50] consider car mass estimation. Reference [103] use the MCC for the square-root CKF in order to estimate velocities, the yaw rate, and wheel rotation of electric vehicles, [201] consider estimating the yaw rate, side slip angle and the longitudinal velocity.

Reference [249] scale the covariance matrix corresponding to the measurement noise of the KF via IGGIII weights and estimate the SoC of lithium-ion batteries of electric vehicles.

Reference [289] consider, under a static environment assumption, a linear relation between Doppler velocities (based on radar measurements) and the ego-velocity. Due to dynamic features, outliers are generated, which are first filtered using a sliding window approach where instances for which the velocity of two subsequent measurements differs too much or where the velocity differs too much from the average in the window are discarded. With the filtered data, robust regression using truncated least squares and the Cauchy loss is performed.

Robust regression can also be used for velocity estimation, see, e.g., [300], who consider the objective

$$\min_{\boldsymbol{\beta}} \left( \sum_{i} \rho_{H}(v_{i} - X_{i}\boldsymbol{\beta}) \right),$$

for the measured velocities  $v_i$  and variables such as the mean traffic speed or the road curvature, that are represented by the  $X_i$ .

Reference [258] apply robust M-estimators such as LTS and LMS, but also consider robustifications of recursive least squares, for vehicle parameter estimation. Such recursive objective are important when considering time-varying systems so that for each time step t, a solution can be efficiently computed, which is in particular important for real-time applications. The objective is

$$\min_{\boldsymbol{\beta}} \left( \sum_{t=t_0}^{T} \lambda^{t-t_0} \rho(Y_t - \boldsymbol{X}_t \boldsymbol{\beta}) \right)$$
 2225

for some forgetting parameter  $\lambda \in ]0, 1]$ . Reference [258] also propose to additionally regularize recursive least squares. They apply these algorithms to mass estimation and tractive force prediction of vehicles in grey-box models. They use the model  $X\beta = Y$  for

$$X = \left(g\cos(\theta), g\sin(\theta) + v', v^2, \frac{v^4}{4r_P^2}\right),$$

$$\beta = \left(mf_{r_0}, m, \frac{\rho_a}{2}Ac_x, \frac{m^2}{c_yw}\right),$$
2232

for the gravitational constant, g, the gradient angle,  $\theta$ , the path radius,  $r_P$ , the rolling resistance coefficient,  $f_{r_0}$ , the mass, m, the vehicle cross-sectional area, A, the longitudinal drag coefficient,  $c_x$ , the air density,  $\rho_a$ , the wheel-concerning stiffness,  $c_{yW}$ , and the velocity, v. X takes the role of the measured input and Y represents the tractive force, which takes the role of the measured output in mass estimation. Note that a robust estimation of  $\beta$  allows for extracting the

desired vehicle parameters, here the mass, from the estimate  $\hat{\beta}$ . In [258], Y itself is computed by the model

$$Y = \frac{T_R - I_W \theta_W''}{r_W},$$

for the rim torque,  $T_R$ , the wheel moment of inertia,  $I_W$ , the dynamic wheel radius,  $r_W$ , and the second derivative  $\theta_W''$  of the wheel rotation angle,  $\theta_W$ . They also provide an overview of variables that need to be estimated as they cannot be directly measured. In the above model, the engine torque and the reduced moment of inertia can be assessed by look-up tables, while the velocity, the path angle, and the path radius can be estimated by simple models. They also point out that in the presence of outliers, the MSE is not the correct criterion for validation.

Mass estimation has also been considered in [60]. Under the assumption of a nearly flat road, the model  $Y = X\beta$  for the longitudinal acceleration Y is approximately valid, where

$$X = \left(\frac{T_e i_g i_f \eta_T}{r_W} - \frac{c_x A \rho_a v^2}{2}, -g\right),$$
$$\beta = \left(\frac{1}{m}, f_{r_0} + \frac{F_{err}}{mg}\right)^T,$$

where  $T_e$  is the engine torque,  $i_g$  the transmission gear,  $i_f$  the final drive ratio,  $\eta_T$  the driveline mechanical efficiency, and where  $F_{err}$  represents the error of a physical model of the driving force. They consider recursive regression where the objective consists of two parts, one for each component of  $\beta$ . The squared loss is replaced by the three-part redescender going back to [123] for the first part of the objective. In their simulations, they confirm real-time capabilities of their algorithm.

Reference [67] consider the estimation of running resistances of a train. To this end, they invoke the differential equation

$$\partial_t v(t) = u(t) - r(v(t)) - w(s(t)), w(s(t)) = \frac{g}{\rho_m} p(s(t))$$
$$+ \frac{k}{\rho_m r_T(s(t))},$$

where u(t) is the tractive and brake effort, r(v(t)) the running resistance corresponding to the velocity, at time t, respectively, and where  $\rho_m$  is the rotational mass factor, p(s(t)) the gradient of the track at s(t),  $r_T(s(t))$  is the radius of the track at s(t), and where k is a gauge factor corresponding to the impact of a curve on the train. For the resistance, they use the model

$$r(v(t)) = r_0 + r_1 v(t) + r_2 v^2(t),$$

for rolling resistance parameters  $r_0$ ,  $r_1$ ,  $r_2$ . Using time discretization with time step size  $\Delta t$ , one gets the regression model  $Y = X\beta$ , for

$$y_k = u_k - w(s_k) - a_k, \quad a_k = \frac{v(t_{k+1}) - v(t_k)}{\Delta t},$$

$$\boldsymbol{\beta} = (r_0, r_1, r_2)^T, \quad \boldsymbol{X}_k = (1, v_k, v_k^2),$$

with the respective quantities at time step k. They consider a plethora of non-robust and robust loss functions, including the Huber, Tukey, Cauchy, and Welsch loss.

Reference [32] consider robust parameter estimation for electric vehicles, including mass, braking parameters, drag and resistance, electric parameters of asynchronous machines (such as resistances, inductivities), and parameters of lithium-ion cells (voltage, SoC, State of Health). They point out that contamination may arise from wrong measurements, disturbed transfer, phases with low system stimulation (when driving with constant speed), wrongly modelled system dynamics, or wrong input parameters such as wheel radii, velocity, driving torque, air density, or acceleration. As for the longitudinal vehicle dynamics, they consider the model  $Y = F_A = X\beta$  for

$$X = \left(a_x, g, gv_x, gv_x^4, 0.5\rho_a v_x^2, a_y^2\right),$$

$$\beta = \left((m, mc_{r,0}, mc_{r,1}, mc_{r,4}, c_w A_{F_z g}, \frac{m^2}{(4c_{\gamma_{Rad}})^T}\right),$$
2303

for the longitudinal velocity,  $v_x$ , the longitudinal acceleration,  $a_x$ , the lateral acceleration,  $a_y$ , the rolling drag forces,  $c_{r,j}$ , the air drag force,  $c_w$ , the surface area projected on the y-z-axis,  $A_{Fz_g}$ , and the curve drag force,  $m^2/(4c_{\gamma_{\rm Rad}})$ . Apart from outlier detection, which has disadvantages when being applied to embedded systems due to a large memory and computational burden due to the recursive estimations, [32] propose a robust version of recursive least squares, including exponential forgetting, regularization and parameter range constraints, see [32, Alg. 3.8], which is solved by an IRWLS procedure. As for the robustness aspect, the weighted RLS objective

$$\min_{\boldsymbol{\beta}} \left( \frac{1}{n} \sum_{t=t_0}^{T} \lambda^{t-t_0} w(r_t^2(\boldsymbol{\beta})) \right)$$

is considered, where w is a weight function such as the Huber weight function. As for electric parameters, they consider the model

$$Y = \partial_{t}u_{S}^{\alpha} + n_{p}\omega_{m}u_{S}^{\gamma} = \begin{pmatrix} \partial_{t}^{2}i_{S}^{\alpha} + \partial_{t}(n_{p}\omega_{m}i_{S}^{\gamma}) \\ \partial_{t}i_{S}^{\alpha} \\ -u_{S}^{\alpha} \\ \partial_{t}i_{S}^{\alpha} + n_{p}\omega_{m}i_{S}^{\gamma} \end{pmatrix} \begin{pmatrix} \sigma_{\mathrm{B}1}L_{S} \\ L_{S}\frac{R_{R}}{L_{R}} \\ R_{S} \\ R_{S}\frac{R_{R}}{L_{R}} \end{pmatrix}$$

$$= X\beta,$$

for currents, i, voltages, u, electric resistances, R, and inductivities, L, where the subscripts S and R refer to the stator and the rotor, respectively, and where superscripts  $\alpha$  and  $\gamma$  refer to the coordinate system of the asynchronous machine.  $\omega_m$  is the mechanical rotor drive,  $n_p$  the number of pole pairs, and  $\sigma_{\rm B1}$  the scattering coefficient. Although they do not apply their robust RLS procedure here, they analyze problems that arise when applying the non-robust variant and propose a Savitzy-Golay smoothing of the signal in order to



2383

2391

2392

2397

2398

2400

2405

2410

2412

2414

2415

2418

2419

2420

compute  $\partial_t^2 i_S^{\alpha}$ . In lithium-ion cells, the model

2331

2333

2334

2336

2338

2339

2340

2341

2343

2347

2351

2353

2355

2358

2360

2362

2363

2365

2368

2372

2376

2377

$$Y^{(k)} = U_{akk}^{(k)} = (1, U_{akk}^{(k-1)}, I_{akk}^{(k)}, I_{akk}^{(k-1)}) \boldsymbol{\beta}$$

for  $\beta = ((1 - a_1 U_{\text{OC}}, a_1, a_2, a_3))$  is assumed, for voltage  $U_{\text{akk}}$ , current  $I_{\text{akk}}$  and open circuit voltage  $U_{\text{OC}}$  of the cell, and quantities  $a_1, a_2, a_3$  that are given in terms of the time step size, inner resistance  $R_0$ , and resistance  $R_1$  and capacity  $C_1$  of the RC branch, respectively. They apply their robust RLS variant here.

### C. BOUNDING BOX ESTIMATION

Reference [154] propose a robust estimation of future bounding boxes, including their uncertainty. Given an anchor box  $\mathbf{B}_0$ , let  $T(t) = [T_x(t), T_y(t), T_w(t), T_h(t)] : \mathbb{R} \to \mathbb{R}^4$  be the transformation at time step t from  $\mathbf{B}_0$  to the ground-truth prediction box  $\mathbf{B}^*(t)$  where the indices represent the x- and y-position of the center, the width and the height of the bounding box, respectively. Then, the proposed confidence-weighted Huber loss is

$$H_k(u, u', \sigma) = \ln(c)$$
+ 
$$\begin{cases} (u - u')^2 / (2\sigma^2), & |u - u'| < k \\ k\sigma^{-2} |u - u'| - k^2 / (2\sigma^2), & |u - u'| \ge k \end{cases}$$

for a normalizing constant c and a scale parameter  $\sigma > 0$ . They propose to set k to the estimated uncertainty  $\hat{\sigma}$ , scaled by some constant factor. As for the objective, they consider minimizing the discrepancies of the dimension-individual means, i.e.,

$$\min_{\boldsymbol{\theta}_{d}^{d},\boldsymbol{\theta}_{\sigma}^{d}} \left( \sum\nolimits_{d} H_{d}(T_{d}^{*}(t),\hat{T}_{d}(t,\boldsymbol{\theta}_{B}^{d}),\hat{\sigma}_{d}(t,\boldsymbol{\theta}_{\sigma}^{d})) \right),$$

where  $\hat{T}_d$  and  $\hat{\sigma}_d$  are estimators for the transformation and the uncertainty by a neural network, with individual parameters  $\boldsymbol{\theta}_B^d$  and  $\boldsymbol{\theta}_\sigma^d$ , respectively. Experiments were performed on the KITTI "raw" dataset. The first 20 frames of a tracklet serve as training sample, the prediction horizon consists of the following 10 frames.

The Huber loss is also referred to as "smooth  $l_1$ -loss", only up to a scaling, in the deep learning literature. For example, [53] use this loss function as orientation loss and bounding box offset loss, [54] for the 3D box regression loss, [175] use it for all regression losses in 3D object detection. In 2D object detection, algorithms such as Fast R-CNN [108] use this loss function. Reference [15] propose to use a convex combination of the IoU loss and the Huber loss.

### D. DETECTION OF ROAD FEATURES

Reference [302] consider the detector YARF (yet another road follower), which uses Robust Statistics in order to detect road features. They propose the model

$$Y_i = \beta_0 - \beta_0^r + \beta_1 X_i + 0.5 \beta_2 X_i^2$$

where  $\beta_0^r$  is the offset from the road spine,  $\beta_0$  the *Y*-intercept of the spine arc,  $\beta_1$  the heading w.r.t. the tangent of the spine arc at  $\beta_0$  and where  $\beta_2$  is the curvature of the spine arc,

where the positions are given by  $(X_i, Y_i)$ . The coefficients are estimated using LMS.

References [234] and [235] consider the problem of road surface extraction from 3D point clouds and apply a robust variant of locally weighted regression based on the Tukey loss, i.e., they minimize

$$\sum_{i} \rho_T(\tilde{r}_i) w(X_i) (Y_i - f_{\boldsymbol{\beta}}(X_i))^2,$$

where  $\tilde{r}_i = r_i/\hat{\sigma}$  for  $\hat{\sigma}$  being the MAD of  $(|r_1|, \dots, |r_n|)$ , where the weight function w is the tri-cube weight function

$$w(X_i) = \left\{ \begin{bmatrix} 1 - \left( \frac{||X_i - X_j||_2}{\max_{j \in N(X_i)} (||X_i - X_j||_2)} \right)^3 \end{bmatrix}^3, \ j \in N(x) \\ 0, \ j \notin N(x), \end{bmatrix}$$

for a local neighborhood  $N(X_i)$  of  $X_i$ , and for some potentially non-linear function  $f_{\beta}$ . The residuals after the fit indicate whether the individual points belong to the road surface or whether they are non-ground/3D surface points.

### E. OTHER APPROACHES

Outlier detection is a popular topic in data analysis. It is therefore out of scope for this paper to list all the literature where some kind of outlier detection has been performed in the context of autonomous driving. Just as an example, consider the work of [345] who have data from n microphone arrays which are located as known 2D-positions  $p_i$ , i = $1, \ldots, n$ , which measure angles of arrival from an object with the goal to determine its position  $p_0$ . In an iterative manner, first the m microphone arrays with the smallest distance to a particular object are identified based on an initial estimate  $\hat{p}_0$  of the object's position, which form a reference set. Then, the matrices  $P_i = (\hat{p}_{ij})_{j=m+1,\dots,n}, i =$  $1, \ldots, m$ , are formed, where  $\hat{p}_{ij}$  is the estimated position of the object when replacing  $p_i$  with  $p_i$ . Using the robust Mahalanobis distance where the mean and covariance of the  $P_i$  are estimated robustly in the spirit of the Gnanadesikan-Kettenring estimator [109], some instances are flagged as "outliers". Finally, the position of the object is estimated using WLS where the outlying instances are downweighted accordingly.

Reference [36] use median regression for trend estimation in GPS time series based on the Theil-Sen estimator

$$\hat{v} = \operatorname{med}_{i < j} \left( \frac{z_j - z_i}{t_j - t_i} \right)$$

for the velocity, where each  $z_i$  represents the coordinate at time  $t_i$ . As a pre-processing step, outlier detection is done where the slope is computed for each data pairs, removing all pairs for which the slope has a distance larger than 2 MADs from the median.

Reference [204] estimate the orientation changes of a vehicle based on radar images. After an MAD-based outlier removal, the surviving pairs of reference and data images are considered and the rotation and scale is estimated using Tukey's biweight function. At the end, the estimation



is refined by minimizing the Cauchy loss, evaluated at Mahalanobis-type residuals arising from the previous estimation step.

Reference [23] propose a whole family of loss functions, including robust ones as special cases, given by

$$\rho(r,\alpha,\tau) := \frac{|\alpha-2|}{\alpha} \left( \left( \frac{\left(\frac{r}{\tau}\right)^2}{|\alpha-2|} + 1 \right)^{\alpha/2} - 1 \right),$$

with a scale parameter  $\tau > 0$  and a shape parameter  $\alpha$ . The special cases  $\alpha = -\infty$ ,  $\alpha = -2$ ,  $\alpha = 0$ ,  $\alpha = 2$  correspond to the Welsch loss, the Geman-McClure loss, a smoothed version of the  $l_1$ -loss and the squared loss, respectively. They apply several particular loss functions from this family to tasks such as monocular depth estimation and fast global registration.

Reference [347] consider the truncated least squares problem

$$\min_{z} \left( \sum_{i} \min \left( \frac{(z - Y_i)^2}{\sigma_i^2}, \tau^2 \right) \right)$$

for the inlier standard deviation  $\sigma_i$  corresponding to  $Y_i$ . They show that general geometric perception problems such as pose, rotation or 3D structure estimation can be formulated as such a problem. They solve it by a convex relaxation. Their relaxation is extended in [348] to robust loss functions such as the Huber loss or Tukey's biweight loss where it is applied to, for example, point cloud registration, pose estimation, shape estimation, and rotation averaging.

Reference [241] propose the version

$$\rho_{H,k}(Y_i, \hat{Y}_i) = \begin{cases} |\hat{Y}_i - Y_i|, & |\hat{Y}_i - Y_i| \le k \\ \frac{(\hat{Y}_i - Y_i)^2 + k^2}{2k}, & |\hat{Y}_i - Y_i| \ge k \end{cases}$$

of the Huber loss function for depth estimation, where the  $Y_i$  are the pixel values in the ground truth depth-map, the  $\hat{Y}_i$  their predictions, and where the threshold k is given by  $k = 0.2 \max_i(|\hat{Y}_i - Y_i|)$ . This loss is one component of an overall loss that is composed by this pixel loss and a loss function for structural similarity and for the intensity gradients of the pixels, respectively. Contamination may arise from inherent blurs in images.

As for GNNs, which are a backbone of many computer vision methods, [105] consider a robust aggregation of the embedded features of neighboring points in GNNs. They replace the usual sum or mean aggregation, which opens the door for distorted aggregated embeddings due to single perturbed points (as the BDP of an arithmetic mean is zero), by a smoothed medoid aggregation, which is computed by

$$\sum\nolimits_{i} w_{i} \boldsymbol{X}_{i}, \quad w_{i} = \frac{\exp\left(-\delta^{-1} \sum_{j} ||\boldsymbol{X}_{j} - \boldsymbol{X}_{i}||\right)}{\sum_{k} \exp\left(-\delta^{-1} \sum_{j} ||\boldsymbol{X}_{j} - \boldsymbol{X}_{k}||\right)}$$

for some parameter  $\delta$  that controls the approximation to the original solution

$$\operatorname{argmin}_{\mathbf{y}}\left(\sum_{i}||X_{i}-\mathbf{y}||\right).$$

The solution to the smoothed medoid problem approaches the arithmetic mean for  $\delta \to \infty$  and the exact medoid for  $\delta \to 0$ . They show that the soft medoid procedure has a BDP of 0.5. As for contamination, they assume that an adversary can perturb a fraction of the aggregation points. Reference [104] propose the Soft Median aggregation which requires less memory capacities than the Soft Medoid aggregation while maintaining the BDP of 0.5. It is given by

$$\operatorname{softmax}(-\boldsymbol{c}\delta^{-1}p^{-1/2})^TX$$

for the vector c consisting of components  $c_j = ||\bar{X} - X_j||$  and for the node attributes  $X \in \mathbb{R}^{n \times p}$  of the graph to which the GNN is applied.

Deep fundamental matrix estimation has applications in 3D perception, for example, for the projected retinal image coordinates p corresponding to 3D coordinates of the corresponding point, a fundamental matrix F satisfies  $p^T F p = 0$ . Having an initial estimate for F, [367] propose to refine F by computing the signed distances  $r_i^2$  and flagging all points for which  $r_i^2$  is larger than a certain multiple of a robust scale estimate as outliers and then consider an LTS approach where only the residuals from the non-flagged instances enter. Reference [254] propose to estimate the inlier distribution during the optimization. In their context, the optimization problem is

$$\min_{\boldsymbol{\theta}} \left( \sum_{i} ||A\boldsymbol{p}_{i}\boldsymbol{\theta}||^{2} \right) \quad \text{s.t.} \quad ||\boldsymbol{\theta}|| = 1,$$

for some matrix A. This problem can approximately be solved by solving iteratively

$$\mathbf{x}^{j+1} = \operatorname{argmin}_{||\mathbf{x}||=1}(||W^{j}(\boldsymbol{\theta})A\mathbf{x}||^{2})$$

for a weight matrix  $W(\theta)$ . They propose to learn the weights by a deep neural network, so that they essentially have a meta-algorithm of IRWLS. Identifying the solution in one step of the IRWLS problem as a right singular vector of  $W(\theta)A$  for the weight matrix  $W(\theta)$ , they show that  $\theta$  can be learned by backpropagation through an SVD layer. This technique is applied to fundamental matrix estimation.

# V. APPLICATIONS IN AUTONOMOUS DRIVING: PREDICTION AND PLANNING

In this section, we collect robust approaches for prediction and planning. The first two subsections are devoted to RL and IL. Here, the ego-vehicle has to learn by experience (typically, via simulations) how to behave in which situations, so the own actions and, implicitly, the evolution of the states of surrounding vehicles, are learned. The third subsection considers MPC, where models for vehicle dynamics are used in order to predict the state evolution for the surrounding traffic participants and the ego-vehicle based on the observed current state. In all cases, reliable perception is important (see



2578

2581

2583

2585

2593

2595

2597

2598

2600

2605

2607

2610

2612

2617

2619

2620

Fig. 1). Nevertheless, robust planning approaches may safeguard partially against misperception, and can, in addition, also cope with other types of peculiarities such as adversarial driving behaviors of the surrounding traffic participants. The fourth subsection addresses Byzantine robustness, which becomes important when performing federated or distributed RL training.

### A. REINFORCEMENT LEARNING

2518

2520

2522

2524

2526

2527

2529

2530

2532

2534

2536

2537

2539

2541

2542

2543

2545

2548

2550

2552

2553

2555

2557

2559

2560

2562

2566

2567

2569

RL considers a Markov decision process  $(S, A, \beth, \gamma, R)$  for a state space S, an action space A, a set  $\Box$  of transitions, a discount factor  $\gamma \in ]0, 1]$ , and a reward function R:  $\mathcal{S} \times \mathcal{A} \times \mathcal{S} \rightarrow \mathbb{R}$  that assigns a real-valued reward to a state-action-state triple  $(s_t, a_t, s_{t+1})$ , where  $s_{t+1}$  is the state into which the system is translated in the next time step after action  $a_t$  was executed in state  $s_t$ . The transition model may either be deterministic, so that  $\exists \in \exists$  is a mapping  $(s, a) \mapsto \Im(s, a) \in \mathcal{S}$ , or stochastic, so that a density value  $P_{\gimel}(s'|s,a)$  is assigned to (s,a). The goal is to learn a policy  $\pi$ which is either deterministic, i.e., a map  $\pi: \mathcal{S} \to \mathcal{A}$  so that  $\pi(s)$  is the action taken when being in state s, or stochastic, i.e.,  $\pi$  :  $\mathcal{S} \times \mathcal{A} \rightarrow [0, \infty[$  so that  $\pi(s, a)$  assigns a density value to the state-action pair (s, a). We abbreviate  $R(s_t, a_t, s_{t+1}) =: R_t$ . The value function for a given state s is the expected future reward that the agent receives when following policy  $\pi$ , i.e.,

$$V^{\pi}(s) = \mathbb{E}_{\pi} \left[ \sum_{t'=t}^{\infty} \gamma^{t'-t} R_t \middle| s_t = s \right].$$

The Q-function similarly assigns a value to a state-action pair (s, a) in the sense that, starting with  $s_t = s$ , one does not let the policy choose the initial action  $a_t$  but starts with a given action a at the initial state s.

In RL or MPC, the term "robustness" is often understood as adversarial robustness, hence many robust RL algorithms perform adversarial training. However, in contrast to adversarial attacks in classical machine learning where a model is trained on a static dataset and where adversarial attacks are computed after model training, decoupling them from the training procedure, adversarial attacks in RL are used for adversarial training where an adversarial agent challenges the ego-agent, indeed affecting the training procedure. This makes the notion of adversarial robustness in RL inherently close to Robust Statistics.

For example, adversarial RL approaches have been applied to train an agent for autonomous driving, see [256], who propose a minimax game where the adversarial agent minimizes the objective that the ego agent aims at maximizing (up to a different regularization parameter). References [247] and [257] suggest similar minimax games. References [256] and [257] apply their method to a scenario where the ego vehicle aims at crossing a 4-way intersection, where adversarial vehicles drive on the lanes the ego vehicle has to cross. Reference [134] consider adversarial attacks against the agent's observations in highway scenarios, which is trained according to maximizing the Jensen-Shannon divergence

between the  $\pi(s,\cdot)$  and  $\pi(\tilde{s},\cdot)$ , for the perturbed state  $\tilde{s}$  of s. In [133], the worst-case observational perturbations are computed by an adversary using the FGSM scheme [111]. They consider highway, intersection, and on-ramp scenarios with episode lengths of 300, 30 and 30 time steps, respectively. They observe much higher computational costs than for standard RL algorithms, which is a consequence of the approximation of the worst-case perturbations by a Bayesian approach. In [130], the management of a fleet of electric vehicles is considered, where one has one agent for each region of the map who can displace vehicles into adjacent regions or to charging stations. Here, the adversarial attack is a perturbation of the observed states of the region's agents, which consist of the number of vacant and low-battery vehicles, information about charging spots, and demand. The objective is a minimax game, and both the region's and the adversary's policies are updated iteratively. Reference [84] propose to discount the adversary's reward and to constrain the number of attacks by an upper bound, encouraging to only attack in critical situations. Their method is applied for left-turn in an intersection and on-ramp merging. Reference [117] consider state attacks and optimize the worst-case discounted reward, while the adversarial agents aim at performing the action that minimizes the victim's reward. In a simulation framework, they consider driving scenarios with an obstacle.

In addition, many approaches concerning robust control are given in the literature. One can distinguish between minimax games where one searches for the policy the maximizes the cumulated reward/minimizes the cumulated cost given the worst-case trajectory or worst-case transition model (similarly as above in the adversarial RL approaches, but with the difference that the adversarial agents trained in these approaches do not necessarily reflect worst-case situations), risk-sensitive criteria where an individual risk measure is used as objective, and constrained criteria where the reward should be maximized subject to several constraints, see [99].

More formally, the worst-case criterion under parameter uncertainty corresponds to the objective

$$\max_{\pi \in \Pi} \left( \min_{P \in \square} \left( \mathbb{E}_{\pi,P} \left[ \sum_{t=0}^{\infty} \gamma^{t} R_{t} \right] \right) \right),$$

for a set  $\square$  of transition matrices, and a set  $\Pi$  of policies, while the worst-case criterion under inherent uncertainty is given by

$$\max_{\pi \in \Pi} \left( \min_{\omega \in \Omega^{\pi}} \left( \mathbb{E}_{\pi,\omega} \left[ \sum_{t=0}^{\infty} \gamma^{t} R_{t} \right] \right) \right),$$

for a set  $\Omega^{\pi}$  of trajectories that are allowed under policy  $\pi$  [101]. E.g., [232] consider the worst-case criterion under parameter uncertainty for finite state-action spaces and apply the method to aircraft routing.

Another example of a minimax criterion is the robust Bellman TD operator introduced in [279]. The objective is the expected squared temporal difference

$$\frac{1}{2} \mathbb{E}_{o_t \sim P_O}[(\delta_{t, w}^{\text{nominal}}(w_t, o_t))^2]$$
 2621

2675

2676

2677

2679

2682

2684

2686

2688

2690

2698

2699

2701

2703

2704

2706

2708

2709

2710

2711

2713

2715

2716



for

2622

2623

2625

2626

2627

2628

2629

2631

2632

2634

2635

2636

2637

2639

2642

2644

2646

2647

2649

2652

2654

2656

2657

2659

2661

2663

2664

2666

2668

2670

2671

$$\delta_{t,w'}^{\text{nominal}}(w_t, o_t) = Y_{t,w'}^{\text{nominal}}(o_t) - Q_{w_t}(s_t, a_t)$$

for the weights w' of the target network, the current parameter  $w_t$  of the approximation  $Q_{w_t}(s, a)$  of the true Q-function, the distribution  $P_Q$  of the observations, and the nominal targets

$$Y_{t,w'}^{\text{nominal}}(o_t) = R_t + \gamma \max_{a'}(Q_{w'}(s_{t+1}, a'))$$

for observation  $o_t = (s_t, a_t, R_t, s_{t+1})$  at time t. In the robust Bellman TD formulation, one still considers the squared TD error but a robust minimax target label

$$Y_{t,w'}^{\text{robust}}(o_t) = R_t + \gamma \min_{\exists \in \mathcal{U}} \left( \sum_{s' \in \mathcal{S}(s_t, a_t)} \exists (s'|s_t, a_t) \max_{a'} (Q_{w'}(s', a')) \right).$$

for the set  $S(s_t, a_t)$  of all possible states at time (t + 1) given  $s_t$  and  $a_t$  under the uncertainty set U.

Reference [44] consider policy gradient descent and replace the squared differences of the predicted *Q*-values for given state-action pairs and the observations by the absolute differences and the Huber losses. They apply their algorithm for autonomous parking and consider scenarios with 100 time steps. In their experiments, the Huber loss allows for quicker convergence, finally resulting in an even decreased training time in comparison with training according to the MSE and the MAE. Other occurences of the Huber loss in RL include the training of ecological behavior in front of red traffic lights [223], vehicle control (left/right turn, acceleration/deceleration, [354]), and in (simulated) environments for a mountain car and a lunar lander [43].

In contrast to the minimax approach where the adversarial realization is considered to be the worst from a given uncertainty set, distributionally robust optimization optimizes an expectation which is not computed w.r.t. the ideal distribution but w.r.t. a set of distributions that contains the ideal distribution. In light of Sec. III, one can interpret this as an optimization of an expectation w.r.t. a contamination ball (although, in the literature, one not necessarily uses the classical contamination balls from Robust Statistics). In [132] (although actually not an RL approach, as there is no learned policy but the optimization problem is solved periodically with new data), the goal is to manage a fleet of electric vehicles according to the mobility demand and charging requirements. Here, the worst-case expected cost (w.r.t. sets of distributions that model the demand and the supply, respectively) is minimized over the number of dispatched vehicles across the regions. Here, the sets of distributions are confidence sets, estimated from historical data.

Reference [282] consider state measurement errors and formulate the idea of smoothness regularizers that should encourage the differences between  $\pi_{\theta}(s)$  and  $\pi_{\theta}(\tilde{s})$  to be small if the difference of s and  $\tilde{s}$  is small. Assuming  $s \in \mathbb{R}^p$ , the smoothness regularizer has the form

$$R_s(\pi_{\theta}) = \mathbb{E}_{s \sim P_S^{\pi_{\theta_t}}} [\max_{\tilde{s} \in B(s, \epsilon)} (D(\pi_{\theta}(s), \pi_{\theta}(\tilde{s}))]$$

for the state visitation distribution  $P_S^{\pi}$  induced by a policy  $\pi$  and the  $l_p$ -ball  $B(s, \epsilon)$  around s with radius  $\epsilon$ . For the distance D, they use the Jeffrey's divergence

$$D_J(P||Q) = \frac{1}{2}D_{KL}(P||Q) + \frac{1}{2}D_{KL}(Q||P)$$

for stochastic policies and the Euclidean norm for deterministic policies. The agent is then trained w.r.t. the objective to maximize the *Q*-function, penalized by the smoothness regularizer.

Reference [131] consider multi-agent RL with electric vehicles and argue that the individual charging patterns lead to additional model uncertainties with the goal to distribute the electric vehicles fairly among different regions while allocating low-battery vehicles to charging stations, minimizing the overall costs. For a cost function c, denote the worst-case state value function by

$$v_c^{\pi}(s) = \min_{\exists \in U_c(\exists_0, r)} \left( \mathbb{E}_{\pi} \left[ \sum_{t=1}^{\infty} \gamma^{t-1} c(s_t, a_t) \middle| s_1 = s \right] \right)$$

for the uncertainty set  $U_c(\gimel_0,r)=\bigotimes_{s\in S,a\in A} \gimel(s,a)$  where each  $\gimel(s,a)$  is a convex contamination ball around the true transition distribution  $\gimel_0(s,a)$  with contamination radius r, i.e.,

$$J(s, a) = \{(1 - r)_+ J_0(s, a) + \min(1, r)Q | Q \in \mathcal{M}_1(S \times A) \}.$$

The objective for finding the optimal policy is then

$$\max_{\pi} (v_r^{\pi}(P_S)) \quad \text{s.t.} \quad v_c^{\pi}(s) \ge \tau \ \forall s \in S,$$

for some threshold  $\tau$  and

$$v_r^{\pi}(s) = \min_{\exists \in U_c(\exists_0, r)} \left( \mathbb{E}_{\pi} \left[ \sum_{t=1}^{\infty} \gamma^{t-1} R_t \middle| s_1 = s \right] \right)$$

and 
$$v_*^{\pi}(P_S) = \mathbb{E}_{s \sim P_S}[v_*^{\pi}(s)] \text{ for } * \in \{c, r\}.$$

### **B. IMITATION LEARNING**

Robust approaches for RL also carry over to IL.

Random perturbations of trajectories, which can be understood as an untargeted adversarial training, have been considered for IL in [19] who trained an autonomous driving agent based on expert trajectories. In [298], one perturbs the action selected by the agent by an adversarial action that should drag the vehicle from the intended path. In their setting, one is provided with future states by an expert. An inverse dynamics model (IDM) is applied to find suitable actions that allow the vehicle to attain these states. The policy is trained according to the reward function

$$-||\mathbf{a}_{\text{IDM}}-(\mathbf{a}_{\theta}+\mathbf{a}_{\omega})||^2$$
,

for the policy's action  $a_{\theta}$  and the adversarial action  $a_{\omega}$ , so the agent should learn to imitate the optimal action by adjusting for the adversarial action. In order to decourage too harsh adversarial actions, they only inject an adversarial action with a certain probability and further restrict the adversarial action to a certain interval.



Reference [183] consider a minimax criterion where an uncertainty set around the true observation is considered. This uncertainty set is given by coordinate-wise  $l_1$ -balls around the true state component. They consider simulated driving scenarios with traffic lights and intersections.

Reference [138] introduce an IL algorithm based on GANs. They start with a regularized form of inverse RL with the objective

$$\operatorname{argmax}_{c}(-J(c) + \min_{\pi}(-H(\pi) + \mathbb{E}_{\pi}[c(s, a)]) - \mathbb{E}_{\pi_{E}}[c(s, a)]),$$

where c denotes a cost function, H the  $\gamma$ -discounted causal entropy and  $\pi_E$  the expert policy. In order to prevent overfitting, they propose to regularize this objective with a convex regularizer J, inducing the additional term -J(c). Denoting this regularized objective by  $\mathrm{IL}_J(\pi_E)$ , and considering the RL objective

$$RL(c) = \operatorname{argmin}_{\pi}(H(\pi) + \mathbb{E}_{\pi}[c(s, a)]),$$

[138, Prop. 3.2] shows that

$$RL \circ IL_J(\pi_E) = \operatorname{argmin}_{\pi}(-H(\pi) + J^*(OM_{\pi} - OM_{\pi_E})),$$

for the occupancy measure

$$OM_{\pi}(s, a) = \pi(a|s) \sum_{t=0}^{\infty} \gamma^{t} P(s_{t} = s|\pi).$$

Now, [138] connect GANs with RL with the choice

$$J(c) = \begin{cases} \mathbb{E}_{\pi_E}[g(c(s, a))], & c < 0\\ \infty, & c \ge 0 \end{cases},$$
$$\begin{cases} -x - \ln(1 - e^x), & x < 0 \end{cases}$$

$$g(x) = \begin{cases} -x - \ln(1 - e^x), & x < 0 \\ \infty, & x \ge 0 \end{cases}$$

for which

$$J^*(\mathrm{OM}_{\pi} - \mathrm{OM}_{\pi_E}) = \max_{D} (\mathbb{E}_{\pi}[D(s, a)] + \mathbb{E}_{\pi_E}[\ln(1 - D(s, a))]),$$

where D is taken from the set of all discriminative classifiers on  $S \times A$ . This leads to the task of finding a saddle point of

$$\mathbb{E}_{\pi}[\ln(D(s,a))] + \mathbb{E}_{\pi_E}[\ln(1-D(s,a))] - \lambda H(\pi).$$

With parametrizations  $D_{\omega}$  and  $\pi_{\theta}$ , this task can be solved in a GAN-style by alternatingly updating the parameters for the discriminator and the policy, respectively.

Reference [220] propose to induce a Lipschitzness of both the discriminator and the policy by replacing the entropy regularizer  $H(\pi)$  with the regularizer

$$R(D) = \frac{1}{|D|} \sum_{(s,a) \in D} |D_{\omega}(s + \delta_{s,a}a) - D_{\omega}(s,a)|,$$

 $\delta_{s,a} = \operatorname{argmax}_{||\boldsymbol{\delta}||_2 \le r}(|D_{\omega}(s+\boldsymbol{\delta},a) - D_{\omega}(s,a)|),$ 

for training data D and discriminator network  $D_{\omega}$ . The motivation is to better cope with observation noise. Their method is applied to robot locomotion.

Reference [176] train an adversarially robust IL agent via a minimax game where the adversary aims at minimizing the objective the agent aims at maximizing (the entropyregularized advantage function). In order to stabilize training, they suggest regularizing the objective of the ego-agent by a distillation loss term.

Similarly, [316] propose to alternatingly train an IL agent and an adversary where the latter learns to perturb the states in order to let the agent fail. Let the attack policy  $\pi_{\rm adv}$  assign a density  $\pi_{\rm adv}(\cdot|s)$  to a state s in order to produce some adversarial state s'. They then distinguish between sensory attacks, where the observed states are perturbed, or physical attacks, where the state itself is perturbed, resulting in a perturbation of the observed state and letting the transition model produce the next state based on the perturbed state. The objective is then to learn a policy under all possible attacks, i.e.,

$$\min_{\pi}(\max_{\pi_{ ext{adv}}}(J(\pi,\pi_{ ext{adv}})))$$

for 2775

$$J(\pi, \pi_{\text{adv}}) = \mathbb{E}\left[\sum_{t} \rho(a_t, \pi_E(s_t)) \middle| a_t \sim \pi(\pi_{\text{adv}}(s_t)), s_{t+1} \sim \mathbb{I}(\cdot|s_t, a_t)] \right]$$
2776

in the case of sensory attacks, or

$$J(\pi, \pi_{\text{adv}}) = \mathbb{E}\left[\sum_{t} \rho(a_t, \pi_E(s_t)) \middle| a_t \sim \pi(\pi_{\text{adv}}(s_t)), s_{t+1} \sim \Im(\cdot | \pi_{\text{adv}}(s_t), a_t)] \right]$$
2779

in the case of physical attacks, respectively, for some loss function  $\rho$  that penalizes the discrepancy between two actions.

A typical approach from Robust Statistics, namely a robustification of the objective, is done in [240] who consider value function estimation and who point out that this is usually done by minimizing the squared Bellman error. I.e., for Bellman operator

$$(\mathcal{T}V)(s) = \mathbb{E}[R_{t+1} + \gamma^{t+1}V(s_{t+1})|s_t = s],$$

this objective is given by

$$\min_{\theta} \left( \sum_{s \in \mathcal{S}} P_{\mathcal{S}}(s) ((\mathcal{T}V_{\theta})(s) - V_{\theta}(s))^{2} \right)$$

for some distribution  $P_S$  on S and an approximation  $V_\theta$  of the true function  $V^\pi$  for which  $(\mathcal{T}V^\pi) = V^\pi$  holds. Reference [240] propose to replace the squared loss by the absolute or the Huber loss and show how these new objectives can be minimized.

Reference [198] consider IL if contamination in the classical Tukey-Huber sense are allowed, i.e., in the pool of offline demonstration data, a fraction of  $\epsilon$  of the instances (state-action pairs) can be arbitrarily corrupted (note that this fraction is deterministic as in the BDP context, not stochastic as in convex contamination settings). They propose to randomly partition the data into B batches and to use the mean of the likelihoods in each batch as the objective, so the overall objective is the median of the means for which they propose a gradient-based optimization algorithm. This contamination



model has also be considered in [365] and [366] for RL with policy gradient. More precisely, in [366], an  $\epsilon$ -fraction of transitions can be modified arbitrarily while in [365], both an  $\epsilon$ -fraction of rewards and transitions can be perturbed arbitrarily, therefore, they call this contamination scheme "strong data corruption".

Reference [366] point out that many of the existing robust RL methods consider offline RL, where they distinguish between online RL, i.e., an adversary can adapt their perturbation in each iteration, and offline RL, where the contamination must be generated prior to training. In [365], in contrast, the  $\epsilon$ -contamination scheme is designed for online learning in the sense that the adversary can decide in each iteration whether to replace the current reward and the new state with arbitrary values, with the restriction that this can only be done in at most  $\epsilon m_{\text{iter}}$  training iterations if  $m_{\text{iter}}$  is the maximum number of iterations.

Reference [70] assume that reference trajectories or parts of reference trajectories are adversarial in the sense that they accomplish the task with illegal means. Having a small initial set of guaranteed benign trajectories, they detect adversarial trajectories by a divergence measure. To this end, they partition trajectories during training into parts corresponding to sub-tasks and learn sub-policies (options, see [18], [295]) for each sub-task. In order to be able to detect adversarial trajectories that only differ from benign ones in some time steps, they propose to use the occupancy measure w.r.t. the clean trajectories, i.e.,

$$OM_{\pi}^{\text{clean}}(s, a) = \sum_{(s_i, a_i) \in \tau_{\text{clean}}} \pi^*(a_i | s_i)$$
$$\sum_{t} \gamma^t P(s_t = s_i | \pi_{\text{clean}})$$

for a clean trajectory  $\tau_{\text{clean}}$  generated by a clean policy  $\pi_{\text{clean}}$  and for the optimal policy  $\pi^*$ . Because this measure is zero if two trajectories are very close without overlapping, [70] combine it with the Fréchet distance

$$FD(\tau) = \min_{\alpha, \beta} (\max_{t \in [0, 1]} (||\tau(\alpha(t)) - \tau_{\text{clean}}(\beta(t))||_2))$$

for functions  $\alpha$ ,:  $[0, 1] \rightarrow \{0, 1, \dots, |\tau|\}$ ,  $\beta$ ,:  $[0, 1] \rightarrow \{0, 1, \dots, |\tau_{clean}|\}$ . Then, a classifier is trained on the two distance measures in order to decide whether the trajectory part is adversarial or benign.

## C. MODEL-PREDICTIVE CONTROL

In MPC, one assumes a model for the system dynamics, i.e.,

$$s_{t+1} = f(s_t, u_t, v_t),$$

where  $u_t$  are the control inputs to the system, which are contained in some space U, and control noise  $v_t$ . In its simplest form, an MPC problem is given by

$$\min_{u \in U} \left( \sum_{t} \rho(r_t) \right) \quad \text{s.t.} \quad s_{t+1} = f(s_t, u_t),$$

for the control errors  $r_t = d(s_t^{sp}, s_t(u_t))$  where  $s_t^{sp}$  is the set-point that the agent should follow at time t and where d is some distance measure. The objective is potentially

conditioned on other constraints such as that the states and control inputs should, at least with a certain probability, be contained in some subspace of  $\mathcal S$  and U, respectively, that correspond to safe or comfortable behavior, or penalized by a term that discourages the control inputs to vary too much over time.

Similar approaches as for RL and IL have also been introduced for MPC, e.g., replacing the quadratic loss for the control errors by the absolute loss as in [79] and [227], by the Cauchy loss [77] or the dynamically scaled covariance loss introduced in [4], which has been used in [77] as loss function for MPC.

A minimax formulation of an MPC in order to deal with worst-case uncertainties goes back to [41]. Reference [362] propose another minimax formulization where the objective contains worst-case losses w.r.t. an uncertainty set on the (discrete) behavior of surrounding vehicles, given as a probability simplex. Experiments on simulated data with a time step of 0.1 s and a planning horizon of 5 s confirm real-time capability. Reference [226] consider the control of maritime vessels and aim at avoiding collisions. Here, the obstacles are overapproximated by balls, and due to tidal effects, their radius changes, i.e., they are modelled as random variables. Assuming that an empirical distribution for each radius exists, their robust MPC approach considers an uncertainty set in the form of contamination balls around each empirical distribution, based on the p-th order Wasserstein distance.

Reference [228] point out that robust control approaches often include robust optimization where the constraints are only known up to some noise term with the goal to keep the constraints satisfied for all possible noise terms for a given uncertainty set, i.e.,  $g(x, \xi) \leq 0$  for all  $\xi \in \mathcal{U}$  for some uncertainty set  $\mathcal{U}$  and some function g, making the approach rather conservative. The other approach is distributionally robust optimization where the supremal expectation of the constraints have to be satisfied w.r.t. a given set of distributions w.r.t. which the expectation is computed, i.e.,

$$\sup_{P \in \square} (\mathbb{E}_P[g(x,\xi)]) \le 0$$

for some set  $\square$  of distributions. Motivated by the functional view from Robust Statistics, [228] consider the supremum bias due to the decomposition

$$\sup_{P \in \beth} (\mathbb{E}_P[g(x,\xi)]) = \mathbb{E}_{\hat{P}}[g(x,\xi)] + \sup_{P \in \beth} (\operatorname{Bias}(P,g,\hat{P}))$$

with

Bias
$$(P, g, \hat{P}) = \int g d(P - \hat{P}).$$

They compute the supremum bias for the commonly used 1-th order Wasserstein and MMD metric, resulting in

$$\sup_{W_1(P,\hat{P})\leq\epsilon} (\operatorname{Bias}(P,g,\hat{P})) = \epsilon L_g$$

2907

2909

2911

2912

2913

2914

2916

2917

2919

2920

2921

2923

2924

2926

2928

2929

2930

2931

2933

2934

2936

2938

2939

2940

2941

2943

2944

2946

2948

2949

2950

2951

2952

2953

2954



2957

2961

2963

2968

2969

2971

2972

2974

2975

2976

2977

2979

2981

2982

2983

2984

2986

2989

2991

2992

2994

2999

3001

3004

for Lipschitz constant  $L_g$  of g w.r.t. the first argument, and

$$\sup_{\mathrm{MMD}(\mathcal{H}_g,P,\hat{P})\leq\epsilon}(\mathrm{Bias}(P,g,\hat{P}))=\epsilon||g||_{\mathcal{H}_g}$$

for the RKHS  $\mathcal{H}_g$  of g, respectively. Due to  $L_g$  and  $||g||_{\mathcal{H}_g}$  being unknown in practice, they propose to control the distributional robustness for the 1-th order Wasserstein distance by

$$\epsilon \max_{i}(||\nabla_{x}g(x_{i},\cdot)||),$$

motivated by  $L_g \geq \sup_x(||\nabla_x g(x,\cdot)||)$ , and for the MMD distance, they prove that the original inequality w.r.t. the supremal expectation is satisfied if there exists  $h \in \mathcal{H}$  for some RKHS  $\mathcal{H}$  such that

$$\max_{i}(h(\xi_{i})) + \epsilon||h||_{\mathcal{H}}) \leq 0 \text{ and } g(x,\xi) \leq h(\xi) \ \forall \xi \in \mathcal{U}.$$

Another common robust MPC strategy is tube-based MPC where one assumes that there is a function  $g: 2^{S} \times U \times 2^{\mathbb{R}^{q}}$  such that  $g(s_{t}, u_{t}, v_{t}) \in g(S, u_{t}, N)$ , where  $v_{t} \in \mathbb{R}^{q}$ ,  $S \subset S$  and  $N \subset \mathbb{R}^{q}$ . Furthermore, if  $S_{1} \subset S_{2}$ , it holds that  $g(S_{1}, u, \mathbb{R}^{q}) \subset g(S_{2}, u, \mathbb{R}^{q})$  for all  $u \in U$  (e.g., [287]). In other words, the set of all possible forward reachable states is overapproximated by a tube.

Reference [287] enhance tube-based robust MPC with collision avoidance constraints and train an autonomous agent for a car. Reference [26] apply robust tube-based MPC to the training of an autonomous driving agent in order to avoid collisions with pedestrians, both uncertain static and uncertain dynamic pedestrians. Reference [25] consider MPC that satisfies safety constraints such as collision avoidance or terminal conditions like a full stop or parking, and allow for the state and controller inputs being as close as possible to a reference input. In simulations with a time step size of 0.05 s and a prediction horizon of 20 s, they confirm real-time performance of their controller. Reference [230] consider a robust tube-based MPC for lane keeping of an autonomous vehicle, [142], [157], [215], [179], [350] (experiencing quicker convergence than standard MPC in their simulations), [20], [57] apply it to path tracking, and [340] to overtaking. Reference [98] consider obstacle avoidance using tube-based MPC on icy and snowy roads and confirm real-time capability in their experiments. Reference [290] use tube-based MPC for collision avoidance with moving obstacles. Reference [222] use tube-based MPC in order to let multiple agents satisfy platooning requirements, i.e., maintaining the same speed. Reference [244] combine  $l_1$ -adaptive control, which lets the system behave as a linear model, disregarding uncertainties and perturbations, with tube-based MPC. Delay (even time-varying) as an additional source of uncertainty is also considered, for example in [199], who apply tube-based MPC to steering, and [163], who consider uncertainties in timing due to multiple sources simultaneously, formulate the problem as tube-based MPC, and perform experiments concerning static

collision avoidance and overtaking. Reference [329] consider tube-based robust MPC for autonomous racing.

 $H_{\infty}$ -control considers the  $H_{\infty}$ -norm of the transfer function G of a linear state space model, i.e.,

$$||G||_{\infty} = \sup_{\omega} (\sigma_{\max}(G(j\omega)))$$
 2959

for the maximum singular value  $\sigma_{\rm max}$ . Optimal  $H_{\infty}$ -control considers minimizing  $||T_{zw}||_{\infty}$  where  $T_{zw}$  denotes the upper left block of the transfer matrix G, however, as the solution is often not unique and difficult to compute, one usually relaxes the problem to satisfying  $||T_{zw}(s)||_{\infty} < \gamma$  for some  $\gamma > 0$ . Reference [275] use  $H_{\infty}$ -control for adaptive cruise control and lane change in queues, [116] for path tracking, cruise control and lane change of electric vehicles, [159] consider double lane change and serpentine maneuvers for electric vehicles, [253], [342] steering while driving at constant speed, [160] path following and lateral stability of autonomous electric vehicles, [165] path following and lateral stability of autonomous vehicles, [236] speed and current control for electric vehicles, [242] collision avoidance, [261] lane-keeping, [95] lateral control, and [137], [377] path-tracking.

Reference [278] consider lane change on highways and model the lane switching behavior of the surrounding vehicles as Markov jump process. Let  $\omega$  be a set of parameters that model the uncertainty of the system. Then, for a sample  $\{\hat{\omega}_i\}$ , they compute the empirical distribution  $\hat{P}_n$  and let the ambiguity set be the contamination ball around  $\hat{P}_n$  w.r.t. the TV distance. The robust MPC approach then solves a minimax problem, i.e., finding the control sequence that minimizes that maximum cost over all such distributions.

See also [355] for further references on robust MPC approaches for autonomous driving.

### D. BYZANTINE ROBUSTNESS

Federated and distributed (reinforcement) learning is done for a lot of recent autonomous driving models, see [319] and references therein. Therefore, it is important to ensure Byzantine-robustness of those approaches. Reference [319] themselves craft poisoning attacks against federated learning in a non-linear, autonomous steering control scenario, [102] propose attacks against trajectory prediction via federated learning.

As for distributed RL, [85] consider Byzantine-robustness and suggest classical outlier detection in each learning round by computing the mean of the medians of the estimated policy gradients of each agent and neglecting those which differ by a least two standard deviations from this estimate. Reference [80] consider a general bandit algorithm and allow for a constant  $\epsilon$ -fraction of agents to be byzantine, and propose to compute the shortest interval containing a fixed fraction of rewards so that the mean reward is then given by the mean of the rewards contained in this interval. Reference [58] consider also a trimmed mean in order to estimate the value function in online and offline

3066

3068

3070

3073

3075

3077

3078

3082

3087

3091

3094

3101

3106

3107

3108

3109

3111

3008

3010

3012

3013

3014

3015

3017

3018

3019

3020

3022

3024

3025

3027

3029

3030

3032

3034

3035

3037

3038

3039

3040

3042

3043

3045

3046

3047

3048

3050

3051

3052

3054

3056

3057

3059

distributed RL. Reference [208] propose a poisoning scheme for federated RL and assume that the attacker can perturb the observations of some of the trained RL agents, but has no information about the underlying MPC. They also consider corrupted critic networks in actor-critic RL. Note that in these settings, the individual distributed agents themselves take the role of the instances in the original understanding of casewise contamination.

Further approaches for Byzantine-robustness that are not directly tailored to federated RL are given in the literature. For example, [35] show that no linear aggregation is Byzantine-robust if one single local model is poisoned. Note that analogy to the non-robustness of the mean or the non-robustness of Bagging. They propose Krum, a technique where essentially a variant of the geometric median is computed, more precisely, the local model with the smallest distance to its nearest neighbors. They show that Krum guarantees Byzantine robustness if the fraction of malicious models is smaller than (n/2 - 1), so one could interpret the fraction of 0.5 of malicious models as "Byzantine-BDP" here. The notion of such a BDP has recently been introduced in [113]. Variants of the geometric median have also been considered for example in [186], [286], and [321], or in [56] and [271] where a geometric median of means of gradients is proposed. Reference [351] consider median and trimmed-mean aggregation of the coordinate-wise gradients reported back from the local learners and analyze statistical error rates. Reference [379] improve their work as the bounds in [351] depend on the dimensionality so that the rates may be sub-optimal in high dimensions and also interpret the minimum fraction of Byzantine models that lead to unreliability of the federated learning procedure as BDP.

See [309] for a recent overview of robust federated learning.

### VI. OUTLOOK AND FUTURE WORK

In this section, we outline some ideas of robust strategies that were not yet fully applied to autonomous driving tasks. Moreover, we provide suggestions for benchmarking studies, where different robust algorithms for each of the individual application areas could be compared in order to assess whether some classes of robust algorithms are better suited than other, and to get an intuition about the amount of contamination in typical datasets from the respective area.

### A. FURTHER STRATEGIES FROM ROBUST STATISTICS

The concept of influence functions is rarely seen in the context of autonomous driving in the sense of Robust Statistics, however, the term "influence function" is often used in a physical sense, i.e., quantifying the impact of one physical variable to some property. Influence functions are used as diagnostic tools in deep learning in general, for example, in [174], and they are one of many approaches of XAI (e.g., [16]). [106] propose adversarial attack against influence functions and show that the interpretation of a

neural network based on the influence function is also fragile and highly vulnerable to adversarial attacks.

A particular application in autonomous driving is given in [301] where influence functions are used in order to predict the impact of a data point on pedestrian detection. More precisely, the influence function is used as proxy in order to predict the differences between the test losses for a model trained on the original data and a model trained on data where one instance has been deleted.

Apart from the quantification of the impact of an observation on the estimator, diagnostics based on influence curves can be used to generally strengthen the understanding of the data, for example, whether there are clusters of points with high impact or by trying to find particular properties that make data points influential. This strategy may not only be applied for perception but also for planning in the sense that certain actions or whole trajectories of adversarial agents are identified as influential on the RL training result.

Nevertheless, apart from diagnostic purposes, the influence curve can also be used in order to robustify an estimator directly through the perspective of local robustness. The "robust losses" introduced in Sec. III-D themselves induce bounded influence curves of the corresponding M-estimator by Eq. 2, however, it is also possible to directly robustify the influence curves. To this end, a so-called asymptotic linear expansion of the estimator in the form

$$\hat{\boldsymbol{\theta}}_n = \hat{\boldsymbol{\theta}}_0 + \frac{1}{n} \sum_{i=1}^n \mathrm{IC}(\boldsymbol{X}_i, T, P) + \mathbf{rem}$$

must be valid, for some consistent initial estimator  $\hat{\theta}_0$  and a remainder term **rem** (see, e.g., [259]). This property holds, for example, for asymptotically normal M-estimators [259], SVMs [120], or regularized M-estimators [324]. Given an influence curve, one can formulate different optimization problems in order to robustify the underlying estimator, for example, minimizing the covariance of the influence curve subject to a bound on the bias, minimizing the MSE [259], or finding the estimator the achieves maximum asymptotic relative efficiency even under the worst-case contamination radius [260]. Such "optimally-robust" estimators do not seem to have been considered so far for applications in autonomous driving, but would potentially increase the performance of the trained models compared to those trained according to the classical robust losses.

Another topic, which becomes increasingly important when dealing with high-dimensional data, is variable selection. Robust variable selection algorithms already have been proposed in the literature, for example, the sparse LTS [7], robust Boosting variants [161], [206], or a trimmed Stability Selection [326]. Such techniques could be applied in situations with high-dimensional state spaces in order to identify relevant variables.

In the reviewed literature, except for those considering Kalman filters where contamination in the innovations has already been regarded, one does often not distinguish between contamination in the responses and contamination in

3117

3119

3121

3122

3124

3125

3126

3127

3128

3129

3131

3132

3133

3134

3135

3136

3138

3139

3140

3141

3143

3145

3146

3148

3149

3150

3151

3153

3155

3156

3158

3159

3160

3162

3163

3165

3166

3167

3168

3169

3170



3173

3175

3178

3180

3181

3182

3183

3187

3188

3189

3190

3195

3197

3202

3204

3209

3211

3214

3216

3217

3218

3219

3221

the regressor variables. This distinction is however important because one can argue that outliers in the responses, given clean predictor columns, may naturally be bounded or that large errors may be detectable in advance, implying that unbounded loss functions with a bounded gradient such as the Huber loss function are not problematic here. However, outliers in the predictor columns are known to be more challenging. This situation would even be natural, as the predictor variables are also measurements in some applications such as location estimation via GPS data, where coordinates or clock offsets enter as predictor variables, or vehicle parameter estimation such as tractive forces or electric parameters, where variables such as velocity or voltages are used as predictor variables. Moreover, contamination in the predictor variables occurs when one cannot assume perfect reference data. For example, bounding box estimation is often accompanied with ground truth coordinates, which may be imperfect due to errors done by human annotators, or the reference trajectories in IL are corrupted. Here, robust estimation techniques that allow for this type of contamination, which is more challenging than just considering contamination in the responses, allow for addressing such situations.

Large measurement errors that are a source of contamination in the data are especially problematic in data with a high number of variables and a rather low number of observations. Here, the fraction of contaminated instances can quickly become very large, as a single contaminated cell already makes an instance an outlier (e.g., [10]). Therefore, cell-wise robust approaches have recently been proposed in the literature, i.e., algorithms that can cope with a certain fraction of contaminated cells, even if all instances would be contaminated. For example, there are cell-wise robust counterparts of location and scatter matrix estimation algorithms [5], [180], regression [39], [90], [181], and clustering [100]. In high-dimensional data with an admissible cell-wise contamination scheme (which could be a random selection of perturbed cells as, e.g., having contamination on the response column only would not allow for any advantage of cell-wise robust over case-wise robust algorithms, see [326]), the application of cell-wise robust procedures could improve the robustness against large case-wise contamination rates, even potentially becoming an alternative to RANSAC and its variants.

Outlier detection algorithms have been applied in advance to the data in many references. Unless one faces univariate samples, one should be aware of several pitfalls when trying to detect outliers in multivariate data (see, e.g., [121]). A single large outlier in a multivariate sample can make other outliers invisible, essentially due to deforming the confidence region in a way that other outliers fall within this region, which is referred to as "masking effect". Similarly, non-contaminated observations can, due to the same reason, be located outside the confidence region so that they are incorrectly flagged as outliers, which is referred to as "swamping effect". Therefore, one should not apply a

classical outlier detection algorithm on the dataset once and consider the non-flagged observations as clean. In addition, when assuming an underlying model, as in regression, simply detecting outliers in a model-agnostic way is unlikely to find instances whose entries are insuspicious but which appear as outliers w.r.t. the assumed model. In such settings, model-based outlier detection, which is essentially done in the iterations of LTS, is necessary. As for cell-wise contamination, some strategies for detecting and imputing cell-wise outliers have been proposed, e.g., [255], [263].

# B. SUGGESTIONS FOR BENCHMARK STUDIES AND FUTURE RESEARCH

This survey paper has provided an overview of robust methods in autonomous driving in a comprehensive way and in a unified notation. It should not only serve as a detailed overview for researchers and practitioners, but also pave the way for organizing and conducting benchmarking studies, which are of interest on their own, but beyond the scope of this work.

For nearly each application area, there are already several robust strategies in the literature. Of course, in the respective papers, comparisons already have been made, but often with some selected comptetitors from the literature. The comparison of a large number of algorithms for one specific problem would be desirable. In particular, the navigation section contains a plethora of robust algorithms that follow different strategies: robust criteria, noise modeling or clipping. While robust criteria and clipping follow a similar idea as robust regression approaches, namely downweighting or even neglecting outlying instances during optimization, noise modeling learns the noise distribution and integrates it into the computation of the posterior distribution for the next state. Both strategies are accompanied with advantages and disadvantages. Noise modeling, in particular when using online algorithms such as variational inference, allow for non-stationary noise distributions and have already been successfully applied in real-world settings where both the measurement and the process noise were heavy-tailed, i.e., both additive and innovation outliers occurred. The computation of the posterior distribution allows for the quantification of estimation uncertainty. On the other hand, noise modeling requires assumptions about the noise distributions, while robust optimization criteria are usually applicable under milder assumptions. Therefore, algorithms from each type should be compared on data with both additive and innovation outliers and where the noise distributions are non-stationary. The iterative nature of both variational inference and the optimization of robust criteria usually induces computational overheads compared to a non-robust algorithm. It should be investigated how this overhead scales on real-world data and in dependence of the amount of contamination.

Benchmarking studies could be both based on simulations and real data. As for simulations, the advantage is that via data generation, one can directly control the type and the amount

3282

3284

3287

3294

3301

3306

3308

3311

3313

3315

3316

3318

3322

3323

3325

3328

3330

3332

3225

3227

3229

3231

3232

3234

3235

3236

3237

3238

3239

3241

3242

3243

3244

3246

3248

3249

3250

3251

3253

3255

3256

3258

3259

3260

3261

3263

3265

3268

3270

3272

3273

3274

3275

3277

3279

of contamination, for example, case-wise contamination with outliers only in the responses, only in the regressors, or both, or cell-wise contamination. This would enable to validate different robust algorithms concerning breakdown. Although one can compute theoretical breakdown points, one should be aware of the facts that on the one hand, the breakdown point corresponds to a worst-case scenario, indicating that an estimator does not necessarily break down once the corresponding fraction of instances or cells is contaminated. On the other hand, the algorithm with which the estimator is computed usually is not regarded when computing a breakdown point, therefore, due to numerical pitfalls such as vanishing gradients, it is possible to have an earlier breakdown than expected. Such an effect has been observed in [327] for neural network training.

As for real data, any type of data base with real data and a benchmarking study on such data is of course also of interest on its own. A future benchmarking study should focus on the comparison of the performance of robust algorithms from each individual subsection in this review paper, including non-robust competitors. In particular, on real data, one cannot determine the true underlying contamination model nor the contamination radius. Therefore, one usually applies both a robust and a non-robust method and decides to use the non-robust estimator henceforth if their performance does not differ much or if the classical estimator performs better. In a more granular approach, for any algorithm whose robustness can be controlled, e.g., by the trimming parameter that decides on the size of the clean subset used for fitting, one should apply the respective algorithm with different robustness properties in order to try to implicitly assess the amount of contamination of the data in the real world.

The same argumentation holds for adversarial and Byzantine robustness. In particular, for Byzantine robustness, each contaminated gradient/model/input from an adversarial machine takes the role of one contaminated instance in a standard dataset. As for adversarial robustness, from the perspective of Robust Statistics, one could ask whether a worst-case analysis is possible, and how the amount of contamination could be quantified. Both questions should be addressed in future research.

If a worst-case perspective, without any restrictions, would be pursued, one would likely consider adversarial actions from an adversarial agent where the worst case would correspond to the maximum acceleration or jaw. However, in particular for planning algorithms, there is one crucial aspect when it comes to perturbations/adversarial actions: Realism. This property has already been identified as important in the literature on adversarial attacks on images, e.g., [308]. It is well-known that training strategies such as RL fail if the environment is too challenging, e.g., [298]. Although such edge cases are important for the safety assessment of an autonomous driving system, focusing on them appears not to be the correct way to assess the robustness of the learning algorithm itself in the context of breakdown.

Moreover, one could ask how the amount of contamination should be quantified here, i.e., whether one should count each adversarial action or each adversarial trajectory.

In order to define a breakdown for learned policies, one should check whether the existing definitions of a breakdown from Robust Statistics can be translated. In Robust Statistics, when learning a parametrized model, a breakdown indicates that the learned parameters can be arbitrarily close to the borders of the underlying parameter set, or made arbitrarily large. It should be assessed whether this is possible for the parameters learned when training a parametrized policy, or the control inputs learned in MPC, as well as the implications on the behavior of the agent. Moreover, robustness should not be confused with safety here. For example, consider an autonomous car and a distribution that is learned on its action space. If the environment is extremely challenging, it can learn just not to move. From the perspective of safety, such a behavior could be interpreted as excellent, but from the perspective of Robust Statistics, it could be interpreted as breakdown since it would correspond to (or be close to, depending on the algorithm) a Dirac distribution on a particular value (zero acceleration). Apart from the quantitative robustness that corresponds to the influence curve and the breakdown point, [122] propose a notion of qualitative robustness of an estimator, which indicates that small changes in the underlying distribution (usually measured in the Prokhorov distance) imply only small changes in the estimates. Regularity of the trained policy has already been considered in [220] and [282], where one focuses on the regularity w.r.t. state perturbations. A unified approach would consider a joint distribution on the observed states (e.g., due to measurement errors or in partially observable settings) and the transitions. An approach in order to assess qualitative robustness, in a simulated setting, could be to identify realistic but challenging scenarios, such as complex urban environments or severe weather conditions, and to gradually change the underlying distribution to increase the mass of such challenging situations, or, in other words, to contaminate an "ideal distribution", which should reflect the real world as much as possible, resulting in a contaminated distribution, similarly as in [131], who concentrated on the transition distribution. One may be able to identify when the trained policy starts to deteriorate in the sense that a certain regularity property of the underlying policy no longer holds once the distribution favors challenging situations too strongly. This amount of contamination could then be interpreted as the BDP.

In the reviewed literature, a robust method for either a particular perception or planning area has been presented. A complete autonomous system however is composed by several modules, at least multiple perception modules and a planning module. It is vital to consider the robustness of the whole system. To this end, one would first inspect each individual module and assess its robustness in order to have prior information for further inspections in the case

3337

3339

3341

3342

3344

3345

3346

3348

3349

3351

3352

3354

3355

3356

3358

3359

3361

3363

3365

3366

3368

3370

3372

3373

3375

3377

3378

3379

3380

3382

3383

3385

3387

3389



3393

3398

3400

3402

3405

3410

3412

3417

3419

3422

3424

3425

3427

3430

3432

3433

3436

3439

3440

3441

3442

3443

3444

3445

3446

that the whole system is not robust. Usually, one may argue that the whole system is not robust if at least one module is not robust. On the other hand, applying robust methods for each subsystem may have the disadvantage of a low overall efficiency, as a consequence from the robustification. For example, [279] consider a state-space model in order to incorporate observation noise. This observation noise itself depends on the perception module. Therefore, one should examine to what extend a certain non-robustness in the perception modules could be compensated during the training of a driving policy.

Once an algorithm has proven to be competitive in terms of its generalization performance, accuracy, or security, a crucial question is whether the running time is sufficiently low in order to be applicable in real-world autonomous driving scenarios. In particular, many of the individual tasks require real-time performance. While robust algorithms tolerate contamination which may let non-robust algorithms break down, they are less efficient than non-robust algorithms, so that more training data are required for convergence. The major drawback however is that the optimization of a non-convex loss function, a minimax loss, or, for adversarial training, the optimization of an adversary, may be required, usually resulting in a considerably higher computation time, which could be the main hindrance for real-world applications, regardless of their performance in terms of safety or security. Several of the reviewed papers already confirm in their experiments, some even on real-world data, that their robust algorithm has real-time performance. In addition, for iterative procedures, robustness can even lead to quicker convergence and even to a reduced computation time than a classical algorithm, e.g., [44], [327]. Nevertheless, research on the real-time capabilities of robust algorithms is necessary, in particular when considering the whole autonomous system with many individual modules.

As for the whole system itself, an even broader research question is the interaction between different properties that a system should satisfy, in particular, safety and security. As for security, the reviewed robust approaches for planning as well as for Byzantine robustness already allow for training with adversarial attacks, directly corresponding to security. For perception where training data are given, adversarial robustness does not fall within the scope of Robust Statistics as adversarial attacks are crafted after model training, while Robust Statistics considers the training procedure itself. As explained in Sec. III, poisoning attacks in contrast are crafted before model training. However, as poisoning attacks are usually restricted by a geometric bound, methods from Robust Statistics can be assumed to fail if the majority of the instances is perturbed. Nevertheless, a potential topic for future research could be the interaction between adversarial robustness (also against poisoning attacks) and robustness in the sense of Robust Statistics, i.e., whether methods from Robust Statistics already increase adversarial robustness or how models that are both robust in the sense of Robust Statistics and adversarially robust can be trained. A combination with Byzantine robustness, i.e., training a federated RL model with both Byzantine and adversarial attacks, could also be considered. As for safety in autonomous driving, the goal is to assess whether an autonomous system can perform undesired actions or with which probability such behavior occurs. Although, in particular for deep-learning-based systems, reasoning whether an outlier in the training data of some perception module caused an undesired action may not be possible, one could at least train robust and non-robust subsystems and evaluate whether the robustness of these subsystems affects the safety of the combined system.

While the overall system in the previous paragraphs corresponds to a single autonomous agent, another topic of interest is collborative navigation. If the individual agents communicate, there are multiple state measurements, depending on whether an individual is inside the lane of sight or at least sufficiently close to another agent. As each agent has a different location, it can happen that the perception for some agents suffers from anomalies such as lightning variations. Therefore, regarding the joint information, one has a similar setting as in federated RL. One may consider the corrupted measurements of one agent as Byzantine information. Of course, computing an average or distance-weighted average of the information would lead to corrupted joint information. Here, one may consider integrating a robust aggregation procedure, such as a trimmed mean, into the algorithm that infers the next states. Nevertheless, in this context, other problems additionally need to be solved, such as communication delays or data loss, as argued in [276], or correlated observations among the individual agents (e.g., [48], [205]). On top of that, [299] consider adversarial interference in the inter-agent communication. Future research may consider Byzantine-robust federated training of robust collaborative agents.

### **ACKNOWLEDGMENT**

The author would like to thank Peter Ruckdeschel, Martin Fränzle, and Eike Möhlmann for helpful comments and/or discussions, as well as three anonymous referees for their valuable comments that helped to improve the quality of the article. Of course, he is solely responsible for any errors. He also thanks the consortium for the successful cooperation.

### **REFERENCES**

- G. Agamennoni, J. I. Nieto, and E. M. Nebot, "An outlier-robust Kalman filter," in *Proc. IEEE Int. Conf. Robot. Autom.*, May 2011, pp. 1551–1558.
- [2] G. Agamennoni, J. I. Nieto, and E. M. Nebot, "Approximate inference in state-space models with heavy-tailed noise," *IEEE Trans. Signal Process.*, vol. 60, no. 10, pp. 5024–5037, Oct. 2012.
- [3] P. Agarwal, "Robust graph-based localization mapping," Ph.D. thesis, Technische Fakultät, Albert-Ludwigs-Universität Freiburg, Freiburg, Germany, 2015.
- [4] P. Agarwal, G. D. Tipaldi, L. Spinello, C. Stachniss, and W. Burgard, "Robust map optimization using dynamic covariance scaling," in *Proc. IEEE Int. Conf. Robot. Autom.*, May 2013, pp. 62–69.

3521

3522

3523

3524

3525

3526

3527

3529

3530

3531

3532

3533

3534

3535

3536

3537

3538

3540

3541

3542

3543

3544

3545

3547

3549

3550

3551

3552

3554

3555

3556

3557

3558

3559

3560

3561

3563

3565

3567

3568

3569

3570

3571

3572

3573

3574

3576

3578

3579

3580

3581

3582

3583

3584

3585

3587

3588

3589

3590

3591

3592

3593



3447

3448

3449

3450

3451

3452

3453

3454

3455

3456

3457

3458

3459

3460

3461

3462

3463

3464

3465

3466

3467

3468

3470

3471

3472

3473

3474

3475

3476

3478

3479

3480

3481

3482

3483

3484

3485

3486

3487

3488

3489

3490

3491

3492

3493

3494

3495

3496

3497

3498

3499

3500

3501

3502

3503

3504

3505

3506

3507

3508

3509

3514

3515

3516

3517

3518

3519

- [5] C. Agostinelli, A. Leung, V. J. Yohai, and R. H. Zamar, "Robust estimation of multivariate location and scatter in the presence of cellwise and casewise contamination," *TEST*, vol. 24, no. 3, pp. 441–461, Sep. 2015.
  - [6] M. Akram, P. Liu, Y. Wang, and J. Qian, "GNSS positioning accuracy enhancement based on robust statistical MM estimation theory for ground vehicles in challenging environments," *Appl. Sci.*, vol. 8, no. 6, p. 876, May 2018.
  - [7] A. Alfons, C. Croux, and S. Gelper, "Sparse least trimmed squares regression for analyzing high-dimensional large data sets," *Ann. Appl. Statist.*, vol. 7, no. 1, pp. 226–248, Mar. 2013.
  - [8] P. Almasi, R. Moni, and B. Gyires-Toth, "Robust reinforcement learning-based autonomous driving agent for simulation and real world," in *Proc. Int. Joint Conf. Neural Netw. (IJCNN)*, Jul. 2020, pp. 1–8.
  - [9] M. T. Alonso, C. Ferigato, D. I. Segura, D. Perrotta, A. Rovira-Garcia, and E. Sordini, "Analysis of 'pre-fit' datasets of gLAB by robust statistical techniques," *Stats*, vol. 4, no. 2, pp. 400–418, May 2021.
  - [10] F. Alqallaf, S. Van Aelst, V. J. Yohai, and R. H. Zamar, "Propagation of outliers in multivariate data," *Ann. Statist.*, vol. 37, no. 1, pp. 311–331, Feb. 2009.
- [11] A. Amini, I. Gilitschenski, J. Phillips, J. Moseyko, R. Banerjee, S. Karaman, and D. Rus, "Learning robust control policies for end-to-end autonomous driving from data-driven simulation," *IEEE Robot. Autom. Lett.*, vol. 5, no. 2, pp. 1143–1150, Apr. 2020.
- [12] A. Angrisano and S. Gaglione, "Mitigation of leverage observation effects in GNSS robust positioning," in *Proc. IEEE Int. Workshop Metrol.* Sea; Learn. Measure Sea Health Parameters (MetroSea), Oct. 2018, pp. 278–282.
- [13] M. O. A. Aqel, M. H. Marhaban, M. I. Saripan, and N. B. Ismail, "Review of visual odometry: Types, approaches, challenges, and applications," *SpringerPlus*, vol. 5, no. 1, pp. 1897–1922, Dec. 2016.
- [14] I. Arasaratnam and S. Haykin, "Cubature Kalman filters," *IEEE Trans. Autom. Control*, vol. 54, no. 6, pp. 1254–1269, Jun. 2009.
- [15] M. u. I. Arif, M. Jameel, and L. Schmidt-Thieme, "Directly optimizing IoU for bounding box localization," in *Proc. Asian Conf. Pattern Recognit.*, 2020, pp. 544–556.
- [16] A. B. Arrieta, N. Díaz-Rodríguez, J. Del Ser, A. Bennetot, S. Tabik, and A. Barbado, "Explainable artificial intelligence (XAI): Concepts, taxonomies, opportunities and challenges toward responsible AI," *Inf. Fusion*, vol. 58, pp. 82–115, Jun. 2020.
- [17] B. W. Babu, S. Kim, Z. Yan, and L. Ren, "S-DVO: Sensor noise model meets dense visual odometry," in *Proc. IEEE Int. Symp. Mixed Augmented Reality (ISMAR)*, Sep. 2016, pp. 18–26.
- [18] P. Bacon, J. Harb, and D. Precup, "The option-critic architecture," in Proc. AAAI Conf. Artif. Intell., vol. 31, 2017, pp. 1726–1734.
- [19] M. Bansal, A. Krizhevsky, and A. Ogale, "ChauffeurNet: Learning to drive by imitating the best and synthesizing the worst," 2018, arXiv:1812.03079.
- [20] H. Bao and R. Huang, "Tube-based model predictive control for unmanned vehicles trajectory tracking," in *Proc. 2nd Int. Conf. Electr. Technol. Autom. Eng. (ETAE)*, May 2025, pp. 555–560.
- [21] J. Bao, X. Mu, X. Yu, Z. Zhu, and H. Qin, "Outlier-robust underwater navigation using a dual-robust-kernel Kalman filter," *IEEE Signal Process. Lett.*, vol. 32, pp. 1485–1489, 2025.
- [22] J. Bao, X. Yu, X. Mu, C. Hu, and H. Qin, "Geometric extended Kalman filter with dual robust kernels for integrated navigation," *IEEE Trans. Instrum. Meas.*, vol. 74, pp. 1–17, 2025.
- [23] J. T. Barron, "A general and adaptive robust loss function," in *Proc. IEEE/CVF Conf. Comput. Vis. Pattern Recognit. (CVPR)*, Jun. 2019, pp. 4331–4339.
- [24] O. Bastani, Y. Ioannou, L. Lampropoulos, D. Vytiniotis, A. Nori, and A. Criminisi, "Measuring neural net robustness with constraints," in Proc. Adv. Neural Inf. Process. Syst., 2016, pp. 2613–2621.
- I. Batkovic, A. Gupta, M. Zanon, and P. Falcone, "Experimental validation of safe MPC for autonomous driving in uncertain environments,"
   IEEE Trans. Control Syst. Technol., vol. 31, no. 5, pp. 2027–2042,
   Sep. 2023.
  - [26] I. Batkovic, U. Rosolia, M. Zanon, and P. Falcone, "A robust scenario MPC approach for uncertain multi-modal obstacles," *IEEE Control Syst. Lett.*, vol. 5, no. 3, pp. 947–952, Jul. 2020.
    - [27] H. Bay, A. Ess, T. Tuytelaars, and L. Van Gool, "Speeded-up robust features (SURF)," *Comput. Vis. Image Understand.*, vol. 110, no. 3, pp. 346–359, Jun. 2008.

- [28] A. Bellés and D. Medina, "Robust PPP-AR using M-estimators for multifault scenarios," in *Proc. IEEE/ION Position, Location Navigat. Symp.* (PLANS), Apr. 2025, pp. 251–257.
- [29] A. Bellés, D. Medina, P. Chauchat, S. Labsir, and J. Vilà-Valls, "Robust error-state Kalman-type filters for attitude estimation," *EURASIP J. Adv. Signal Process.*, vol. 2024, no. 1, p. 75, Jul. 2024.
- [30] A. Bellés, D. Medina, P. Chauchat, and J. Vilà-Valls, "Reliable GNSS joint position and attitude estimation in harsh environments through robust statistics," in *Proc. IEEE Aerosp. Conf. (AERO)*, Mar. 2022, pp. 1–9.
- [31] P. Bergström and O. Edlund, "Robust registration of point sets using iteratively reweighted least squares," *Comput. Optim. Appl.*, vol. 58, no. 3, pp. 543–561, Jul. 2014.
- [32] S. Beyer, "Robuste Parameterschätzung für Elektrofahrzeuge," Ph.D. thesis, Fakultät für Elektrotechnik und Informationstechnik, Universitätsbibliothek der Universität der Bundeswehr München, Munich. Germany. 2019.
- [33] M. J. Black and P. Anandan, "A framework for the robust estimation of optical flow," in *Proc. 4th Int. Conf. Comput. Vis.*, May 1993, pp. 231–236.
- [34] M. J. Black and P. Anandan, "The robust estimation of multiple motions: Parametric and piecewise-smooth flow fields," *Comput. Vis. Image Understand.*, vol. 63, no. 1, pp. 75–104, Jan. 1996.
- [35] P. Blanchard, E. M. E. Mhamdi, R. Guerraoui, and J. Stainer, "Machine learning with adversaries: Byzantine tolerant gradient descent," in *Proc. Adv. Neural Inf. Process. Syst.*, vol. 30, 2017, pp. 118–128.
- [36] G. Blewitt, C. Kreemer, W. C. Hammond, and J. Gazeaux, "MIDAS robust trend estimator for accurate GPS station velocities without step detection," *J. Geophys. Res., Solid Earth*, vol. 121, no. 3, pp. 2054–2068, Mar. 2016.
- [37] B. Xu, A. A. Razzaqi, and Y. Liu, "Cooperative localisation of AUVs based on Huber-based robust algorithm and adaptive noise estimation," *J. Navigat.*, vol. 72, no. 4, pp. 875–893, 2019.
- [38] A. Borkar, M. Hayes, and M. T. Smith, "Robust lane detection and tracking with ransac and Kalman filter," in *Proc. 16th IEEE Int. Conf. Image Process. (ICIP)*, Nov. 2009, pp. 3261–3264.
- [39] L. Bottmer, C. Croux, and I. Wilms, "Sparse regression for large data sets with outliers," Eur. J. Oper. Res., vol. 297, no. 2, pp. 782–794, Mar. 2022.
- [40] H. Calatrava, D. Medina, and P. Closas, "Towards robust collaborative DGNSS in the presence of outliers," in *Proc. IEEE/ION Position*, *Location Navigat. Symp. (PLANS)*, Apr. 2025, pp. 328–336.
- [41] Campo and Morari, "Robust model predictive control," in *Proc. Amer. control Conf.*, vol. 24, Jun. 1987, pp. 1021–1026.
- [42] N. Carlini and D. Wagner, "Towards evaluating the robustness of neural networks," in *Proc. IEEE Symp. Secur. Privacy (SP)*, May 2017, pp. 39–57.
- [43] J. Obando-Ceron and P. S. Castro, "Revisiting rainbow: Promoting more insightful and inclusive deep reinforcement learning research," in *Proc. Int. Conf. Mach. Learn.*, 2020, pp. 1373–1383.
- [44] K. H. Chan, A. Mustapha, and M. A. Jubair, "Comparative analysis of loss functions in TD3 for autonomous parking," J. Soft Comput. Data Mining, vol. 5, no. 1, pp. 1–14, Jun. 2024.
- [45] G. Chang, "Robust Kalman filtering based on Mahalanobis distance as outlier judging criterion," *J. Geodesy*, vol. 88, no. 4, pp. 391–401, Apr. 2014.
- [46] L. Chang, B. Hu, G. Chang, and A. Li, "Huber-based novel robust unscented Kalman filter," *IET Sci., Meas. Technol.*, vol. 6, no. 6, pp. 502–509, Nov. 2012.
- [47] L. Chang, K. Li, and B. Hu, "Huber's M-estimation-based process uncertainty robust filter for integrated INS/GPS," *IEEE Sensors J.*, vol. 15, no. 6, pp. 3367–3374, Jun. 2015.
- [48] T.-K. Chang, K. Chen, and A. Mehta, "Resilient and consistent multirobot cooperative localization with covariance intersection," *IEEE Trans. Robot.*, vol. 38, no. 1, pp. 197–208, Feb. 2022.
- [49] B. Chen, X. Liu, H. Zhao, and J. C. Principe, "Maximum correntropy Kalman filter," *Automatica*, vol. 76, pp. 70–77, Feb. 2017.
- [50] Q. Chen, B. Yu, C. Zhong, Z. Jiang, D. You, and Y. Cai, "Study on vehicle state and tire-road friction coefficient estimation based on maximum correntropy generalized high-degree cubature Kalman filter," *Trans. Inst. Meas. Control*, pp. 1–12, Oct. 2024.
- [51] W. Chen, L. Chen, R. Wang, and M. Pollefeys, "LEAP-VO: Long-term effective any point tracking for visual odometry," in *Proc. IEEE/CVF Conf. Comput. Vis. Pattern Recognit. (CVPR)*, Jun. 2024, pp. 19844–19853.

3595

3596 3597

3598

3599

3600

3601

3602

3603

3604

3605

3606

3607

3608

3609

3610

3611

3612

3613

3614

3615

3616

3617

3618

3619

3620

3621

3622

3623

3624

3625

3626

3627

3628

3629

3630

3631

3632

3633

3634

3635

3636

3637

3638

3639

3640

3641

3642

3643

3644

3645

3647

3648

3649

3650

3651

3652

3653

3654

3657

3658

3659

3660

3661



3666

3667

3668

3669

3670

3671

3672

3673

3674

3675

3676

3677

3678

3679

3680

3681

3682

3683

3684

3685

3686

3687

3688

3689

3690

3691

3692

3693

3694

3695

3696

3697

3698

3699

3700

3702

3703

3704

3705

3706

3707

3708

3709

3710

3711

3712

3713

3714

3715

3716

3717

3718

3719

3720

3721

3722

3723

3724

3725

3726

3727

3728

3729

3730

3731

3732

3733

3734

3735

3736

3737

3738

- [52] W. Chen, Z. Li, Z. Chen, Y. Sun, and Y. Liu, "Multiple similarity measure-based maximum correntropy criterion Kalman filter with adaptive kernel width for GPS/INS integration navigation," *Measurement*, vol. 222, Nov. 2023, Art. no. 113666.
- [53] X. Chen, K. Kundu, Z. Zhang, H. Ma, S. Fidler, and R. Urtasun, "Monocular 3D object detection for autonomous driving," in *Proc. IEEE Conf. Comput. Vis. Pattern Recognit. (CVPR)*, Jun. 2016, pp. 2147–2156.
- [54] X. Chen, H. Ma, J. Wan, B. Li, and T. Xia, "Multi-view 3D object detection network for autonomous driving," in *Proc. IEEE Conf. Comput. Vis. Pattern Recognit. (CVPR)*, Jul. 2017, pp. 1907–1915.
- [55] Y. Chen, W. Li, and Y. Du, "A novel robust adaptive Kalman filter with application to urban vehicle integrated navigation systems," *Measurement*, vol. 236, Aug. 2024, Art. no. 114844.
- [56] Y. Chen, L. Su, and J. Xu, "Distributed statistical machine learning in adversarial settings: Byzantine gradient descent," in *Proc. ACM Meas. Anal. Comput. Syst.*, 2017, pp. 1–25.
- [57] Y. Chen, Y. Sun, J. Li, J. He, and C. He, "Tube-based robust model predictive control for autonomous vehicle with complex road scenarios," *Appl. Sci.*, vol. 15, no. 12, p. 6471, Jun. 2025.
- [58] Y. Chen, X. Zhang, K. Zhang, M. Wang, and X. Zhu, "Byzantine-robust online and offline distributed reinforcement learning," in *Proc. Int. Conf. Artif. Intell. Statist.*, 2022, pp. 3230–3269.
- [59] D. Chetverikov and D. Stepanov, "Robust Euclidean alignment of 3D point sets," in *Proc. 1st Hung. Conf. Comput. Graph. Geometry*, 2002, pp. 70–75.
- [60] W. T. Chor, C. P. Tan, A. S. M. Bakibillah, Z. Pu, and J. Y. Loo, "Robust vehicle mass estimation using recursive least M-squares algorithm for intelligent vehicles," *IEEE Trans. Intell. Vehicles*, vol. 9, no. 1, pp. 165–177, Jan. 2024.
- [61] S. Chu, H. Qian, S. Yan, and P. Ding, "Adaptive robust maximum correntropy cubature Kalman filter for spacecraft attitude estimation," *Adv. Space Res.*, vol. 72, no. 8, pp. 3376–3385, Oct. 2023.
- [62] A. I. Comport, E. Malis, and P. Rives, "Accurate quadrifocal tracking for robust 3D visual odometry," in *Proc. IEEE Int. Conf. Robot. Autom.*, Apr. 2007, pp. 40–45.
- [63] A. I. Comport, E. Malis, and P. Rives, "Real-time quadrifocal visual odometry," Int. J. Robot. Res., vol. 29, nos. 2–3, pp. 245–266, Feb. 2010.
- [64] O. G. Crespillo, A. Andreetti, and A. Grosch, "Design and evaluation of robust M-estimators for GNSS positioning in urban environments," in *Proc. Int. Tech. Meeting The Inst. Navigat.*, San Diego, CA, USA, Feb. 2020, pp. 21–24.
- [65] O. G. Crespillo, D. Medina, J. Skaloud, and M. Meurer, "Tightly coupled GNSS/INS integration based on robust M-estimators," in *Proc. IEEE/ION Position, Location Navigat. Symp. (PLANS)*, Apr. 2018, pp. 1554–1561.
- [66] B. Cui, W. Chen, D. Weng, J. Wang, X. Wei, and Y. Zhu, "Variational resampling-free cubature Kalman filter for GNSS/INS with measurement outlier detection," *Signal Process.*, vol. 237, Dec. 2025, Art. no. 110036.
- [67] A. Cunillera, R. M. Lentink, N. van Oort, and R. M. P. Goverde, "Robust train motion model calibration based on M-estimation," *Authorea Preprints*, pp. 1–10, Oct. 2023.
- [68] S. Das, "Robust state estimation methods for robotics applications," Ph.D. thesis, Dept. Mech. Aerosp. Eng., West Virginia Univ., Morgantown, WV, USA, 2023.
- [69] S. Das, C. Kilic, R. Watson, and J. Gross, "A comparison of robust Kalman filters for improving wheel-inertial odometry in planetary rovers," in *Proc. I<sub>ON</sub> GNSS+*, *Int. Tech. Meeting Satell. Division Inst. Navigat.*, Oct. 2021, pp. 2621–2632.
- [70] P. Dasgupta, "Divide and repair: Using options to improve performance of imitation learning against adversarial demonstrations," 2023, arXiv:2306.04581.
- [71] P. L. Davies and U. Gather, "Breakdown and groups," Ann. Statist.,
   vol. 33, no. 3, pp. 977–1035, Jun. 2005.
  - [72] D. De Palma and G. Indiveri, "Output outlier robust state estimation," Int. J. Adapt. Control Signal Process., vol. 31, no. 4, pp. 581–607, Apr. 2017.
  - [73] Z. Deng, Y. Yao, B. Deng, and J. Zhang, "A robust loss for point cloud registration," in *Proc. IEEE/CVF Int. Conf. Comput. Vis. (ICCV)*, Oct. 2021, pp. 6118–6127.
- [74] Y. Ding, G. Pagès, P. Asseman, and É. Chaumette, "Robust tightly coupled GNSS/INS experimental assessment for autonomous aircraft inspection," in *Proc. I<sub>ON</sub> GNSS+*, *Int. Tech. Meeting Satell. Division Inst. Navigat.*, Oct. 2021, pp. 3452–3463.

- [75] Y. Ding, P. Chauchat, G. Pages, and P. Asseman, "Learning-enhanced adaptive robust GNSS navigation in challenging environments," *IEEE Robot. Autom. Lett.*, vol. 7, no. 4, pp. 9905–9912, Oct. 2022.
- [76] Y. Ding, F. Feriol, Y. Watanabe, P. Asseman, G. Pages, and D. Vivet, "Adaptive robust-statistics GNSS navigation based on environmental context detection," in *Proc. Int. Tech. Meeting The Inst. Navigat.*, Feb. 2023, pp. 138–152.
- [77] P. D. Domanski and M. Lawrynczuk, "Impact of MPC embedded performance index on control quality," *IEEE Access*, vol. 9, pp. 24787–24795, 2021.
- [78] D. L. Donoho and P. J. Huber, "The notion of breakdown point," in A Festschrift for Erich L. Lehmann. Belmont, CA, USA: Wadsworth International Group, 1983, pp. 157–184.
- [79] A. Dötlinger and R. M. Kennel, "Near time-optimal model predictive control using an L1-norm based cost functional," in *Proc. IEEE Energy Convers. Congr. Expo. (ECCE)*, Sep. 2014, pp. 3504–3511.
- [80] A. Dubey and A. Pentland, "Private and Byzantine-proof cooperative decision-making," 2022, arXiv:2205.14174.
- [81] S. R. Eftekhari, S. A. Davari, P. Naderi, C. Garcia, and J. Rodriguez, "Robust loss minimization for predictive direct torque and flux control of an induction motor with electrical circuit model," *IEEE Trans. Power Electron.*, vol. 35, no. 5, pp. 5417–5426, May 2020.
- [82] F. El-Hawary and Y. Jing, "Robust regression-based EKF for tracking underwater targets," *IEEE J. Ocean. Eng.*, vol. 20, no. 1, pp. 31–41, Jan. 1995.
- [83] M. Elsisi, M. Altius, S.-F. Su, and C.-L. Su, "Robust Kalman filter for position estimation of automated guided vehicles under cyberattacks," *IEEE Trans. Instrum. Meas.*, vol. 72, pp. 1–12, 2023.
- [84] J. Fan, X. Lei, X. Chang, J. Mišić, V. B. Mišić, and Y. Yao, "Less is more: A stealthy and efficient adversarial attack method for DRL-based autonomous driving policies," *IEEE Internet Things J.*, vol. 12, no. 15, pp. 30215–30227, Aug. 2025.
- [85] F. X. Fan, Y. Ma, Z. Dai, J. Wei, C. Tan, and B. K. H. Low, "Fault-tolerant federated reinforcement learning with theoretical guarantee," in Proc. Adv. Neural Inf. Process. Syst., 2021, pp. 1007–1021.
- [86] Y. Fan, S. Qiao, G. Wang, and H. Zhang, "An improved Sage-Husa variational robust adaptive Kalman filter with uncertain noise covariances," *IEEE Sensors J.*, vol. 24, no. 18, pp. 28921–28930, Sep. 2024.
- [87] H. Fang, M. A. Haile, and Y. Wang, "Robust extended Kalman filtering for systems with measurement outliers," *IEEE Trans. Control Syst. Technol.*, vol. 30, no. 2, pp. 795–802, Mar. 2022.
- [88] Y. Fei, B. Xu, X. Wang, and Y. Guo, "A novel current estimation and cooperative localization method under unknown current and non-Gaussian noise," *IEEE Trans. Instrum. Meas.*, vol. 74, pp. 1–13, 2025.
- [89] D. Feng, C. Haase-Schütz, L. Rosenbaum, H. Hertlein, C. Gläser, F. Timm, W. Wiesbeck, and K. Dietmayer, "Deep multi-modal object detection and semantic segmentation for autonomous driving: Datasets, methods, and challenges," *IEEE Trans. Intell. Transp. Syst.*, vol. 22, no. 3, pp. 1341–1360, Mar. 2021.
- [90] P. Filzmoser, S. Höppner, I. Ortner, S. Serneels, and T. Verdonck, "Cellwise robust m regression," *Comput. Statist. Data Anal.*, vol. 147, Jul. 2020, Art. no. 106944.
- [91] A. T. M. Fisch, I. A. Eckley, and P. Fearnhead, "Innovative and additive outlier robust Kalman filtering with a robust particle filter," *IEEE Trans. Signal Process.*, vol. 70, pp. 47–56, 2022.
- [92] M. A. Fischler and R. C. Bolles, "Random sample consensus: A paradigm for model fitting with applications to image analysis and automated cartography," *Commun. ACM*, vol. 24, no. 6, pp. 381–395, 1981.
- [93] A. W. Fitzgibbon, "Robust registration of 2D and 3D point sets," *Image Vis. Comput.*, vol. 21, nos. 13–14, pp. 1145–1153, Dec. 2003.
- [94] A. Fontan, J. Civera, and M. Milford, "Adaptive outlier thresholding for bundle adjustment in visual SLAM," in *Proc. IEEE Int. Conf. Robot. Autom. (ICRA)*, May 2024, pp. 3969–3976.
- [95] G. Gagliardi, M. Lupia, G. Cario, and A. Casavola, "Optimal  $H_{\infty}$  control for lateral dynamics of autonomous vehicles," *Sensors*, vol. 21, no. 12, p. 4072, Jun. 2021.
- [96] S. Gaglione, A. Innac, S. Pastore Carbone, S. Troisi, and A. Angrisano, "Robust estimation methods applied to GPS in harsh environments," in *Proc. Eur. Navigat. Conf. (ENC)*, May 2017, pp. 14–25.
- [97] M. A. Gandhi and L. Mili, "Robust Kalman filter based on a generalized maximum-likelihood-type estimator," *IEEE Trans. Signal Process.*, vol. 58, no. 5, pp. 2509–2520, May 2010.

3813

3814

3815

3816

3818

3819

3820

3821

3822

3823

3825

3827

3828

3830

3831

3832

3833

3834

3836

3837

3838

3839

3840

3841

3842

3843

3844

3845

3846

3847

3849

3850

3851

3852

3853

3854

3855

3856

3857

3858

3859

3860

3861

3862

3863

3864

3865

3866

3867

3868

3869

3870

3872

3873

3874

3877

3878

3879

3880

3881

3882

3883



3744

3745

3746

3747

3748

3749

3750

3751

3752

3753

3754

3755

3756

3757

3758

3759

3760

3761

3762

3763

3764

3765

3766

3767

3768

3769

3770

3771

3772

3773

3774

3775

3779

3780

3781

3782

3783

3784

3785

3786

3787

3788

3789

3790

3791

3792

3793

3795

3796

3797

3804

3805

3806

- [98] Y. Gao, "Model predictive control for autonomous and semiautonomous vehicles," Ph.D. thesis, Dept. Mech. Eng., Univ. California, Berkeley, CA, USA, 2014.
- 3742 [99] J. García and F. Fernández, "A comprehensive survey on safe reinforce-3743 ment learning," J. Mach. Learn. Res., vol. 16, no. 1, pp. 1437–1480, 2015.
  - [100] L. A. García-Escudero, D. Rivera-García, A. Mayo-Iscar, and J. Ortega, "Cluster analysis with cellwise trimming and applications for the robust clustering of curves," *Inf. Sci.*, vol. 573, pp. 100–124, Sep. 2021.
  - [101] J. L. García-Lapresta and D. Pérez-Román, "Measuring consensus in weak orders," in *Consensual Processes*. Berlin, Germany: Springer, 2011, pp. 213–234.
  - [102] S. Garg, H. Jönsson, G. Kalander, A. Nilsson, B. Pirange, V. Valadi, and J. Östman, "Poisoning attacks on federated learning for autonomous driving," 2024, arXiv:2405.01073.
  - [103] P. Ge, C. Zhang, T. Zhang, L. Guo, and Q. Xiang, "Maximum correntropy square-root cubature Kalman filter with state estimation for distributed drive electric vehicles," *Appl. Sci.*, vol. 13, no. 15, p. 8762, 2023.
  - [104] S. Geisler, T. S. Schmidt, H. Şirin, D. Zügner, A. Bojchevski, and S. Günnemann, "Robustness of graph neural networks at scale," in *Proc. Adv. Neural Inf. Process. Syst.*, 2021, pp. 7637–7649.
  - [105] S. Geisler, D. Zügner, and S. Günnemann, "Reliable graph neural networks via robust aggregation," in *Proc. Adv. Neural Inf. Process.* Syst., 2020, pp. 13272–13284.
  - [106] A. Ghorbani, A. Abid, and J. Zou, "Interpretation of neural networks is fragile," in *Proc. AAAI Conf. Artif. Intell.*, 2017, pp. 3681–3688.
  - [107] R. Girod, M. Hauswirth, P. Pfreundschuh, M. Biasio, and R. Siegwart, "A robust baro-radar-inertial odometry M-estimator for multicopter navigation in cities and forests," in *Proc. IEEE Int. Conf. Multisensor Fusion Integr. Intell. Syst. (MFI)*, Sep. 2024, pp. 1–8.
  - [108] R. Girshick, "Fast R-CNN," in Proc. IEEE Int. Conf. Comput. Vis. (ICCV), Dec. 2015, pp. 1440–1448.
  - [109] R. Gnanadesikan and J. R. Kettenring, "Robust estimates, residuals, and outlier detection with multiresponse data," *Biometrics*, vol. 28, no. 1, pp. 81–124, Mar. 1972.
  - [110] T. Gonçalves and A. I. Comport, "Real-time direct tracking of color images in the presence of illumination variation," in *Proc. IEEE Int. Conf. Robot. Autom.*, May 2011, pp. 4417–4422.
- 3776 [111] I. J. Goodfellow, J. Shlens, and C. Szegedy, "Explaining and harnessing adversarial examples," 2014, *arXiv:1412.6572*.
  - [112] L. Gosch, D. Sturm, S. Geisler, and S. Günnemann, "Revisiting robustness in graph machine learning," in *Proc. Workshop Trustworthy Socially Responsible Mach. Learn.*, 2023, pp. 1–29.
  - [113] R. Guerraoui, N. Gupta, and R. Pinot, "Byzantine machine learning: A primer," ACM Comput. Surv., vol. 56, no. 7, pp. 1–39, Jul. 2024.
  - [114] A. Guillard, P. Thevenon, C. Milner, and C. Macabiau, "Benefits of CNN-based multipath detection for robust GNSS positioning," in *Proc. I<sub>ON</sub> GNSS+*, *Int. Tech. Meeting Satell. Division Inst. Navigat.*, Oct. 2023, pp. 283–297.
  - [115] J. Guo, L. Ren, X. Zhu, J. Zhuang, B. Jiang, C. Liu, and L. Wang, "Pseudo-Huber loss function-based affine registration algorithm of point clouds," in *Proc. 39th Youth Academic Annu. Conf. Chin. Assoc. Autom.* (YAC), Jun. 2024, pp. 1034–1039.
  - [116] M. Guo, C. Bao, Q. Cao, F. Xu, X. Miao, and J. Wu, "Fault-tolerant control study of four-wheel independent drive electric vehicles based on drive actuator faults," *Machines*, vol. 12, no. 7, p. 450, Jun. 2024.
  - [117] W. Guo, G. Liu, Z. Zhou, J. Wang, Y. Tang, and M. Wang, "Robust training in multiagent deep reinforcement learning against optimal adversary," *IEEE Trans. Syst. Man, Cybern. Syst.*, vol. 55, no. 7, pp. 4957–4968, Jul. 2025.
- 3798 [118] W. Guo, B. Tondi, and M. Barni, "An overview of backdoor attacks 3799 against deep neural networks and possible defences," *IEEE Open J.* 3800 *Signal Process.*, vol. 3, pp. 261–287, 2022.
- [119] S. Gupta, A. Mohanty, and G. Gao, "Urban localization using robust filtering at multiple linearization points," EURASIP J. Adv. Signal Process., vol. 2023, no. 1, p. 100, Oct. 2023.
  - [120] R. Hable, "Asymptotic normality of support vector machine variants and other regularized kernel methods," J. Multivariate Anal., vol. 106, pp. 92–117, Apr. 2012.
- [121] F. Hampel, E. Ronchetti, P. Rousseeuw, and W. Stahel, Robust Statistics:
   The Approach Based on Influence Functions, vol. 114. Hoboken, NJ,
   USA: Wiley, 2011.
- [122] F. R. Hampel, "A general qualitative definition of robustness," *Ann. Math. Statist.*, vol. 42, no. 6, pp. 1887–1896, Dec. 1971.

- [123] F. R. Hampel, "The influence curve and its role in robust estimation," J. Amer. Stat. Assoc., vol. 69, no. 346, pp. 383–393, Jun. 1974.
- [124] G. Han, F. Liu, J. Deng, W. Bai, X. Deng, and K. Li, "An adaptive vehicle tracking enhancement algorithm based on fuzzy interacting multiple model robust cubature Kalman filtering," *Circuits, Syst., Signal Process.*, vol. 43, no. 1, pp. 191–223, Jan. 2024.
- [125] S.-J. Han, J. Kang, K.-W. Min, and J. Choi, "DiLO: Direct light detection and ranging odometry based on spherical range images for autonomous driving," *ETRI J.*, vol. 43, no. 4, pp. 603–616, Aug. 2021.
- [126] P. Hao, O. Karakuş, and A. Achim, "Robust Kalman filters based on the sub-Gaussian  $\alpha$ -stable distribution," *Signal Process.*, vol. 224, pp. 1–12, Nov. 2024.
- [127] B. He, L. Zheng, Y. Jin, and Y. Li, "A robust adaptive estimator for sideslip angle and tire-road forces under time-varying and abnormal noise," *IEEE Sensors J.*, vol. 25, no. 9, pp. 15723–15734, May 2025.
- [128] M. He, C. Zhu, Q. Huang, B. Ren, and J. Liu, "A review of monocular visual odometry," Vis. Comput., vol. 36, no. 5, pp. 1053–1065, May 2020.
- [129] R. He, Y. Shan, and K. Huang, "Robust cooperative localization with failed communication and biased measurements," *IEEE Robot. Autom. Lett.*, vol. 9, no. 3, pp. 2997–3004, Mar. 2024.
- [130] S. He, S. Han, and F. Miao, "Robust electric vehicle balancing of autonomous mobility-on-demand system: A multi-agent reinforcement learning approach," in *Proc. IEEE/RSJ Int. Conf. Intell. Robots Syst.* (IROS), Oct. 2023, pp. 5471–5478.
- [131] S. He, Y. Wang, S. Han, S. Zou, and F. Miao, "A robust and constrained multi-agent reinforcement learning electric vehicle rebalancing method in AMoD systems," in *Proc. IEEE/RSJ Int. Conf. Intell. Robots Syst. (IROS)*, Oct. 2023, pp. 5637–5644.
- [132] S. He, Z. Zhang, S. Han, L. Pepin, G. Wang, D. Zhang, J. A. Stankovic, and F. Miao, "Data-driven distributionally robust electric vehicle balancing for autonomous mobility-on-demand systems under demand and supply uncertainties," *IEEE Trans. Intell. Transp. Syst.*, vol. 24, no. 5, pp. 5199–5215, May 2023.
- [133] X. He, W. Huang, and C. Lv, "Trustworthy autonomous driving via defense-aware robust reinforcement learning against worst-case observational perturbations," *Transp. Res. C, Emerg. Technol.*, vol. 163, Jun. 2024, Art. no. 104632.
- [134] X. He and C. Lv, "Towards safe autonomous driving: Decision making with observation-robust reinforcement learning," *Automot. Innov.*, vol. 6, no. 4, pp. 509–520, Nov. 2023.
- [135] D. Hendrycks and T. Dietterich, "Benchmarking neural network robustness to common corruptions and perturbations," 2019, arXiv:1903.12261.
- [136] C. Hennig, "Dissolution point and isolation robustness: Robustness criteria for general cluster analysis methods," *J. Multivariate Anal.*, vol. 99, no. 6, pp. 1154–1176, Jul. 2008.
- [137] S. Hima, B. Lusseti, B. Vanholme, S. Glaser, and S. Mammar, "Trajectory tracking for highly automated passenger vehicles," *IFAC Proc. Volumes*, vol. 44, no. 1, pp. 12958–12963, Jan. 2011.
- [138] J. Ho and S. Ermon, "Generative adversarial imitation learning," in *Proc. Adv. Neural Inf. Process. Syst.*, 2016, pp. 4565–4573.
- [139] J. Hou, H. He, Y. Yang, T. Gao, and Y. Zhang, "A variational Bayesian and Huber-based robust square root cubature Kalman filter for lithiumion battery state of charge estimation," *Energies*, vol. 12, no. 9, p. 1717, May 2019.
- [140] E. Hu and L. Sun, "VODRAC: Efficient and robust correspondence-based point cloud registration with extreme outlier ratios," *J. King Saud Univ. Comput. Inf. Sci.*, vol. 35, no. 1, pp. 38–55, Jan. 2023.
- [141] G. Hu, K. Khosoussi, and S. Huang, "Towards a reliable SLAM back-end," in *Proc. IEEE/RSJ Int. Conf. Intell. Robots Syst.*, Nov. 2013, pp. 37–43.
- [142] K. Hu and K. Cheng, "Robust tube-based model predictive control for autonomous vehicle path tracking," *IEEE Access*, vol. 10, pp. 134389–134403, 2022.
- [143] F. Huang, W. Wen, J. Zhang, C. Wang, and L.-T. Hsu, "Dynamic object-aware LiDAR odometry aided by joint weightings estimation in urban areas," *IEEE Trans. Intell. Vehicles*, vol. 9, no. 2, pp. 3345–3359, Feb. 2024.
- [144] J. Huang, T. Birdal, Z. Gojcic, L. J. Guibas, and S.-M. Hu, "Multiway non-rigid point cloud registration via learned functional map synchronization," *IEEE Trans. Pattern Anal. Mach. Intell.*, vol. 45, no. 2, pp. 2038–2053, Feb. 2023.

3885

3886

3890

3891

3892

3893

3894

3895

3896

3897

3898

3899

3900

3901

3902

3903

3904

3905

3906

3907

3908

3909

3910

3911

3912

3913

3914

3915

3916

3917

3918

3919

3923

3924

3925

3929

3930

3931

3936

3937

3938

3939



3955

3956

3957

3958

3959

3960

3961

3962

3963

3964

3965

3966

3968

3969

3970

3971

3972

3973

3974

3975

3976

3977

3978

3979

3980

3981

3982

3983

3984

3985

3986

3987

3988

3989

3990

3991

3992

3993

3995

3997

3999

4000

4001

4002

4003

4004

4005

4006

4007

4008

4010

4011

4012

4013

4015

4016

4017

4018

4019

4020

4021

4022

4024

4025

4026

- [145] T. Huang, L. Peng, R. Vidal, and Y.-H. Liu, "Scalable 3D registration via truncated entry-wise absolute residuals," in *Proc. IEEE/CVF Conf. Comput. Vis. Pattern Recognit. (CVPR)*, Jun. 2024, pp. 27477–27487.
- [146] Y. Huang, M. Bai, Y. Li, Y. Zhang, and J. Chambers, "An improved variational adaptive Kalman filter for cooperative localization," *IEEE Sensors J.*, vol. 21, no. 9, pp. 10775–10786, May 2021.
  - [147] Y. Huang, Y. Zhang, N. Li, and J. Chambers, "A robust Gaussian approximate fixed-interval smoother for nonlinear systems with heavytailed process and measurement noises," *IEEE Signal Process. Lett.*, vol. 23, no. 4, pp. 468–472, Apr. 2016.
  - [148] Y. Huang, Y. Zhang, P. Shi, and J. Chambers, "Variational adaptive Kalman filter with Gaussian-inverse-Wishart mixture distribution," *IEEE Trans. Autom. Control*, vol. 66, no. 4, pp. 1786–1793, Apr. 2021.
  - [149] Y. Huang, Y. Zhang, P. Shi, Z. Wu, J. Qian, and J. A. Chambers, "Robust Kalman filters based on Gaussian scale mixture distributions with application to target tracking," *IEEE Trans. Syst. Man, Cybern. Syst.*, vol. 49, no. 10, pp. 2082–2096, Oct. 2019.
  - [150] Y. Huang, Y. Zhang, Z. Wu, N. Li, and J. Chambers, "A novel adaptive Kalman filter with inaccurate process and measurement noise covariance matrices," *IEEE Trans. Autom. Control*, vol. 63, no. 2, pp. 594–601, Feb. 2018.
  - [151] Y. Huang, Y. Zhang, B. Xu, Z. Wu, and J. Chambers, "A new outlier-robust student's t based Gaussian approximate filter for cooperative localization," *IEEE/ASME Trans. Mechatronics*, vol. 22, no. 5, pp. 2380–2386, Oct. 2017.
  - [152] Y. Huang, Y. Zhang, Y. Zhao, and J. A. Chambers, "A novel robust Gaussian-student's t mixture distribution based Kalman filter," IEEE Trans. Signal Process., vol. 67, no. 13, pp. 3606–3620, Jul. 2019.
  - [153] P. J. Huber and E. Ronchetti, *Robust Statistics*. Hoboken, NJ, USA: Wiley, 2009.
  - [154] M. Hudnell, T. Price, and J.-M. Frahm, "Robust aleatoric modeling for future vehicle localization," in *Proc. IEEE/CVF Conf. Comput. Vis. Pattern Recognit. Workshops (CVPRW)*, Jun. 2019, pp. 2944–2951.
  - [155] A. Jaegle, S. Phillips, and K. Daniilidis, "Fast, robust, continuous monocular egomotion computation," in *Proc. IEEE Int. Conf. Robot. Autom. (ICRA)*, May 2016, pp. 773–780.
- 3920 [156] A. Jeddi, M. J. Shafiee, and A. Wong, "A simple fine-tuning is all you need: Towards robust deep learning via adversarial fine-tuning," 2020, arXiv:2012.13628.
  - [157] D. Jeong and S. B. Choi, "Tube-based robust model predictive control for tracking control of autonomous articulated vehicles," *IEEE Trans. Intell.* Vehicles, vol. 9, no. 1, pp. 2184–2196, Jan. 2024.
- [158] Z. Jiang, G. Battistelli, L. Chisci, N. Forti, and W. Zhou, "Outlier-robust centralized and distributed variational Bayesian moving horizon estimation," *IEEE Trans. Signal Process.*, vol. 73, pp. 2527–2541, 2025.
  - [159] X. Jin, Q. Wang, Z. Yan, and H. Yang, "Nonlinear robust control of trajectory-following for autonomous ground electric vehicles with active front steering system," AIMS Math., vol. 8, no. 5, pp. 11151–11179, 2023.
- [160] X. Jin, Q. Wang, Z. Yan, H. Yang, and G. Yin, "Integrated robust control of path following and lateral stability for autonomous in-wheel-motor-driven electric vehicles," *Proc. Inst. Mech. Eng., D, J. Automobile Eng.*, vol. 239, no. 5, pp. 1517–1535, Apr. 2025.
  - [161] X. Ju and M. Salibián-Barrera, "Robust boosting for regression problems," Comput. Statist. Data Anal., vol. 153, Jan. 2021, Art. no. 107065.
  - [162] S. Julier and J. Uhlmann, "New extension of the Kalman filter to nonlinear systems," *Proc. SPIE*, vol. 3068, pp. 182–193, Jul. 1997.
- [163] D. Kalaria, Q. Lin, and J. M. Dolan, "Delay-aware robust control for safe autonomous driving," in *Proc. IEEE Intell. Vehicles Symp. (IV)*,
   Jun. 2022, pp. 1565–1571.
- 3943 [164] R. E. Kalman, "A new approach to linear filtering and prediction problems," *J. Basic Eng.*, vol. 82, no. 1, pp. 35–45, Mar. 1960.
- [165] N. Kang, H. Tang, and Y. Han, "Robust integrated control of autonomous vehicles path following with response performance improvement considering lateral stability," *Proc. Inst. Mech. Eng., D, J. Automobile Eng.*, Oct. 2024, Art. no. 09544070241285507.
- [166] C. Karlgaard and H. Schaub, "Adaptive Huber-based filtering using
   projection statistics: Application to spacecraft attitude estimation," in
   Proc. AIAA Guid., Navigat. Control Conf. Exhib., Aug. 2008, p. 7389.
- [167] C. D. Karlgaard and H. Schaub, "Adaptive nonlinear Huber-based navigation for rendezvous in elliptical orbit," *J. Guid., Control, Dyn.*, vol. 34, no. 2, pp. 388–402, Mar. 2011.

- [168] I. A. Kazerouni, L. Fitzgerald, G. Dooly, and D. Toal, "A survey of state-of-the-art on visual SLAM," Expert Syst. Appl., vol. 205, Nov. 2022, Art. no. 117734.
- [169] C. Kerl, J. Sturm, and D. Cremers, "Robust odometry estimation for RGB-D cameras," in *Proc. IEEE Int. Conf. Robot. Autom.*, May 2013, pp. 3748–3754.
- [170] S. Khalid, N. Rehman, S. Abrar, and L. Mihaylova, "Robust Bayesian filtering using Bayesian model averaging and restricted variational," in *Proc. 21st Int. Conf. Inf. Fusion (FUSION)*, Jul. 2018, pp. 361–368.
- [171] P. Kim, H. Lee, and H. J. Kim, "Autonomous flight with robust visual odometry under dynamic lighting conditions," *Auto. Robots*, vol. 43, no. 6, pp. 1605–1622, Aug. 2019.
- [172] S. Klose, P. Heise, and A. Knoll, "Efficient compositional approaches for real-time robust direct visual odometry from RGB-D data," in *Proc. IEEE/RSJ Int. Conf. Intell. Robots Syst.*, Nov. 2013, pp. 1100–1106.
- [173] N. L. Knight and J. Wang, "A comparison of outlier detection procedures and robust estimation methods in GPS positioning," *J. Navigat.*, vol. 62, no. 4, pp. 699–709, Oct. 2009.
- [174] P. W. Koh and P. Liang, "Understanding black-box predictions via influence functions," in *Proc. Int. Conf. Mach. Learn.*, 2017, pp. 1885–1894.
- [175] J. Ku, A. D. Pon, and S. L. Waslander, "Monocular 3D object detection leveraging accurate proposals and shape reconstruction," in *Proc. IEEE/CVF Conf. Comput. Vis. Pattern Recognit. (CVPR)*, Jun. 2019, pp. 11859–11868.
- [176] S. Kuutti, S. Fallah, and R. Bowden, "ARC: Adversarially robust control policies for autonomous vehicles," in *Proc. IEEE Int. Intell. Transp. Syst. Conf. (ITSC)*, Sep. 2021, pp. 522–529.
- [177] D. Lee, M. Jung, W. Yang, and A. Kim, "LiDAR odometry survey: Recent advancements and remaining challenges," *Intell. Service Robot.*, vol. 17, no. 2, pp. 95–118, Mar. 2024.
- [178] J.-K. Lee, Y.-K. Baik, H. Cho, K. Kim, and D. H. Kim, "1-point RANSAC-based method for ground object pose estimation," 2020, arXiv:2008.03718.
- [179] T.-Y. Lee and Y. Jeong, "A tube-based model predictive control for path tracking of autonomous articulated vehicle," *Actuators*, vol. 13, no. 5, p. 164, 2024.
- [180] A. Leung, V. Yohai, and R. Zamar, "Multivariate location and scatter matrix estimation under cellwise and casewise contamination," *Comput. Statist. Data Anal.*, vol. 111, pp. 59–76, Jul. 2017.
- [181] A. Leung, H. Zhang, and R. Zamar, "Robust regression estimation and inference in the presence of cellwise and casewise contamination," *Comput. Statist. Data Anal.*, vol. 99, pp. 1–11, Jul. 2016.
- [182] J. Li, Q. Hu, and M. Ai, "Point cloud registration based on one-point RANSAC and scale-annealing biweight estimation," *IEEE Trans. Geosci. Remote Sens.*, vol. 59, no. 11, pp. 9716–9729, Nov. 2021.
- [183] J. Li, L. Tao, W. Zou, Y. Zhang, B. Shuai, and J. Duan, "Towards robust motion control in multi-source uncertain scenarios by robust policy iteration," *Commun. Transp. Res.*, vol. 5, Dec. 2025, Art. no. 100191.
- [184] Q. Li, Y. Ben, S. M. Naqvi, J. A. Neasham, and J. A. Chambers, "Robust student's *t*-based cooperative navigation for autonomous underwater vehicles," *IEEE Trans. Instrum. Meas.*, vol. 67, no. 8, pp. 1762–1777, Aug. 2018.
- [185] R. Li, H. Xu, and R. Zheng, "Cauchy kernel-based maximum correntropy extended Kalman filter for cooperative localization of multi-UUVs," in *Proc. 3rd Int. Symp. Intell. Unmanned Syst. Artif. Intell.*, May 2024, pp. 290–293.
- [186] S. Li, E. Ngai, and T. Voigt, "Byzantine-robust aggregation in federated learning empowered industrial IoT," *IEEE Trans. Ind. Informat.*, vol. 19, no. 2, pp. 1165–1175, Feb. 2023.
- [187] S. Li, Z. Wang, F. Juefei-Xu, Q. Guo, X. Li, and L. Ma, "Common corruption robustness of point cloud detectors: Benchmark and enhancement," *IEEE Trans. Multimedia*, vol. 27, pp. 848–859, 2025.
- [188] Y. Li, Z. Gao, C. Yang, and Q. Xu, "A novel UWB/INS tight integration model based on ranging offset calibration and robust cubature Kalman filter," *Measurement*, vol. 237, Sep. 2024, Art. no. 115186.
- [189] Y. Li, L. Hou, Y. Yang, and J. Tong, "Huber's M-estimation-based cubature Kalman filter for an INS/DVL integrated system," *Math. Problems Eng.*, vol. 2020, pp. 1–12, Sep. 2020.
- [190] Y. Li, J. Li, J. Qi, and L. Chen, "Robust cubature Kalman filter for dynamic state estimation of synchronous machines under unknown measurement noise statistics," *IEEE Access*, vol. 7, pp. 29139–29148, 2019.

4101

4102

4103

4104

4105

4106

4107

4108

4109

4110

4111

4112

4113

4114

4116

4117

4118

4119

4120

4122

4123

4124

4125

4126

4128

4129

4130

4132

4133

4134

4135

4136

4137

4138

4140

4141

4142

4143

4144

4145

4146

4147

4148

4150

4151

4152

4154

4155

4156

4157

4158

4160

4161

4162

4163

4164

4165

4166

4167

4168

4169

4170

4171

4172



4027

4028

4029

4030

4031

4032

4033

4034

4035

4036

4037

4038

4039 4040

4041

4042

4043

4044

4045

4046

4047

4048

4049

4050

4051

4052

4053

4054

4055

4056

4057

4058

4059

4060

4061

4062

4063

4064

4065

4066

4067

4068

4069

4071

4072

4073

4074

4075

4076

4077

4078

4079 4080

4081

4082

4083

4084

4085

4087

4088

4089

4090

4091

4092

4093

4094

4095

4096

4097

4098

4099

- [191] Y. Li and L. Zhang, "A robust Kalman filter based on Gaussian-exponential distribution for SINS/USBL integration navigation system," Proc. Inst. Mech. Eng., M, J. Eng. Maritime Environ., vol. 238, no. 4, pp. 865–875, Nov. 2024.
- [192] H. Lim, K. Han, G. Shin, G. Kim, S. Hong, and H. Myung, "ORORA: Outlier-robust radar odometry," 2023, arXiv:2303.01876.
- [193] H. Lim, B. Kim, D. Kim, E. Mason Lee, and H. Myung, "Quatro++: Robust global registration exploiting ground segmentation for loop closing in LiDAR SLAM," *Int. J. Robot. Res.*, vol. 43, no. 5, pp. 685–715, Apr. 2024.
- [194] L. Lin, X. Zhang, and Z. Xiao, "Integration of SINS, laser Doppler velocimeter, and monocular visual odometry for autonomous navigation in complex road environments," *Optik*, vol. 295, Dec. 2023, Art. no. 171513.
- [195] J. Liu, Q. Kong, F. Yin, Z. Cai, M. Sun, and B. Chen, "Design and implementation of the correntropy-based filter for GNSS vector tracking and positioning," *IEEE Trans. Aerosp. Electron. Syst.*, early access, Jul. 14, 2025, doi: 10.1109/TAES.2025.3588478.
- [196] L. Liu, W. Bi, B. Zhang, Z. Huang, A. Zhang, and S. Xu, "TORKF: A dual-driven Kalman filter for outlier-robust state estimation and application to aircraft tracking," *Aerospace*, vol. 12, no. 8, p. 660, Jul. 2025.
- [197] L. Lili, R. Mu, and N. Cui, "Huber-based robust tracking method of hypersonic cruise vehicle," in *Proc. China Aeronaut. Sci. Technol. Conf.*, 2023, pp. 484–501.
- [198] L. Liu, Z. Tang, L. Li, and D. Luo, "Robust imitation learning from corrupted demonstrations," 2022, arXiv:2201.12594.
- [199] W. Liu, G. Chen, and A. Knoll, "Matrix inequalities based robust model predictive control for vehicle considering model uncertainties, external disturbances, and time-varying delay," *Frontiers Neurorobotics*, vol. 14, Jan. 2021, Art. no. 617293.
- [200] X. Liu, X. Liu, Y. Yang, and W. Zhang, "An INS/LiDAR integrated navigation algorithm based on robust Kalman filter," in *Proc. Int. Conf. Guid.*, *Navigat. Control Adv. Guid.* (*ICGNC*), Tianjin, China, Oct. 2021, pp. 1027–1037.
- [201] Y. Liu, D. Cui, and C. Xie, "Measurement and estimation of vehicle state based on improved maximum correntropy square-root cubature Kalman filter," J. Meas. Eng., pp. 1–14, Jun. 2025.
- [202] Y. Liu, J. Zhang, L. Fang, Q. Jiang, and B. Zhou, "Multimodal motion prediction with stacked transformers," in *Proc. IEEE/CVF Conf. Comput. Vis. Pattern Recognit. (CVPR)*, Jun. 2021, pp. 7573–7582.
- [203] D. G. Lowe, "Object recognition from local scale-invariant features," in Proc. 7th IEEE Int. Conf. Comput. Vis., vol. 2, Sep. 1999, pp. 1150–1157.
- [204] D. L. S. Lubanco, A. Hashem, M. Pichler-Scheder, A. Stelzer, R. Feger, and T. Schlechter, "R<sup>3</sup>O: Robust radon radar odometry," *IEEE Trans. Intell. Vehicles*, vol. 9, no. 1, pp. 231–246, Jan. 2024.
- [205] L. Luft, T. Schubert, S. I. Roumeliotis, and W. Burgard, "Recursive decentralized collaborative localization for sparsely communicating robots," *Robot., Sci. Syst.*, vol. 12, pp. 1–9, Jan. 2016.
- [206] R. W. Lutz, M. Kalisch, and P. Bühlmann, "Robustified L<sub>2</sub> boosting," Comput. Statist. Data Anal., vol. 52, no. 7, pp. 3331–3341, Mar. 2008.
- [207] C. Ma, S. Pan, W. Gao, H. Wang, and L. Liu, "Variational Bayesian-based robust adaptive filtering for GNSS/INS tightly coupled positioning in urban environments," *Measurement*, vol. 223, Dec. 2023, Art. no. 113668.
- [208] E. Ma, P. Rathi, and S. R. Etesami, "Local environment poisoning attacks on federated reinforcement learning," 2023, arXiv:2303.02725.
- [209] T. Ma, R. Zhang, S. Gao, H. Li, and Y. Zhang, "A variational Bayesian truncated adaptive filter for uncertain systems with inequality constraints," *IET Signal Process.*, vol. 2024, no. 1, Jan. 2024, Art. no. 3809689.
- [210] K. MacTavish and T. D. Barfoot, "At all costs: A comparison of robust cost functions for camera correspondence outliers," in *Proc. 12th Conf. Comput. Robot Vis.*, Jun. 2015, pp. 62–69.
- [211] W. Maddern, A. Stewart, C. McManus, B. Upcroft, W. Churchill, and P. Newman, "Illumination invariant imaging: Applications in robust vision-based localisation, mapping and classification for autonomous vehicles," in *Proc. Vis. Place Recognit. Changing Environ. Workshop, IEEE Int. Conf. Robot. Autom. (ICRA)*, vol. 2, Hong Kong, May 2014, p. 5
- [212] A. Madry, A. Makelov, L. Schmidt, D. Tsipras, and A. Vladu, "Towards deep learning models resistant to adversarial attacks," 2017, arXiv:1706.06083.

- [213] R. A. Maronna, R. D. Martin, V. J. Yohai, and M. Salibián-Barrera, Robust Statistics: Theory and Methods (With R). Hoboken, NJ, USA: Wiley, 2019
- [214] T. Masuda, K. Sakaue, and N. Yokoya, "Registration and integration of multiple range images for 3-D model construction," in *Proc. 13th Int. Conf. Pattern Recognit.*, vol. 1, Aug. 1996, pp. 879–883.
- [215] S. Mata, A. Zubizarreta, and C. Pinto, "Robust tube-based model predictive control for lateral path tracking," *IEEE Trans. Intell. Vehicles*, vol. 4, no. 4, pp. 569–577, Dec. 2019.
- [216] D. Medina, "Robust GNSS carrier phase-based position attitude estimation," Ph.D. thesis, Dept. Comput. Sci. Eng., Universidad Carlos III de Madrid, Madrid, Spain, 2022.
- [217] D. Medina, H. Li, J. Vila-Valls, and P. Closas, "On robust statistics for GNSS single point positioning," in *Proc. IEEE Intell. Transp. Syst. Conf.* (ITSC), Oct. 2019, pp. 3281–3287.
- [218] D. Medina, H. Li, J. Vilà-Valls, and P. Closas, "Robust statistics for GNSS positioning under harsh conditions: A useful tool?" Sensors, vol. 19, no. 24, p. 5402, 2019.
- [219] M. Meilland, A. Comport, and P. Rives, "Real-time dense visual tracking under large lighting variations," in *Proc. Brit. Mach. Vis. Conf.*, 2011, pp. 45.1–45.11.
- [220] F. Memarian, A. Hashemi, S. Niekum, and U. Topcu, "On the benefits of inducing local lipschitzness for robust generative adversarial imitation learning," 2021, arXiv:2107.00116.
- [221] D. Ming, X. Wu, Y. Wang, Z. Zhu, H. Ge, and R. Liu, "A real-time monocular visual SLAM based on the bundle adjustment with adaptive robust kernel," *J. Intell. Robotic Syst.*, vol. 107, no. 3, p. 35, Mar. 2023.
- [222] U. Montanaro, S. Dixit, and S. Fallah, "Adaptive control and robust MPC for linearising longitudinal vehicle dynamics for platooning applications," in *Proc. IAVSD Int. Symp. Dyn. Vehicles Roads Tracks*, Gothenburg, Sweden, Aug. 2020, pp. 1052–1061.
- [223] S. R. Mousa, S. Ishak, R. M. Mousa, J. Codjoe, and M. Elhenawy, "Deep reinforcement learning agent with varying actions strategy for solving the eco-approach and departure problem at signalized intersections," *Transp. Res. Record: J. Transp. Res. Board*, vol. 2674, no. 8, pp. 119–131, Aug. 2020.
- [224] J. Murrugarra-Llerena, L. N. Kirsten, and C. R. Jung, "Can we trust bounding box annotations for object detection?" in *Proc. IEEE/CVF* Conf. Comput. Vis. Pattern Recognit., Jun. 2022, pp. 4813–4822.
- [225] R. Muthukrishnan, E. Boobalan, and R. Reka, "Performance of RANSAC techniques under classical and robust methods," in *Proc. IJIRCCE*, vol. 2, 2014, pp. 1–5.
- [226] J. M. Nadales, A. Hakobyan, D. M. D. L. Peña, D. Limon, and I. Yang, "Risk-aware Wasserstein distributionally robust control of vessels in natural waterways," *IEEE Trans. Control Syst. Technol.*, vol. 32, no. 4, pp. 1471–1478, Jul. 2024.
- [227] R. Nebeluk and M. Ławryńczuk, "Nonlinear model predictive control with L<sub>1</sub> cost-function using neural networks for multivariable processes," *IFAC-PapersOnLine*, vol. 56, no. 2, pp. 1591–1596, 2023.
- [228] Y. Nemmour, B. Schölkopf, and J.-J. Zhu, "Approximate distributionally robust nonlinear optimization with application to model predictive control: A functional approach," in *Proc. Learn. Dyn. Control*, 2021, pp. 1255–1269.
- [229] R. A. Newcombe, S. J. Lovegrove, and A. J. Davison, "DTAM: Dense tracking and mapping in real-time," in *Proc. Int. Conf. Comput. Vis.*, Nov. 2011, pp. 2320–2327.
- [230] M. Nezami, H. S. Abbas, N. T. Nguyen, and G. Schildbach, "Robust tube-based LPV-MPC for autonomous lane keeping," *IFAC-PapersOnLine*, vol. 55, no. 35, pp. 103–108, 2022.
- [231] H. T. Nguyen and A. W. M. Smeulders, "Fast occluded object tracking by a robust appearance filter," *IEEE Trans. Pattern Anal. Mach. Intell.*, vol. 26, no. 8, pp. 1099–1104, Aug. 2004.
- [232] A. Nilim and L. El Ghaoui, "Robust control of Markov decision processes with uncertain transition matrices," *Operations Res.*, vol. 53, no. 5, pp. 780–798, Oct. 2005.
- [233] H. Nurminen, T. Ardeshiri, R. Piche, and F. Gustafsson, "Robust inference for state-space models with skewed measurement noise," *IEEE Signal Process. Lett.*, vol. 22, no. 11, pp. 1898–1902, Nov. 2015.
- [234] A. Nurunnabi, F. N. Teferle, R. C. Lindenbergh, J. Li, and S. Zlatanova, "Robust approach for urban road surface extraction using mobile laser scanning 3D point clouds," *Int. Arch. Photogramm., Remote Sens. Spatial Inf. Sci.*, vols. XLIII-B1-2022, pp. 59–66, May 2022.



4246

4247

4248

4249

4250

4252

4253

4254

4255

4256

4257

4258

4259

4261

4262

4263

4264

4265

4266

4268

4269

4270

4271

4272

4273

4274

4275

4276

4277

4278

4279

4280

4281

4283

4284

4285

4286

4287

4288

4289

4290

4291

4293

4294

4295

4296

4297

4298

4299

4300

4301

4302

4303

4304

4305

4307

4308

4309

4310

4312

4313

4314

4315

- [235] A. Nurunnabi, G. West, and D. Belton, "Robust locally weighted regression techniques for ground surface points filtering in mobile laser scanning three dimensional point cloud data," *IEEE Trans. Geosci.* Remote Sens., vol. 54, no. 4, pp. 2181–2193, Apr. 2016.
- 4177 [236] F. Oudjama, A. Boumediene, K. Saidi, and D. Boubekeur, "Robust speed 4178 control in nonlinear electric vehicles using H-infinity control and the LMI 4179 approach," *J. Intell. Syst. Control*, vol. 2, no. 3, pp. 170–182, Sep. 2023.
- [237] C.-H. Park and J.-H. Chang, "Robust range estimation algorithm based on hyper-tangent loss function," *IET Signal Process.*, vol. 14, no. 5, pp. 314–321, Jul. 2020.
- [238] S. Park, T. Schöps, and M. Pollefeys, "Illumination change robustness in direct visual SLAM," in *Proc. IEEE Int. Conf. Robot. Autom. (ICRA)*, May 2017, pp. 4523–4530.
- 4186 [239] Á. P. Bustos and T.-J. Chin, "Guaranteed outlier removal for rotation search," in *Proc. IEEE Int. Conf. Comput. Vis. (ICCV)*, Dec. 2015, pp. 2165–2173.
- 4189 [240] A. Patterson, V. Liao, and M. White, "Robust losses for learning value functions," *IEEE Trans. Pattern Anal. Mach. Intell.*, vol. 45, no. 5, pp. 6157–6167, May 2023.
- 4192 [241] S. Paul, B. Jhamb, D. Mishra, and M. S. Kumar, "Edge loss functions for deep-learning depth-map," *Mach. Learn. with Appl.*, vol. 7, Mar. 2022,
   4194 Art. no. 100218.
  - [242] D. Penco, J. Davins-Valldaura, E. Godoy, P. Kvieska, and G. Valmorbida, "Self-scheduled h control of autonomous vehicle in collision avoidance maneuvers," *IFAC-PapersOnLine*, vol. 54, no. 8, pp. 148–153, 2021.

4195

4196

4197

4198

4199

4200

4201

4202

4203

- [243] L. Peng, C. Kümmerle, and R. Vidal, "On the convergence of IRLS and its variants in outlier-robust estimation," in *Proc. IEEE/CVF Conf. Comput. Vis. Pattern Recognit. (CVPR)*, Jun. 2023, pp. 17808–17818.
- [244] K. Pereida and A. P. Schoellig, "All models are wrong: Robust adaptive model predictive control for safe and high accuracy trajectory tracking in the presence of model errors," Tech. Rep., 2019.
- 4204 [245] J. M. Phillips, R. Liu, and C. Tomasi, "Outlier robust ICP for minimizing fractional RMSD," in *Proc. 6th Int. Conf. 3-D Digit. Imag. Model.* 4206 (3DIM), Aug. 2007, pp. 427–434.
- 4207 [246] R. Piché, S. Särkkä, and J. Hartikainen, "Recursive outlier-robust filtering
   4208 and smoothing for nonlinear systems using the multivariate student-t
   4209 distribution," in Proc. IEEE Int. Workshop Mach. Learn. Signal Process.,
   4210 Sep. 2012, pp. 1–6.
- 4211 [247] L. Pinto, J. Davidson, R. Sukthankar, and A. Gupta, "Robust adversarial 4212 reinforcement learning," in *Proc. Int. Conf. Mach. Learn.*, 2017, 4213 pp. 2817–2826.
- 4214 [248] D. Qi, J. Feng, Y. Li, L. Wang, and B. Song, "A robust hierarchical estimation scheme for vehicle state based on maximum correntropy square-root cubature Kalman filter," *Entropy*, vol. 25, no. 3, p. 453, 2023.
- 4217 [249] W. Qi, W. Qin, and Z. Yun, "Closed-loop state of charge estimation of Li 4218 ion batteries based on deep learning and robust adaptive Kalman filter,"
   4219 Energy, vol. 307, Oct. 2024, Art. no. 132805.
- 4220 [250] Q. Qiang, L. Baojun, L. Yingchun, L. Xia, and S. Wang, "Robust
   4221 UKF orbit determination method with time-varying forgetting factor
   4222 for angle/range-based integrated navigation system," *Chin. J. Aeronaut.*,
   4223 vol. 37, no. 11, pp. 420–434, Nov. 2024.
- 4224 [251] T. Qin, P. Li, and S. Shen, "VINS-Mono: A robust and versatile monocular visual-inertial state estimator," *IEEE Trans. Robot.*, vol. 34, no. 4, pp. 1004–1020, Aug. 2018.
- 4227 [252] Y. Qu, R. Ma, and Z. Gao, "Heavy-tailed filtering with reduced sensitivity
   4228 to inaccurate noise covariance," Signal Process., vol. 238, Jul. 2025,
   4229 Art. no. 110209.
- 4230 [253] R. C. Rafaila and G. Livint, "H-infinity control of automatic vehicle steering," in *Proc. Int. Conf. Exposit. Electr. Power Eng. (EPE)*, 4232 Oct. 2016, pp. 31–36.
- 4233 [254] R. Ranftl and V. Koltun, "Deep fundamental matrix estimation," in *Proc.*4234 *Eur. Conf. Comput. Vis. (ECCV)*, 2018, pp. 292–309.
- 4235 [255] J. Raymaekers and P. J. Rousseeuw, "Handling cellwise outliers by sparse regression and robust covariance," 2019, arXiv:1912.12446.
- 4237 [256] Y. Ren, J. Duan, S. E. Li, Y. Guan, and Q. Sun, "Improving generalization of reinforcement learning with minimax distributional soft actor-critic," in *Proc. IEEE 23rd Int. Conf. Intell. Transp. Syst. (ITSC)*, Sep. 2020, pp. 1–6.
- <sup>4241</sup> [257] Y. Ren, G. Zhan, L. Tang, S. E. Li, J. Jiang, K. Li, and J. Duan,
   <sup>4242</sup> "Improve generalization of driving policy at signalized intersections
   <sup>4243</sup> with adversarial learning," *Transp. Res. C, Emerg. Technol.*, vol. 152,
   <sup>4244</sup> Jul. 2023, Art. no. 104161.

- [258] S. Rhode, Robust and Regularized Algorithms for Vehicle Tractive Force Prediction and Mass Estimation, vol. 62. Karlsruhe, Germany: KIT Scientific Publishing, 2018.
- [259] H. Rieder, Robust Asymptotic Statistics, vol. 1. Berlin, Germany: Springer, 1994.
- [260] H. Rieder, M. Kohl, and P. Ruckdeschel, "The cost of not knowing the radius," *Stat. Methods Appl.*, vol. 17, no. 1, pp. 13–40, Feb. 2008.
- [261] F. Roselli, M. Corno, S. M. Savaresi, M. Giorelli, D. Azzolini, and A. Irilli, "H<sub>∞</sub> control with look-ahead for lane keeping in autonomous vehicles," in *Proc. IEEE Conf. Control Technol. Appl.* (CCTA), Aug. 2017, pp. 2220–2225.
- [262] P. J. Rousseeuw, "Least median of squares regression," J. Amer. Stat. Assoc., vol. 79, no. 388, pp. 871–880, 1984.
- [263] P. J. Rousseeuw and W. V. D. Bossche, "Detecting deviating data cells," Technometrics, vol. 60, no. 2, pp. 135–145, Apr. 2018.
- [264] P. J. Rousseeuw and K. Van Driessen, "An algorithm for positive-breakdown regression based on concentration steps," in *Studies in Classification, Data Analysis, and Knowledge Organization*. Berlin, Germany: Springer, 2000, pp. 335–346.
- [265] P. J. Rousseeuw and K. V. Driessen, "Computing LTS regression for large data sets," *Data mining Knowl. Discovery*, vol. 12, no. 1, pp. 29–45, 2006.
- [266] W. Ruan, X. Yi, and X. Huang, "Adversarial robustness of deep learning: Theory, algorithms, and applications," in *Proc. 30th ACM Int. Conf. Inf. Knowl. Manage.*, Oct. 2021, pp. 4866–4869.
- [267] P. Ruckdeschel, "Ansätze zur robustifizierung des Kalman-filters," Ph.D. thesis, Fakultät für Mathematik, Physik und Informatik, Univ. Bayreuth, Bayreuth, Germany, 2001.
- [268] P. Ruckdeschel and N. Horbenko, "Yet another breakdown point notion: EFSBP," *Metrika*, vol. 75, no. 8, pp. 1025–1047, Nov. 2012.
- [269] P. Ruckdeschel, B. Spangl, and D. Pupashenko, "Robust Kalman tracking and smoothing with propagating and non-propagating outliers," *Stat. Papers*, vol. 55, no. 1, pp. 93–123, Feb. 2014.
- [270] F. Ruwisch and S. Schön, "Feature map aided robust high precision GNSS positioning in harsh urban environments," *IEEE Trans. Intell. Transp. Syst.*, early access, May 26, 2025, doi: 10.1109/TITS.2025.3569975.
- [271] A. Saday, I. Demirel, Y. Yıldırım, and C. Tekin, "Federated multiarmed bandits under Byzantine attacks," *IEEE Trans. Artif. Intell.*, vol. 6, no. 6, pp. 1488–1501, Jun. 2025.
- [272] A. Samadzadeh and A. Nickabadi, "SRVIO: Super robust visual inertial odometry for dynamic environments and challenging loopclosure conditions," *IEEE Trans. Robot.*, vol. 39, no. 4, pp. 2878–2891, Aug. 2023.
- [273] S. Särkkä and J. Hartikainen, "Non-linear noise adaptive Kalman filtering via variational Bayes," in *Proc. IEEE Int. Workshop Mach. Learn. Signal Process. (MLSP)*, Sep. 2013, pp. 1–6.
- [274] S. Sarkka and A. Nummenmaa, "Recursive noise adaptive Kalman filtering by variational Bayesian approximations," *IEEE Trans. Autom. Control*, vol. 54, no. 3, pp. 596–600, Mar. 2009.
- [275] R. Schmied, "Mixed  $H_2/H_\infty$  and predictive adaptive cruise control: Design, evaluation and comparison/eingereicht von Roman Schmied," Ph.D. thesis, Institut für Design und Regelung Mechatronischer Systeme, Universität Linz, Linz, Austria, 2017.
- [276] P. Schmuck and M. Chli, "CCM-SLAM: Robust and efficient centralized collaborative monocular simultaneous localization and mapping for robotic teams," *J. Field Robot.*, vol. 36, no. 4, pp. 763–781, Jun. 2019.
- [277] D. Schneider, "Optimierte Schätzverfahren für intelligente Batteriesysteme," Ph.D. thesis, Institut für Innovative Mobilität, Technische Universität München, Munich, Germany, 2024.
- [278] M. Schuurmans, A. Katriniok, C. Meissen, H. E. Tseng, and P. Patrinos, "Safe, learning-based MPC for highway driving under lane-change uncertainty: A distributionally robust approach," *Artif. Intell.*, vol. 320, Jul. 2023, Art. no. 103920.
- [279] S. D.-C. Shashua and S. Mannor, "Deep robust Kalman filter," 2017, arXiv:1703.02310.
- [280] F. Shen, C. Shen, A. van den Hengel, and Z. Tang, "Approximate least trimmed sum of squares fitting and applications in image analysis," *IEEE Trans. Image Process.*, vol. 22, no. 5, pp. 1836–1847, May 2013.
- [281] H. Shen, G. Wen, Y. Lv, and J. Zhou, "A stochastic event-triggered robust unscented Kalman filter-based USV parameter estimation," *IEEE Trans. Ind. Electron.*, vol. 71, no. 9, pp. 11272–11282, Dec. 2023.

4388

4389

4390

4391

4394

4396

4397

4398

4399

4400

4401

4402

4403

4404

4405

4406

4407

4408

4409

4410

4411

4414

4415

4416

4417

4418

4419

4420

4421

4424

4425

4426

4427

4428

4429

4430

4431

4432

4433

4434

4435

4436

4438

4439

4440

4441

4442

4443

4444

4445

4446

4447

4448

4449

4450

4451

4452

4453

4454

4455

4456

4457



4322

4323

4324

4325

4326

4327

- 4316 [282] Q. Shen, Y. Li, H. Jiang, Z. Wang, and T. Zhao, "Deep reinforcement learning with robust and smooth policy," in *Proc. Int. Conf. Mach. Learn.*, 2020, pp. 8707–8718.
- [283] J. Shi, H. Yang, and L. Carlone, "Optimal and robust category-level perception: Object pose and shape estimation from 2-D and 3-D semantic keypoints," *IEEE Trans. Robot.*, vol. 39, no. 5, pp. 4131–4151, Oct. 2023.
  - [284] K. Si, P. Li, Z.-p. Yuan, K. Qiao, B. Wang, and X. He, "Distributionally robust Kalman filtering for INS/GPS tightly coupled integration with model uncertainty and measurement outlier," *IEEE Trans. Instrum. Meas.*, vol. 72, 2023, Art. no. 2521213.
  - [285] D. Simon, Optimal State Estimation: Kalman, H Infinity, and Nonlinear Approaches. Hoboken, NJ, USA: Wiley, 2006.
- 4328 [286] A. P. Singh and R. Tali, "Byzantine resilient federated REINFORCE (GM-FedREINFORCE)," in *Proc. Int. Conf. Mach. Learn. Appl.* 4330 (*ICMLA*), Dec. 2023, pp. 825–830.
- 4331 [287] R. Soloperto, J. Köhler, F. Allgöwer, and M. A. Müller, "Collision avoidance for uncertain nonlinear systems with moving obstacles using robust model predictive control," in *Proc. 18th Eur. Control Conf. (ECC)*, Jun. 2019, pp. 811–817.
- 4335 [288] H. W. Sorenson, "Least-squares estimation: From Gauss to Kalman,"
  4336 IEEE Spectr., vol. S-7, no. 7, pp. 63–68, Jul. 1970.
- 4337 [289] V.-J. Štironja, L. Petrović, J. Peršić, I. Marković, and I. Petrović, "RAVE:
   4338 A framework for radar ego-velocity estimation," in *Proc. IEEE Int. Conf.* 4339 Multisensor Fusion Integr. Intell. Syst. (MFI), Sep. 2024, pp. 1–6.
- 4340 [290] H. Sun, L. Dai, and P. Wang, "An efficient moving obstacle avoidance scheme for UAVs via output feedback robust MPC," *IEEE Trans. Aerosp.* 4342 *Electron. Syst.*, vol. 60, no. 5, pp. 6199–6212, May 2024.
- 4343 [291] L. Sun, "RANSIC: Fast and highly robust estimation for rotation search and point cloud registration using invariant compatibility," *IEEE Robot.*4345 *Autom. Lett.*, vol. 7, no. 1, pp. 143–150, Jan. 2022.
- 4346 [292] W. Sun, J. Zhao, W. Ding, and P. Sun, "Robust UKF relative positioning approach for tightly coupled vehicle ad hoc networks based on adaptive M-estimation," *IEEE Sensors J.*, vol. 23, no. 9, pp. 9959–9971, May 2023.
- [293] X. Sun, P. Li, J. Zhang, Z. Chen, and B. He, "Robust AUV navigation with non-Gaussian noise: Enhanced UKF with maximum correntropy and M-estimation methods," *Robot. Auto. Syst.*, vol. 192, Oct. 2025, Art. no. 105007.
- 4354 [294] Z. Sun, W. Gao, X. Tao, S. Pan, P. Wu, and H. Huang, "Semi-tightly coupled robust model for GNSS/UWB/INS integrated positioning in challenging environments," *Remote Sens.*, vol. 16, no. 12, p. 2108, Jun. 2024.
- 4358 [295] R. S. Sutton, D. Precup, and S. Singh, "Between MDPs and semi-MDPs:
   4359 A framework for temporal abstraction in reinforcement learning," Artif.
   4360 Intell., vol. 112, nos. 1–2, pp. 181–211, Aug. 1999.
- 4361 [296] C. Szegedy, W. Zaremba, I. Sutskever, J. Bruna, D. Erhan, I. Goodfellow,
   4362 and R. Fergus, "Intriguing properties of neural networks," 2013,
   4363 arXiv:1312.6199.
- 4364 [297] Y. Tang, M. Wang, Y. Yang, Z. Lan, and Y. Yue, "Robust large-scale collaborative localization based on semantic submaps with extreme outliers," in *IEEE/ASME Trans. Mechatronics*, vol. vol. 29, 2024, pp. 2649–2660.
- 4368 [298] Z. Tang, "Robust imitation learning from observation," Ph.D. thesis,
   4369 Dept. Elect. & Comput. Eng., Univ. Illinois Urbana-Champaign, Champaign, IL, USA., 2020.
- 4371 [299] T. Kargar Tasooji and R. Parasuraman, "Distributed fault-tolerant 4372 multi-robot cooperative localization in adversarial environments," 2025, 4373 arXiv:2507.06750.
- 4374 [300] A. T. Thorgeirsson, S. Scheubner, S. Funfgeld, and F. Gauterin, "An
   4375 investigation into key influence factors for the everyday usability of
   4376 electric vehicles," *IEEE Open J. Veh. Technol.*, vol. 1, pp. 348–361, 2020.
- 4377 [301] B. Thörnblom, "Predicting impact of training data for pedestrian detection in autonomous vehicles using influence functions," Tech. Rep., 2019.
- 4380 [302] C. E. Thorpe and T. Kanade, Second Annual Report for Perception for Outdoor Navigation. Pittsburgh, PA, USA: Carnegie Mellon University, Robotics Institute, 1991.
- [303] Y. Tian, Y. Chang, F. H. Arias, C. Nieto-Granda, J. P. How, and L. Carlone,
   "Kimera-multi: Robust, distributed, dense metric-semantic SLAM for
   multi-robot systems," *IEEE Trans. Robot.*, vol. 38, no. 4, pp. 2022–2038,
   Aug. 2022.

- [304] S. Truzman, G. Revach, N. Shlezinger, and I. Klein, "Outlier-insensitive Kalman filtering using NUV priors," in *Proc. IEEE Int. Conf. Acoust.*, Speech Signal Process. (ICASSP), Jun. 2023, pp. 1–5.
- [305] S. Truzman, G. Revach, N. Shlezinger, and I. Klein, "Outlier-insensitive Kalman filtering: Theory and applications," *IEEE Sensors J.*, vol. 24, no. 23, pp. 39467–39477, Dec. 2024.
- [306] D. Tschirschwitz, C. Benz, M. Florek, H. Norderhus, B. Stein, and V. Rodehorst, "Drawing the same bounding box twice? Coping noisy annotations in object detection with repeated labels," in *Proc. DAGM German Conf. Pattern Recognit.*, 2023, pp. 605–623.
- [307] C.-H. Tseng, S.-F. Lin, and D.-J. Jwo, "Robust Huber-based cubature Kalman filter for GPS navigation processing," *J. Navigat.*, vol. 70, no. 3, pp. 527–546, May 2017.
- [308] J. Tu, M. Ren, S. Manivasagam, M. Liang, B. Yang, R. Du, F. Cheng, and R. Urtasun, "Physically realizable adversarial examples for LiDAR object detection," in *Proc. IEEE/CVF Conf. Comput. Vis. Pattern Recognit. (CVPR)*, Jun. 2020, pp. 13713–13722.
- [309] M. P. Uddin, Y. Xiang, M. Hasan, J. Bai, Y. Zhao, and L. Gao, "A systematic literature review of robust federated learning: Issues, solutions, and future research directions," ACM Comput. Surv., vol. 57, no. 10, pp. 1–62, Oct. 2025.
- [310] H. Velasco, H. Laniado, M. Toro, V. Leiva, and Y. Lio, "Robust three-step regression based on comedian and its performance in cell-wise and case-wise outliers," *Mathematics*, vol. 8, no. 8, p. 1259, Aug. 2020.
- [311] R. v. Mises, "On the asymptotic distribution of differentiable statistical functions," Ann. Math. Statist., vol. 18, no. 3, pp. 309–348, Sep. 1947.
- [312] E. A. Wan and R. Van Der Merwe, "The unscented Kalman filter for nonlinear estimation," in *Proc. IEEE Adapt. Syst. signal Process.*, Oct. 2002, pp. 153–158.
- [313] W. Wan, J. Feng, B. Song, and X. Li, "Huber-based robust unscented Kalman filter distributed drive electric vehicle state observation," *Energies*, vol. 14, no. 3, p. 750, 2021.
- [314] G. Wang, Z. Zhang, C. Yang, L. Ma, and W. Dai, "Robust EKF based on shape parameter mixture distribution for wireless localization with time-varying skewness measurement noise," *IEEE Trans. Instrum. Meas.*, vol. 74, pp. 1–10, 2025.
- [315] J. Wang, L.-j. Qian, J. Chen, L. Xuan, and X. Chen, "Multi-innovation adaptive UKF with robust estimation using QS decomposition for vehicle state estimation," *Proc. Inst. Mech. Eng.*, D, J. Automobile Eng., Jan. 2025, Art. no. 09544070241313090.
- [316] J. Wang, Z. Zhuang, Y. Wang, and H. Zhao, "Adversarially robust imitation learning," in *Proc. Conf. Robot Learn.*, 2021, pp. 320–331.
- [317] L. Wang, H. Chen, F. Lian, W. Zhang, and J. Liu, "Robust Bayesian recursive ensemble Kalman filter under the nonstationary heavy-tailed noise," *IEEE Sensors J.*, vol. 25, no. 1, pp. 749–762, Jan. 2025.
- [318] R. Wang, D. Becker, and T. Hobiger, "Stochastic modeling with robust Kalman filter for real-time kinematic GPS single-frequency positioning," GPS Solutions, vol. 27, no. 3, p. 153, Jul. 2023.
- [319] S. Wang, Q. Li, Z. Cui, J. Hou, and C. Huang, "Bandit-based data poisoning attack against federated learning for autonomous driving models," *Expert Syst. Appl.*, vol. 227, Oct. 2023, Art. no. 120295.
- [320] S. Wang, Y. Zhang, A. Vora, A. Perincherry, and H. Li, "Satellite image based cross-view localization for autonomous vehicle," 2022, arXiv:2207.13506.
- [321] X. Wang, H. Zhang, A. Bilal, H. Long, and X. Liu, "WGM-dSAGA: Federated learning strategies with Byzantine robustness based on weighted geometric median," *Electronics*, vol. 12, no. 5, p. 1190, Mar. 2023.
- [322] Y. Wang, S. Sun, and L. Li, "Adaptively robust unscented Kalman filter for tracking a maneuvering vehicle," *J. Guid.*, *Control*, *Dyn.*, vol. 37, no. 5, pp. 1696–1701, Sep. 2014.
- [323] Y. Wang, Q. Yu, and Y. Shen, "Robust Bayesian cooperative positioning for intelligent vehicles using GNSS and V2V range measurements," *IEEE Trans. Wireless Commun.*, early access, Jun. 6, 2025, doi: 10.1109/TWC.2025.3575159.
- [324] T. Werner, "Asymptotic linear expansion of regularized M-estimators," Ann. Inst. Stat. Math., vol. 74, no. 1, pp. 167–194, Feb. 2022.
- [325] T. Werner, "Quantitative robustness of instance ranking problems," *Ann. Inst. Stat. Math.*, vol. 75, no. 2, pp. 335–368, Apr. 2023.
- [326] T. Werner, "Trimming stability selection increases variable selection robustness," Mach. Learn., vol. 112, no. 12, pp. 4995–5055, Dec. 2023.



4532

4533

4534

4535

4536

4537

4538

4539

4540

4541

4542

4543

4544

4546

4547

4548

4549

4550

4551

4552

4553

4554

4555

4556

4557

4558

4559

4561

4562

4563

4564

4565

4566

4567

4568

4569

4570

4571

4572

4574

4575

4576

4577

4578

4579

4580

4581

4582

4584

4586

4587

4588

4589

4590

4591

4592

4593

4594

4596

4597

4598

4599

4600

4601

4602

4603

- [327] T. Werner, "Global quantitative robustness of regression feed-4458 forward neural networks," Neural Comput. Appl., vol. 36, no. 32, 4459 pp. 19967-19988, Nov. 2024. 4460
- 4461 M. West, "Robust sequential approximate Bayesian estimation," J. Roy. Stat. Soc. Ser. B, Stat. Methodol., vol. 43, no. 2, pp. 157–166, Jan. 1981. 4462
- [329] A. Wischnewski, "Robust and data-driven control for autonomous 4463 racing," Ph.D. thesis, Lehrstuhl für Steuerungs- und Regelungstechnik, 4464 Technische Universität München, Munich, Germany, 2023. 4465

4466

4467

4468

4470

4471

4472

4473

4497

4498

4499

4500

- [330] D. Withers and P. Newman, "Modelling scene change for large-scale long term laser localisation," in Proc. IEEE Int. Conf. Robot. Autom. (ICRA), May 2017, pp. 6233-6239.
- J. Wörmann, "Knowledge augmented machine learning with applications in autonomous driving: A survey," 2022, arXiv:2205.04712.
- [332] F. Wu, C. Sun, H. Li, and S. Zheng, "Real-time center of gravity estimation for intelligent connected vehicle based on HEKF-EKF," Electronics, vol. 12, no. 2, p. 386, Jan. 2023.
- [333] P. Wu, S. Chen, and D. N. Metaxas, "MotionNet: Joint perception and 4474 4475 motion prediction for autonomous driving based on bird's eye view maps," in Proc. IEEE/CVF Conf. Comput. Vis. Pattern Recognit. (CVPR), 4476 Jun. 2020, pp. 11382-11392. 4477
- [334] Q. Wu, L. Chen, Y. Li, Z. Wang, S. Yao, and H. Li, "Reweighted 4478 4479 robust particle filtering approach for target tracking in automotive radar application," Remote Sens., vol. 14, no. 21, p. 5477, Oct. 2022. 4480
- W. Wu, J. Li, C. Chen, B. Yang, X. Zou, Y. Yang, Y. Xu, R. Zhong, and 4481 R. Chen, "AFLI-Calib: Robust LiDAR-IMU extrinsic self-calibration 4482 based on adaptive frame length LiDAR odometry," ISPRS J. Pho-4483 togramm. Remote Sens., vol. 199, pp. 157-181, May 2023. 4484
- M. Xia, T. Zhang, L. Zhang, B. Yang, and Y. Shi, "A mixture distribution-based robust SINS/USBL integration navigation with time-4486 4487 varying delays," IEEE Trans. Instrum. Meas., vol. 73, pp. 1-10, 2024.
- L. Xiong, J. Shen, and X. Bi, "A Huber based unscented Kalman filter 4488 4489 terrain matching algorithm for underwater autonomous vehicle," in Proc. 3rd Int. Conf. Comput. Sci. Appl. Eng., Oct. 2019, pp. 1-8. 4490
- [338] P. Xiong, M. Tegegn, J. S. Sarin, S. Pal, and J. Rubin, "It is all about data: 4491 A survey on the effects of data on adversarial robustness," ACM Comput. 4492 4493 Surv., vol. 56, no. 7, pp. 1-41, Jul. 2024.
- X. Xiong, W. Chen, Z. Liu, and Q. Shen, "DS-VIO: Robust and 4494 efficient stereo visual inertial odometry based on dual stage EKF," 2019, 4495 arXiv:1905.00684. 4496
  - [340] L. Xu, W. Zhuang, G. Yin, G. Li, and C. Bian, "Robust overtaking control of autonomous electric vehicle with parameter uncertainties," Proc. Inst. Mech. Eng., D, J. Automobile Eng., vol. 233, no. 13, pp. 3358-3376, Nov. 2019.
- [341] N. Xu, R. Qin, and S. Song, "Point cloud registration for LiDAR and photogrammetric data: A critical synthesis and performance analysis 4502 4503 on classic and deep learning algorithms," ISPRS Open J. Photogramm. Remote Sens., vol. 8, Apr. 2023, Art. no. 100032. 4504
- [342] Y. Xu, J. Shao, S. Gao, and Y. Zhou, "Emergency autonomous steering 4505 control research based on receding horizon H<sub>∞</sub> control and minimax 4506 4507 criteria," IEEE Access, vol. 9, pp. 151781-151792, 2021.
- F. Yan, Z. Li, and Z. Zhou, "Robust and efficient edge-based visual 4508 odometry," Comput. Vis. Media, vol. 8, no. 3, pp. 467-481, Sep. 2022. 4509
- [344] J. Yan, F. Zhu, Y. Huang, and Y. Zhang, "Robust decentralized 4510 4511 cooperative localization for multirobot system against measurement outliers," IEEE Internet Things J., vol. 11, no. 10, pp. 17934-17947, 4512 May 2024. 4513
- [345] Q. Yan, J. Chen, and L. De Strycker, "An outlier detection method based 4514 on Mahalanobis distance for source localization," Sensors, vol. 18, no. 7, 4515 p. 2186, Jul. 2018. 4516
- 4517 [346] H. Yang, P. Antonante, V. Tzoumas, and L. Carlone, "Graduated nonconvexity for robust spatial perception: From non-minimal solvers to 4518 4519 global outlier rejection," IEEE Robot. Autom. Lett., vol. 5, no. 2, pp. 1127-1134, Apr. 2020. 4520
- H. Yang and L. Carlone, "One ring to rule them all: Certifiably robust 4521 geometric perception with outliers," in Proc. Adv. Neural Inf. Process. 4522 Syst., 2020, pp. 18846-18859. 4523
- [348] H. Yang and L. Carlone, "Certifiably optimal outlier-robust geometric 4524 perception: Semidefinite relaxations and scalable global optimization," 4525 IEEE Trans. Pattern Anal. Mach. Intell., vol. 45, no. 3, pp. 2816–2834. 4526 Mar. 2023. 4527
- S.-W. Yang and C.-C. Wang, "Simultaneous egomotion estimation, 4528 [349] segmentation, and moving object detection," J. Field Robot., vol. 28, 4529 no. 4, pp. 565-588, Jul. 2011. 4530

- [350] X. Yang, F. Wu, L. Gui, and S. Zhong, "A tube-based model predictive control method for intelligent vehicles path tracking," Cluster Comput., vol. 27, no. 8, pp. 10343-10357, Nov. 2024.
- [351] D. Yin, Y. Chen, K. Ramchandran, and P. L. Bartlett, "Byzantine-robust distributed learning: Towards optimal statistical rates," in Proc. Int. Conf. Mach. Learn., 2018, pp. 5650-5659.
- [352] Z. Yin, J. Yang, Y. Ma, S. Wang, D. Chai, and H. Cui, "A robust adaptive extended Kalman filter based on an improved measurement noise covariance matrix for the monitoring and isolation of abnormal disturbances in GNSS/INS vehicle navigation," Remote Sens., vol. 15, no. 17, p. 4125, Aug. 2023.
- [353] K. Yousif, A. Bab-Hadiashar, and R. Hoseinnezhad, "An overview to visual odometry and visual SLAM: Applications to mobile robotics," Intell. Ind. Syst., vol. 1, no. 4, pp. 289-311, Dec. 2015.
- A. Yu, R. Palefsky-Smith, and R. Bedi, "Deep reinforcement learning 4545 for simulated autonomous vehicle control," Course Project Rep., Winter, vol. 2016, pp. 1-7, Jun. 2016.
- [355] S. Yu, M. Hirche, Y. Huang, H. Chen, and F. Allgöwer, "Model predictive control for autonomous ground vehicles: A review," Auto. Intell. Syst., vol. 1, no. 1, pp. 1-17, Aug. 2021.
- [356] X. Yu, Z. Qu, and G. Jin, "Robust adaptive filters and smoothers for linear systems with heavy-tailed multiplicative/additive noises," IEEE Trans. Aerosp. Electron. Syst., vol. 60, no. 5, pp. 6717-6733, Oct. 2024.
- [357] W. Yue, J. Ren, and W. Bai, "An online outlier-robust extended Kalman filter via EM-algorithm for ship maneuvering data," Measurement, vol. 250, Jun. 2025, Art. no. 117104.
- [358] S. Zair, S. Le Hégarat-Mascle, and E. Seignez, "Outlier detection in GNSS pseudo-range/Doppler measurements for robust localization," Sensors, vol. 16, no. 4, p. 580, Apr. 2016.
- [359] N. S. Zewge and H. Bang, "A distributionally robust fusion framework for autonomous multisensor spacecraft navigation during entry phase of Mars entry, descent, and landing," Remote Sens., vol. 15, no. 4, p. 1139, Feb. 2023.
- [360] C. Zhang, M. H. Ang, and D. Rus, "Robust LiDAR localization for autonomous driving in rain," in Proc. IEEE/RSJ Int. Conf. Intell. Robots Syst. (IROS), Oct. 2018, pp. 3409-3415.
- [361] H. Zhang, "Robust statistics vs. machine learning vs. Bayesian inference: Insights into handling faulty GNSS measurements in field robotics," 2025, arXiv:2504.06015
- [362] L. Zhang, G. Pantazis, S. Han, and S. Grammatico, "An efficient riskaware branch MPC for automated driving that is robust to uncertain vehicle behaviors," in Proc. IEEE 63rd Conf. Decis. Control (CDC), Dec. 2024, pp. 8207-8212.
- [363] T. Zhang and C. Tomasi, "Fast, robust, and consistent camera motion estimation," in Proc. IEEE Comput. Soc. Conf. Comput. Vis. Pattern Recognit., Jun. 1999, pp. 164-170.
- [364] W. Zhang and S. Song, "Distributionally robust state estimation for highly maneuvering target tracking with model uncertainty and impulsive measurement outliers," IEEE Sensors J., vol. 25, no. 6, pp. 9876–9886, Mar. 2025.
- [365] X. Zhang, Y. Chen, J. Zhu, and W. Sun, "Robust policy gradient against strong data corruption," in Proc. Int. Conf. Mach. Learn., 2021, pp. 12391-12401.
- [366] X. Zhang, Y. Chen, J. Zhu, and W. Sun, "Corruption-robust offline reinforcement learning," in Proc. Int. Conf. Artif. Intell. Statist., 2021, pp. 5757-5773.
- [367] Z. Zhang, "Determining the epipolar geometry and its uncertainty: A review," Int. J. Comput. Vis., vol. 27, pp. 161-195, Mar. 1998.
- Z. Zhang, X. Zhou, C. Wang, W. Zhao, G. Wu, T. Jiang, and M. Wang, "Adaptive robust federal Kalman filter for multisensor fusion positioning systems of intelligent vehicles," IEEE Sensors J., vol. 24, no. 10, pp. 17269-17281, May 2024.
- [369] J. Zhao and L. Mili, "Robust unscented Kalman filter for power system dynamic state estimation with unknown noise statistics." *IEEE Trans*. Smart Grid, vol. 10, no. 2, pp. 1215-1224, Mar. 2019.
- [370] J. Zhao, G. Yu, and Y. Liu, "Assessing robustness of classification using an angular breakdown point," Ann. Statist., vol. 46, no. 6B, pp. 3362-3389, Dec. 2018.
- [371] P. Zhao and Z. Wan, "Robust nonparametric regression under poisoning attack," in Proc. AAAI Conf. Artif. Intell., 2023, pp. 17007-17015.
- X. Zhao, Q. Li, C. Wang, H. Dou, and B. Liu, "Robust depth-aided visualinertial-wheel odometry for mobile robots," IEEE Trans. Ind. Electron., vol. 71, no. 8, pp. 9161-9171, Aug. 2024.

4605

4606

4607

4608

4609

4610

4611

4612

4613

4614

4615

4616

4617

- [373] X. Zhao, C. Wen, S. M. Prakhya, H. Yin, R. Zhou, Y. Sun, J. Xu, H. Bai, and Y. Wang, "Multimodal features and accurate place recognition with robust optimization for LiDAR-visual-inertial SLAM," *IEEE Trans. Instrum. Meas.*, vol. 73, pp. 1–16, 2024.
- [374] Z. Yang and H. Zhao, "A novel Bayesian-based INS/GNSS integrated positioning method with both adaptability and robustness in urban environments," *Chin. J. Aeronaut.*, vol. 37, no. 6, pp. 205–218, Jun. 2024.
- [375] Z. Li, X. Zhu, M. Cen, and X. Ding, "Robust surface matching for automated detection of local deformations using least-median-ofsquares estimator," *Photogramm. Eng. Remote Sens.*, vol. 67, no. 11, pp. 1283–1292, 2001.
- [376] P. Zhou, X. Guo, X. Pei, and C. Chen, "T-LOAM: Truncated least squares LiDAR-only odometry and mapping in real time," *IEEE Trans. Geosci. Remote Sens.*, vol. 60, 2022, Art. no. 5701013.
- 4618 [377] X. Zhou, Z. Wang, and J. Wang, "Popov-H<sub>∞</sub> robust path-tracking control
   4619 of autonomous ground vehicles with consideration of sector-bounded
   4620 kinematic nonlinearity," J. Dyn. Syst., Meas., Control, vol. 143, no. 11,
   4621 Nov. 2021, Art. no. 111004.
- 4622 [378] Y. Zhou, Z. Zheng, J. Huang, C. Wang, G. Xu, Y. Xuchen, and B. Zha,
   4623 "Distributed maximum correntropy cubature information filtering for tracking unmanned aerial vehicle," *IEEE Sensors J.*, vol. 23, no. 9,
   4625 pp. 9925–9935, May 2023.
- 4626 [379] B. Zhu, L. Wang, Q. Pang, S. Wang, J. Jiao, and D. Song, "Byzantine-robust federated learning with optimal statistical rates," in *Proc. Int. Conf. Artif. Intell. Statist.*, 2023, pp. 3151–3178.
- [380] F. Zhu, Y. Huang, C. Xue, L. Mihaylova, and J. Chambers, "A sliding window variational outlier-robust Kalman filter based on student's t-noise modeling," *IEEE Trans. Aerosp. Electron. Syst.*, vol. 58, no. 5, pp. 4835–4849, Oct. 2022.

- [381] J. Zubizarreta, I. Aguinaga, and J. M. M. Montiel, "Direct sparse mapping," *IEEE Trans. Robot.*, vol. 36, no. 4, pp. 1363–1370, Aug. 2020.
- [382] D. Zügner, "Adversarial robustness of graph neural networks," Ph.D. thesis, Fakultäat für Informatik, Technische Universität München, Munich, Germany, 2022.



**TINO WERNER** received the B.Sc. and M.Sc. degrees in mathematics and the Dr. rer. nat. degree in statistics from the Carl von Ossietzky Universität Oldenburg, in 2014, 2016, and 2020, respectively.

Since 2016, he has been with the Carl von Ossietzky Universität Oldenburg. From 2020 to 2021, he was with the research institute OFFIS, Oldenburg. Since 2022, he has been with German Aerospace Center, Institute of Systems Engineer-

ing for Future Mobility, Oldenburg. His research interests include robust statistics, machine learning, and model validation.

. . .

4633

4634

4635

4636

4637